# POWDER CORE DIELECTRIC WAVEGUIDES

Thesis by

WILLIAM M. BRUNO

In Partial Fulfillment of the Requirements

for the Degree of

Doctor of Philosophy

California Institute of Technology

Pasadena, California

1986

(Submitted January 31, 1986)

ACKNOWLEDGEMENTS

I would like to express my gratitude to Professor William B. Bridges, my thesis advisor, for his guidance and support. He provided many ideas of fundamental importance to the work presented here, including that of using a powder as the core material of a dielectric waveguide. His advice, both in regard to this thesis and other matters, was indispensable.

I thank Professor David Rutledge for his encouragement and technical advice, and his graduate students for many fruitful discussions. Dayalan Kasilingam, especially, was helpful to me both in personal matters and in ones related to this research. I am indebted also to Pete Balcewicz, Joel Paslaski and Larry Begay for their friendly help. A special gratitude is due Laura Rodriguez for her excellent secretarial work and for typing the manuscript.

Finally, I am grateful to everyone who has encouraged me during my years at Caltech, particularly Henry Sucov, and most of all, Jeanne-Marie Hand and my family.

## ABSTRACT

Flexible dielectric waveguides have been demonstrated at 10 GHz and 94 GHz by filling hollow, low dielectric constant polymer tubes with low-loss, high-dielectric constant powders. Flexible guides with losses as low as 0.12 dB/cm were demonstrated at 94 GHz. These guides also exhibited negligible bending loss for radii of curvature greater than 4 cm.

The theory of 3-region cylindrical dielectric waveguide was used to design the powder-filled tube guides, and measured wavelengths for the $HE_{11}$ mode are in agreement with theoretical values. Sets of dispersion curves were calculated numerically from the theory for waveguide parameters typical to our guides.

A powder-filled rectangular groove in the surface of a plastic substrate has also been demonstrated as a dielectric waveguide at 94 GHz. Guide wavelengths measured for these channel guides for various combinations of guide dimensions, powders, and substrate materials agree with values predicted by the approximate theory of Marcatili for the $E^{y}_{11}$ mode. Measured transmission losses were as low as 0.09 dB/cm.

The 94 GHz loss tangents of the powders were calculated by extending Marcatili's theory to relate channel guide attenuation to material losses. These calculated values of loss tangent increased with powder packing fraction, as predicted by theories of electromagnetic wave propagation in random heterogeneous media. Estimates of the 94 GHz loss tangents of the solid constituent materials were then obtained from these theories using the powder loss tangents.

Powder channel ring resonators had Q's as high as 2400 at 94 GHz in an 8 cm diameter ring. Directional coupling from adjacent straight channel guides was used to form a transmission filter. Marcatili's approximate theory of bending loss for channel guide appears to be inadequate for predicting the curvature losses of these resonators.

In a 10 GHz experiment, the coupling between two parallel powder channel waveguides was measured as a function of their separation. The measured coupling was at variance with that predicted by Marcatili's approximate analysis for parallel channel waveguides.

TABLE OF CONTENTS

## INTRODUCTION

Dielectric waveguides have been studied since the early part of the twentieth century. Probably the earliest reported work (1910) is that of Hondros and Debye (Ref. 1), who studied a cylindrical dielectric rod as a structure capable of guiding an electromagnetic wave. Since the late sixties, dielectric waveguides, usually consisting of glass fibers, have been investigated extensively for applications in optical communications (Ref. 2). More recently, with the growing interest in millimeter wave technology for such applications as radar, satellite communications, radio astronomy, and atmospheric studies, dielectric waveguides of various sorts have been studied for use in millimeter wave systems. In particular, they have been investigated as a means of realizing low attenuation transmission (Ref. 3), leaky wave antennas (Ref. 4), and integrated circuits (Ref. 5), to list just a few examples.

Our original motivation for studying millimeter wave dielectric waveguides was to develop an alternative to conventional rectangular metal guide. Metal guide used at millimeter wave frequencies is rigid and expensive (typically 40 dollars per meter for WR-10 W-band extruded copper waveguide, exclusive of end flanges). An attractive alternative would be an inexpensive, flexible dielectric guide analogous to optical fiber. Flexible millimeter wave guides

consisting of cylindrical plastic rods had been demonstrated before (Ref. 3), but these guides were 'unclad' and thus subject to loss from nearby objects. A cladding was needed to isolate the higher-index 'core' from its environment, as in modern optical fibers. In addition, the cladding would need to be thin to maintain flexibility.

For a thin cladding to be effective, its dielectric constant would have to be much smaller than that of the core so that the fields of the guided mode would decrease rapidly with distance in the cladding. Unfortunately, all the known flexible solids with low millimeter wave losses, such as Teflon$^{R}$ and polypropylene, have small dielectric constants (about 2). Our solution to this problem was to fill low-loss, low-dielectric constant plastic tubing with low-loss, high-dielectric constant powder to form the core of a flexible waveguide. In section A of Chapter I we discuss the theory of these 3-region (core/cladding/surrounding medium) dielectric waveguides and present dispersion curves for sets of parameters typical to our guides. Experimental investigations of these powder core guides are described in Section B.

In our first experiments on 94 GHz powder-filled tube waveguides, we found it difficult to pack the powder uniformly into the thin tubes. Packing nonuniformity caused the measured guide wavelength to vary with position. Also, the guides were so flexible that undesired

bending would occur during the measurement of guide wavelength, causing a loss of measurement accuracy. Although these problems with the powder-filled tubes were eventually overcome, an investigation of a rigid 94 GHz powder core waveguide was begun in the meantime to obtain good agreement between theory and experiment. This guide consisted of a powder-filled rectangular channel in the surface of a block of low-loss polymer (Teflon$^{R}$ or polypropylene). Since the powder was loaded from the side rather than the ends, the problem of packing uniformity was also eliminated. In Chapter II we describe the guide wavelength and attenuation measurements performed on these channel guides and present a method of obtaining the 94 GHz powder loss tangents from the measured values of waveguide attenuation.

Although powder channel waveguide was originally intended for measurement purposes, it appears to be interesting in its own right, especially for low-cost millimeter wave integrated circuits. Such circuits would require simple passive components like filters and directional couplers. Experimental investigations of ring resonator transmission filters made from powder channel waveguide are the subject of Chapter III. In Chapter IV, we describe the design and performance of a directional coupler consisting of two parallel powder channel waveguides.

This thesis has four appendices. In Appendix I, we describe our search for powder materials. In solid form, these materials needed very large dielectric constants and moderately low losses at millimeter wave frequencies for the corresponding powder to be suitable as a core for our waveguides. In Appendix II, we review theories of electromagnetic wave propagation in granular materials. Theories relating the attenuation of a wave propagating in a powder to the dielectric properties of the bulk solid from which the powder is derived are used to estimate the 94 GHz loss tangents of the solid materials from which our powders were obtained. Appendix III reviews the theory of the transmission method used for measuring the Q of our ring resonators. Finally, in Appendix IV, we estimate the radiation loss of powder channel guides caused by periodic imperfections in the waveguide parameters.

REFERENCES

1. E. Hondros and P. Debye, 'Elektromagnetischen Wellen an Dielektrischen Drahten,' Annalen Der Physik, Vol. 32, 1910, pp. 465-476.

2. D. Gloge, 'Optical fiber theory: Opportunities for advancement abound,' Radio Science, Vol. 12, No. 4, July-August 1977, pp. 479-490.

3. D. Jablonski, 'Attenuation characteristics of circular dielectric waveguide at millimeter wavelengths,' IEEE Transactions on Microwave Theory and Techniques, Vol. MTT-26, No. 9, Sept. 1978, pp. 667-671.

4. K.L. Klohn, R.E. Horn, H. Jacobs, and E. Freibergs, 'Silicon waveguide frequency scanning linear array antenna,' IEEE Transactions on Microwave Theory and Techniques, Vol. MTT-26, No. 10, Oct. 1978, pp. 764-773.

5. R.M. Knox, 'Dielectric waveguide microwave integrated circuits - an overview,' IEEE Transactions on Microwave Theory and Techniques, Vol. MTT-24, No. 11, Nov. 1976, pp. 806-814.

# I THREE REGION WAVEGUIDES

## Introduction

A flexible waveguide for use at millimeter wave frequencies, can be obtained by filling low-loss, low-dielectric constant plastic tubing with low-loss, high-dielectric constant powder to form the core of the guide. This chapter presents experimental and theoretical work on powder-filled tube dielectric waveguides for millimeter waves.

## A. Theory

### 1. The Characteristic Equation

Since the dielectric tubes employed in this study had to have walls thin compared to a wavelength to ensure flexibility, we could not take the usual simplifying approach, common to optical fibers, of treating a 3-region guide with thick cladding as a 2-region guide by ignoring the presence of the outermost region. Furthermore, since the differences in refractive index between the materials used here were large, approximations based on small index differences, common in optical fiber analysis, (Ref.I-1) were inapplicable. Consequently, the exact analytical theory of lossless 3-region cylindrical dielectric waveguides, given by Kuhn, (Ref. I-2) was used to predict

propagation constants for the modes of powder-filled tube guides.

The geometry of a 3-region cylindrical dielectric waveguide is shown in Fig. I-1. Region 1 is the core of the waveguide, and region 2 is the cladding. For the fields of the propagating modes to be well confined to the waveguide, it must have $\varepsilon_{r1} > \varepsilon_{r2} > \varepsilon_{r3}$. Since the materials are assumed to be lossless in this first-order analysis, $\varepsilon_{r1}$ and $\varepsilon_{r2}$ are real. For low-loss guide, it is usually sufficient to treat the loss as a perturbation, that is, ignore its effect on the propagation constant, $\beta(\omega)$.

To find the propagation constants for the modes of 3-region cylindrical dielectric waveguide, it is necessary to find the solutions to the wave equation for which the tangential field components are continuous at the two material boundaries. Kuhn's approach was to solve for the forms of the axial fields and then use these in Maxwell's curl equations to derive expressions for the other field components. The characteristic equation giving the propagation constants is then obtained from the equations expressing the continuity of the tangential fields at the boundaries.

The 3-region guide solutions require a distinction between modes not necessary in the 2-region case. Propagating modes are classified as either 'core' modes or 'cladding' modes (Ref. I-2). The

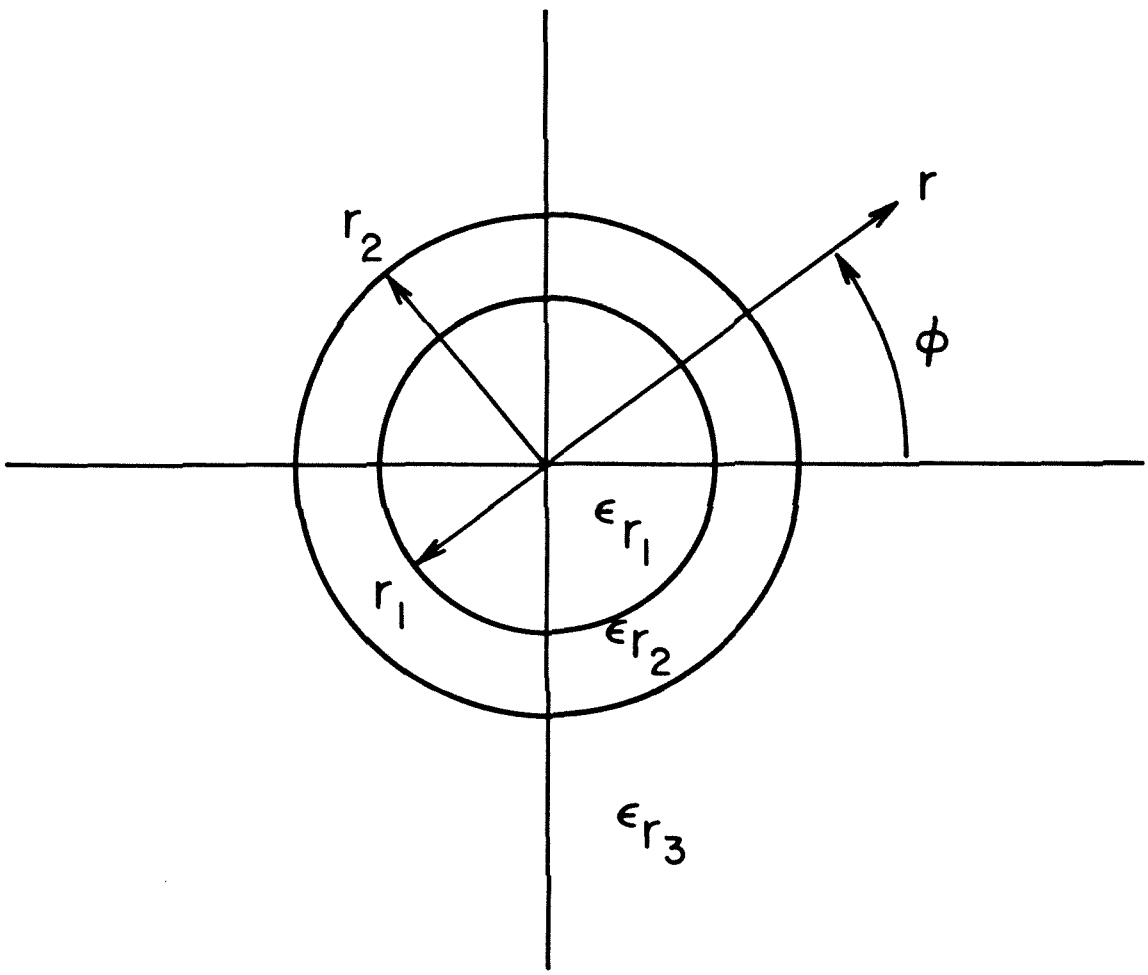


Figure I-1: Cross section of 3-region cylindrical dielectric waveguide

mathematical functions used to describe the field variations are different for these two classes of modes.

If the propagation constant, $\beta$, of a mode satisfies $\beta > \sqrt{\varepsilon_{r2}}k_0$ where $k_0 = \omega\sqrt{\mu_0\varepsilon_0}$, then the mode is a core mode. Core modes propagate with phase velocities less than $c/\sqrt{\varepsilon_{r2}}$ but greater than $c/\sqrt{\varepsilon_{r1}}$. On the other hand, modes for which $\beta < \sqrt{\varepsilon_{r2}}k_0$ are called cladding modes. These modes have phase velocities less than $c/\sqrt{\varepsilon_{r3}}$ but greater than $c/\sqrt{\varepsilon_{r2}}$. In general, cladding modes have larger phase velocities than core modes because a larger fraction of the power of a cladding mode propagates outside the core of the waveguide. Of course, for any propagating mode the propagation constant must lie between the value for a plane wave in free space, $k_0$, and a plane wave in the core dielectric, $k_0\sqrt{\varepsilon_{r1}}$. Modes with values of $\beta$ lying outside this interval are cut off (Fig. I-2).

Consider the system of cylindrical coordinates shown in Fig. I-1, with the z-direction coinciding with the longitudinal axis of the waveguide. The z components of the fields of a <u>core</u> mode can be found using separation of variables. They are

$$\begin{aligned} E_{1z} &= AJ_m(k_1r)\cos(m\phi)\exp(-j\beta z + j\omega t) \\ H_{1z} &= BJ_m(k_1r)\sin(m\phi)\exp(-j\beta z + j\omega t) \\ E_{2z} &= [CI_m(k_2r) + DK_m(k_2r)]\cos(m\phi)\exp(-j\beta z + j\omega t) \\ H_{2z} &= [EI_m(k_2r) + FK_m(k_2r)\sin(m\phi)\exp(-j\beta z + j\omega t) \end{aligned} \qquad \text{(I-1)}$$

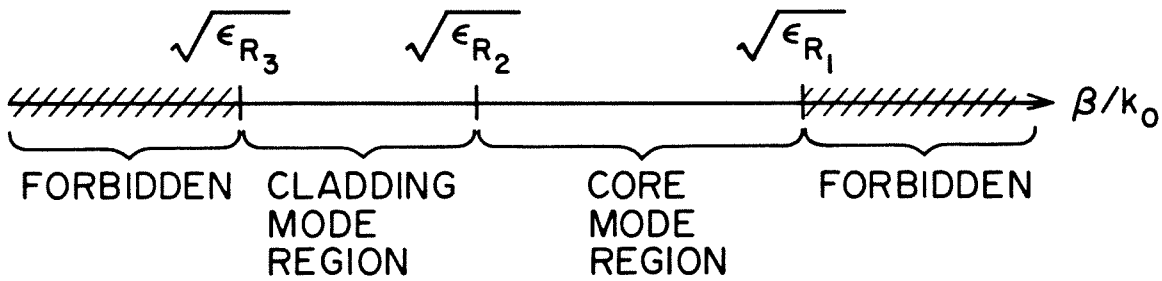


Figure I-2: Core mode and cladding mode regions of a 3-region cylindrical dielectric waveguide

$$E_{3z} = GK_m(k_3 r)\cos(m\phi)\exp(-j\beta z + j\omega t)$$

$$H_{3z} = PK_m(k_3 r)\sin(m\phi)\exp(-j\beta z + j\omega t).$$

We note that the radial variation of these field components is governed by Bessel's equation and that the fields in region 1 cannot depend on the Bessel function $Y_m(k_1 r)$ since it diverges at the origin. Similarly, $I_m(k_3 r)$ is omitted from the form of the solutions in region 3 since it increases monotonically with r.

Here m is the azimuthal eigenvalue, A,B,C,D,E,F,G, and P are constants and the real constants $k_1$, $k_2$, $k_3$ are defined by

$$\begin{aligned} k_1^2 &= \varepsilon_{r1} k_0^2 - \beta^2 \\ k_2^2 &= \beta^2 - \varepsilon_{r2} k_0^2 \\ k_3^2 &= \beta^2 - \varepsilon_{r3} k_0^2. \end{aligned} \qquad \text{(I-2)}$$

The remaining radial and azimuthal field components can be expressed in terms of the z-components using Maxwell's curl equations. (See, for example, Ref. I-3 or I-4.) These field components will exhibit similar functional variations with $(r,\phi,z)$ as the z-components in each region since they are related to the z-components by differentiation. Note that, for the core modes, the z-components of the electric and magnetic fields are oscillatory with r in the core region (Bessel function $J_m$), smoothly vary in the cladding region (modified Bessel functions $I_m$, $K_m$), and decay exponentially in the exterior region ($K_m$ only).

By contrast, for a cladding mode, the constant $k_2$ becomes

imaginary, so we define $k_2'$ as

$$(k_2')^2 = \varepsilon_{r2}k^2_0 - \beta^2, \qquad \text{(I-3)}$$

while $k_1$, and $k_3$ remain as before, and the field components $E_{2z}$, $H_{2z}$ become

$$E_{2z} = [C'J_m(k_2'r) + D'Y_m(k_2'r)]\cos(m\phi)\exp(-j\beta z + j\omega t) \qquad \text{(I-4)}$$

$$H_{2z} = [E'J_m(k_2'r) + F'Y_m(k_2'r)]\sin(m\phi)\exp(-j\beta z + j\omega t).$$

The z-components of the fields in regions 1 and 3 retain the same forms as for core modes.

Equating the tangential field components at the boundaries between regions yields a set of eight linear homogeneous equations for the eight constants (A,B.C,...P.). Setting the secular determinant of this system to zero yields the characteristic equation. This equation is rather complicated and must be solved numerically. For core modes it may may be written (Ref. 5)

$$G_1\eta_1^2 + G_2\eta_1 + G_3 = 0, \qquad \text{(I-5)}$$

where

$$G_1 = ad - bc$$

$$G_2 = (ad' - cb') + (da' - bc')$$

$$G_3 = a'd' - b'c'$$

$$a = \varepsilon_{r1}(\varepsilon_{r2}\Delta_2 - \varepsilon_{r3}\Delta_5)$$

$$a' = \varepsilon_{r2}Q_1Q_2(\xi - 1) - \varepsilon_{r2}(\varepsilon_{r2}\Delta_3 + \varepsilon_{r3}\Delta_1\eta_6)$$

$$b = \varepsilon_{r2}(\xi - 1)\,Q_2$$

$$b' = Q_1(\varepsilon_{r2}\Delta_2 - \varepsilon_{r3}\Delta_5) + \varepsilon_{r2}\Delta_1 Q_2$$

$$c = \varepsilon_{r1}(\xi - 1)\, Q_2$$

$$c' = \varepsilon_{r2}Q_1(\Delta_2 - \Delta_5) + \varepsilon_{r2}\Delta_1 Q_2$$

$$d = \varepsilon_{r2}(\Delta_2 - \Delta_5)$$

$$d' = Q_1 Q_2(\xi - 1) - \varepsilon_{r2}(\Delta_3 + \Delta_1\eta_6)$$

$$\Delta_1 = \eta_2 - \xi\eta_3$$

$$\Delta_2 = \xi\eta_4 - \eta_5$$

$$\Delta_3 = \xi\eta_3\eta_4 - \eta_2\eta_5 \qquad \text{(I-6)}$$

$$\Delta_4 = \xi(\eta_2 - \eta_3)(\eta_4 - \eta_5)$$

$$\Delta_5 = (\xi - 1)\eta_6$$

$$\eta_1 = J_m'(x)/xJ_m(x)$$

$$\eta_2 = -I_m'(u_1)/u_1 I_m(u_1)$$

$$\eta_3 = -K_m'(u_1)/u_1 K_m(u_1)$$

$$\eta_4 = -I_m'(u_2)/u_2 I_m(u_2)$$

$$\eta_5 = -K_m'(u_2)/u_2 K_m(u_2)$$

$$\eta_6 = -K_m'(w)/wK_m(w)$$

$$\xi = I_m(u_2)K_m(u_1)/I_m(u_1)K_m(u_2)$$

$$Q_1 = (m\beta/k_0)(1/x^2 + 1/u_1^2)$$

$$Q_2 = (m\beta/k_0)(1/w^2 - 1/u_2^2)$$

$$x = r_1k_1 \qquad u_1 = r_1k_2$$

$$u_2 = u_1r_2/r_1 \qquad w = r_2k_3.$$

For cladding modes, all the quantities are the same except

$$\eta_2 = J_m'(u_1)/u_1J_m(u_1) \qquad \eta_3 = Y_m'(u_1)/u_1Y_m(u_1)$$

$$\eta_4 = J_m'(u_2)/u_2J_m(u_2) \qquad \eta_5 = Y_m'(u_2)/u_2Y_m(u_2) \qquad \text{(I-7)}$$

$$\xi = J_m(u_2)Y_m(u_1)/J_m(u_1)Y_m(u_2)$$

$$Q_1 = (m\beta/k_0)\ (1/x^2 - 1/u_1^2) \qquad Q_2 = (m\beta/k_0)(1/u_2^2 + 1/w^2)$$

$$u_1 = r_1\ k_2'.$$

## 2. Classification of Modes

As in the case of a simple 2-region dielectric rod, when the azimuthal eigenvalue, m, equals zero, a great simplification is possible. The characteristic equation reduces to two much simpler equations. These are

$$\varepsilon_{r1}\eta_1(\varepsilon_{r2}\Delta_2 - \varepsilon_{r3}\Delta_5) - (\varepsilon_{r2})^2\Delta_3 - \varepsilon_{r2}\varepsilon_{r3}\Delta_1\eta_6 = 0, \qquad \text{(I-8)}$$

which yields TM modes, and

$$\eta_1(\Delta_2 - \Delta_5) - \Delta_3 - \Delta_1\eta_6 = 0, \qquad \text{(I-9)}$$

which yields TE modes. Since m = 0 the fields of these modes have no circumferential variation. TM and TE modes are designated $TM_{01}$, $TM_{02}$, $TM_{03}$,... and $TE_{01}$, $TE_{02}$,... where the first subscript specifies m = 0 (redundant), and the second gives the order in which the modes goes through cutoff to become guided as the frequency is increased.

Again, as in the case of the 2-region dielectric rod, all modes for which m is not zero are termed 'hybrid' modes because longitudinal components of both E and H are present. Several methods have been proposed (Refs. 2,5) for classifying hybrid modes for 3-region guide, but no method has been universally accepted. Most schemes classify

hybrid modes into one of two categories, $HE_{mn}$ and $EH_{mn}$. However, the criterion used to determine whether a mode is HE or EH is still a subject of controversy.

Since most schemes for classifying hybrid modes of 3-region guide are based on ones previously applied to simple dielectric rods, a discussion of methods for classifying hybrid modes of these 2-region guides is necessary to understand those proposed for 3-region guide. One of the earliest schemes for the dielectric rod was proposed by R.E. Beam in 1949 (Ref. I-6). Beam's method is based on the relative contributions of $E_z$ and $H_z$ to a transverse field component at some reference point. If $E_z$ makes the larger contribution, the mode is designated EH. If the contribution from $H_z$ is larger, the mode is classified as HE. In this scheme, the choice of the names HE and EH is reasonable because they are meant to express the hybrid character of the modes and to indicate which longitudinal field component is more significant in some sense. In addition, there is historical precedent for this choice of names. They are adapted from names given to modes of metal guides: TE modes of metal guides have been called H modes and TM modes have been called E modes, particularly in the British literature.

Although the spirit of this naming scheme makes sense, Beam's method is arbitrary because it depends on the particular transverse

component chosen to judge the relative importance of $H_z$ and $E_z$. Objecting to the arbitrariness of Beam's method, Snitzer (Ref. I-7) proposed a scheme for dielectric rods based on a factorization of the characteristic equation into the form $F1(\beta)*F2(\beta) = 0$. Since all modes result from either $F1 = 0$ or $F2 = 0$, the factorization divides the modes into two sets. Snitzer observed two differences between the sets. First, modes stemming from $F1 = 0$ obey different cut-off conditions than ones associated with $F2 = 0$. Second, the sign of the amplitude coefficient ratio A/B (c.f. Eq. I-1) is negative for hybrid modes belonging to one set and positive for hybrid modes from the other set. Since it had become conventional by this time to refer to the fundamental mode as $HE_{11}$, Snitzer proposed that all hybrid modes for which the sign of A/B is the same as for the fundamental be designated $HE_{mn}$. Hybrid modes for which A/B has the opposite sign were to be designated $EH_{mn}$. Here n is the order in which a mode of a given class (either HE of EH) goes through cut-off to become guided.

Although Snitzer's scheme allows the unambiguous classification of hybrid modes into two sets, the use of the names HE and EH is now at variance with Beam's scheme: modes called HE do not have longitudinal H dominant over longitudinal E. Similarly, EH modes are not 'E-like.' In fact, the opposite is true (Refs. I-4, I-8). The magnitude of A/B in normalized units of impedance is always greater than unity for hybrid modes of the dielectric rod designated HE by Snitzer and less

than unity for modes called EH. Hence, Snitzer's HE modes are truly 'E-like' and the EH modes are 'H-like.'

Other classification schemes have been proposed for the dielectric rod (Refs. I-9, I-10). The most commonly used of these other methods (Refs. I-10, I-11) is based on cut-off conditions of hybrid modes. It results in a classification of hybrid modes identical to Snitzer's.

In the case of the dielectric rod, Snitzer's method and its equivalents have gained wide acceptance (Refs. I-4, I-8, and I-11). For 3-region guide, however, no classification scheme has yet received wide acceptance. Following Snitzer, Kuhn (Ref. I-2) used the sign of A/B to classify hybrid modes of 3-region guide as either $HE_{mn}$ or $EH_{mn}$. However, he does not show the existence of any important physical differences between hybrid modes for which the sign of A/B is different. Since the sign of A/B, in itself, is not particularly significant, the separation of hybrid modes into two categories using this criterion is not meaningful.

Safaai-Jazi and Yip (Ref. I-5) have proposed a classification scheme based on a factorization of the characteristic equation of 3-region guide into the form $F3(\beta)*F4(\beta) = 0$. Hybrid modes whose propagation constants are found from $F3(\beta) = 0$ are designated $HE_{mn}$ and those whose propagation constants are given by $F4(\beta) = 0$ are called

$EH_{mn}$. Here again, the authors do not show any general physical differences between modes in each of the two classes. Furthermore, there is more than one way to express the characteristic equation of 3-region guide as a product of two functions of $\beta$ set to zero. Different factorizations may result in different classifications of the modes.

As a scheme for classifying hybrid modes of 3-region dielectric waveguide, we propose here that the magnitude of the ratio of the longitudinal fields be compared to the wave impedance of a plane wave travelling at the same phase velocity. That is, we define a wave impedance, Z, as

$$Z = \sqrt{\mu_0/\varepsilon_0}/(\beta/k_0) = 377 \text{ ohms}/(\beta/k_0).$$

If, for a particular hybrid mode, the ratio $|A/B|$ (which, in some sense, is the magnitude of the ratio of $E_{1z}$ to $H_{1z}$, the longitudinal fields in the core region) evaluated far above the cut-off frequency is greater than Z, then the mode is to be called $HE_{mn}$. Modes for which $|A/B|$ is less than Z will be $EH_{mn}$. The subscript m will denote the azimuthal eigenvalue while n will give the order in which a mode of a particular class goes through cut-off to become guided as frequency is increased. According to this scheme, the fundamental mode will be named $HE_{11}$, in accordance with the established convention.

With this method, hybrid modes can be classified unambiguously into physically distinct categories whose names reflect the distinction. Although it would be preferable for historical reasons to have the first letter in the name of a hybrid mode, rather than the second, indicate the dominant longitudinal component, such a choice would cause extra confusion since the fundamental mode of optical fibers is called $HE_{11}$ by convention. Secondly, our proposed method is in agreement with Snitzer's well-accepted scheme for the dielectric rod where the second letter of the name of a hybrid mode indicates the dominant longitudinal component, as explained earlier.

The reason for examining $|A/B|/Z$ for each hybrid mode far above cut-off is that its value varies with frequency. However, when evaluated far above cut-off, $|A/B|/Z$ approaches unity for all hybrid modes. The classification scheme presented here is based on whether unity is approached from above or below.

## 3. Formulas Useful Near Cut-off

When designing a dielectric waveguide it is useful to know the cut-off conditions for the modes. In general, solving equation I-5 is quite tedious. However, approximations can be used to find the cut-off conditions. For 3-region cylindrical dielectric waveguide these can be obtained from the characteristic equation for cladding

modes (Eq. I-5) using the following Bessel function identities as described in Ref. I-12.

$$tJ_m'(t) = tJ_{m-1}(t) - mJ_m(t)$$
$$tY_m'(t) = tY_{m-1}(t) - mY_m(t)$$
$$tK_m'(t) = -tK_{m-1}(t) - mK_m(t)$$

Near cut-off, $\beta$ approaches $\sqrt{\varepsilon_{r3}}k_o$ and w approaches zero. Using the small argument approximations given in Table 1, the following cut-off conditions are derived:

$$\varepsilon_{r1}\eta_1'(\xi - 1) + \varepsilon_{r2}\Delta_1' = 0 \text{ for TM modes,} \qquad \text{(I-10)}$$
$$\text{and } \eta_1'(\xi - 1) + \Delta_1' = 0 \text{ for TE modes.} \qquad \text{(I-11)}$$

The TE and TM modes of 3-region guide are seen to obey different cut-off conditions, unlike the 2-region guide where the cut-off conditions for the $TE_{0n}$ and $TM_{0n}$ modes are the same.

For modes with $m > 1$, the cut-off condition is

$$(\eta_1' - (m/x^2) - (R_1/(2E_1)))(\eta_1' - (m/x^2) - (R_2/(2E_1))) = 0, \qquad \text{(I-12)}$$

where

$$R_1 = E_2 + \sigma((E_2')^2 + 4\varepsilon_{r1}\varepsilon_{r3}E_3^2)^{1/2}$$
$$R_2 = E_2 - \sigma((E_2')^2 + 4\varepsilon_{r1}\varepsilon_{r3}E_3^2)^{1/2}$$

TABLE I-1

Small argument approximations

| n | $K_{n-1}(t)/(tK_n(t))$ |
|---|---|
| $n \geq 2$ | $1/(2(n-1))$ |
| $n = 1$ | $\ln(2/(\gamma t))$ |
| $n = 0$ | $-1/(t^2 \ln(\gamma t/2))$ |

$\gamma = 1.781...$ (Euler's constant)

$$E_1 = -\varepsilon_{r1}C_1$$

$$E_2 = (\varepsilon_{r1} + \varepsilon_{r2})(mC_1/u_1^2 - C_2) + \varepsilon_{r2}(\varepsilon_{r1} + \varepsilon_{r3})\Delta_4'$$

$$E_2' = (\varepsilon_{r1} - \varepsilon_{r2})(mC_1/u_1^2 - C_2) + \varepsilon_{r2}(\varepsilon_{r1} - \varepsilon_{r3})\Delta_4'$$

$$E_3 = mC_1(1/x^2 - 1/u_1^2) - \varepsilon_{r2}\Delta_4'$$

$$\sigma = 1$$

$$C_1 = (\xi - 1)((\varepsilon_{r2} + \varepsilon_{r3})\Delta_2' - \varepsilon_{r3}(\xi - 1)/(m - 1))$$

$$C_2 = (\xi - 1)((\varepsilon_{r2} + \varepsilon_{r3})\Delta_3' + \varepsilon_{r3}\Delta_1'/(m - 1)).$$

For $m = 1$,

$$E_1 = \varepsilon_{r1}(\xi - 1)$$

$$E_2 = -(\varepsilon_{r1} + \varepsilon_{r2})(\Delta_1' + (\xi - 1)/u_1^2)$$

$$E_2' = -(\varepsilon_{r1} - \varepsilon_{r2})(\Delta_1' + (\xi - 1)/u_1^2)$$

$$E_3 = (\xi - 1)(1/x^2 - 1/u_1^2)$$

$$\sigma = \mathrm{sgn}(\xi - 1).$$

In all of the above equations for cut-off conditions,

$$\Delta_1' = \eta_2' - \xi\eta_3'$$

$$\Delta_2' = \xi\eta_4' - \eta_5'$$

$$\Delta_3' = \xi\eta_3'\eta_4' - \eta_2'\eta_5'$$

$$\Delta_4' = \xi(\eta_2' - \eta_3')(\eta_4' - \eta_5')$$

$$\eta_1' = J_{m-1}(x)/(xJ_m(x))$$

$$\eta_2' = J_{m-1}(u_1)/u_1J_m(u_1))$$

$$\eta_3' = Y_{m-1}(u_1)/(u_1Y_m(u_1))$$

$$\eta_4' = J_{m-1}(u_2)/(u_2J_m(u_2))$$

$$\eta_5' = Y_{m-1}(u_2)/(u_2Y_m(u_2)).$$

## 4. Numerical Results

Computer programs were written which solved the 3-region characteristic equation (Eq. I-5) for m = 1 ($HE_{1n}$ and $EH_{1n}$ modes) and m = 0 ($TE_{0n}$ and $TM_{0n}$ modes). Examples of computed values for propagation constant for different parameters appropriate to 10 GHz waveguides are given in part B of this chapter. As reported there, the agreement between theoretical and experimental values was excellent.

Here we present dispersion curves obtained with the programs for 3-region dielectric waveguides useful at microwave frequencies. These guides have much thinner cladding regions ($r_2 = 1.25r_1$) than their optical counterparts. In addition, the refractive index difference between core and cladding is much larger than for optical fibers.

Sets of dispersion curves are given for $\varepsilon_{r1}$ equal to 4, 8, and 12 (Figs. I-3 through I-5). For each set $\varepsilon_{r3}$ equals 1 (air) and $\varepsilon_{r2}$ equals 2.08 (TFE teflon). The abscissa is $k_o r_1 = 2\pi f r_1/c$. It may be thought of as frequency for a guide with fixed core radius, $r_1$, or as core radius for operation at a fixed frequency.

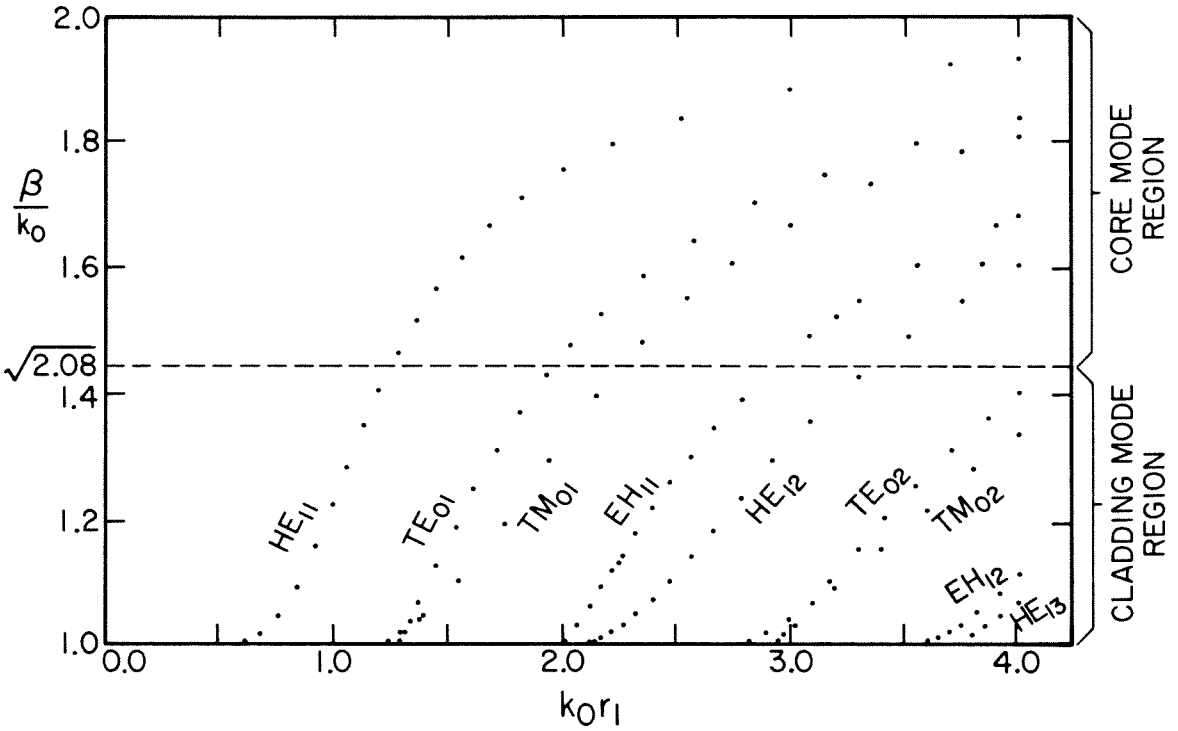


Figure I-3: Dispersion curves of 3-region cylindrical dielectric waveguide. $\varepsilon_{r1} = 4$, $\varepsilon_{r2} = 2.08$, and $\varepsilon_{r3} = 1$. $r_2 = 1.25\ r_1$.

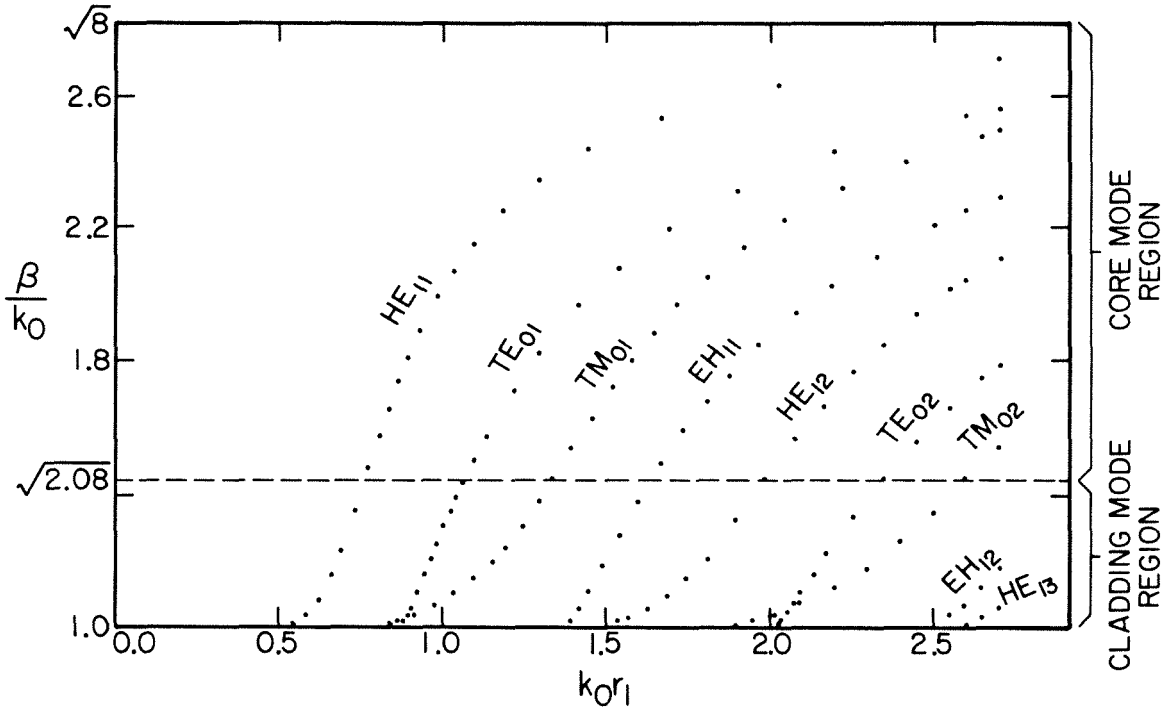


Figure I-4: Dispersion curves of 3-region cylindrical dielectric waveguide. $\varepsilon_{r1} = 8$, $\varepsilon_{r2} = 2.08$, $\varepsilon_{r3} = 1$. $r_2 = 1.25\ r_1$.

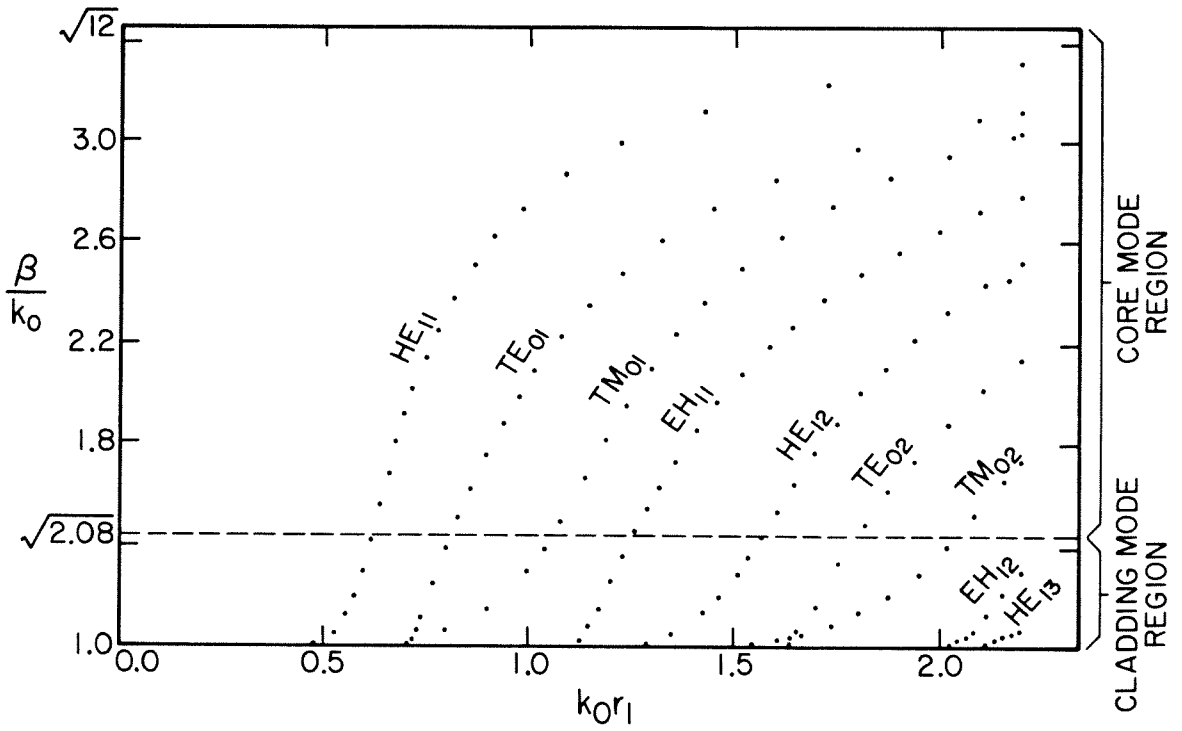


Figure I-5: Dispersion curves of 3-region cylindrical dielectric waveguide. $\varepsilon_{r1} = 12$, $\varepsilon_{r2} = 2.08$, $\varepsilon_{r3} = 1$. $r_2 = 1.25\ r_1$.

The most noticeable differences between Figures I-3 through I-5 and dispersion curves for 2-region guides are the crossovers of the $TE_{0n}$ and $TM_{0n}$ modes in Figures I-3 through I-5. (The $TE_{0n}$ and $TM_{0n}$ modes of dielectric rods do not cross.) Safaai-Jazi and Yip (Ref. I-12) have reported that these modes also cross for 3-region optical guides where the refractive index difference between core and cladding is small. (Their results were obtained from the exact 3-region analysis, not an approximation based on small refractive index difference.) Hence, these crossovers must be attributable to finite cladding thickness.

Another difference between the dispersion curves of 2-region and 3-region guides involves mode cut-offs, as mentioned earlier. For 2-region guides, the $TE_{0n}$ and $TM_{0n}$ modes have identical cut-offs, as do the $EH_{1,n}$ and $HE_{1,n+1}$ modes. However, for 3-region guide, these pairs of modes do not have identical cut-offs, as shown in Figs. I-3 through I-5. Values of $k_o r_1$ at cut-off calculated from equations I-11, I-12, and I-13 are presented in Table I-2.

## B. Experimental Work on 3-Region Guides

Flexible dielectric waveguides were demonstrated at both 10 GHz and 94 GHz by filling hollow, low-dielectric-constant polymer tubes with

TABLE I-2

Calculated values of $k_0 r_1$ at cut-off for 3-region guide with $r_2 = 1.25 r_1$ and $\varepsilon_{r3} = 1.$

| Mode | $\varepsilon_{r1}/\varepsilon_{r2} = 4/2.08$ | $\varepsilon_{r1}/\varepsilon_{r2} = 8/2.08$ | $\varepsilon_{r1}/\varepsilon_{r2} = 12/2.08$ |
|---|---|---|---|
| $TM_{01}$ | 1.24 | .82 | 0.65 |
| $TE_{01}$ | 1.28 | 0.88 | 0.71 |
| $EH_{11}$ | 2.02 | 1.34 | 1.09 |
| $HE_{12}$ | 2.07 | 1.42 | 1.15 |
| $TM_{02}$ | 2.77 | 1.86 | 1.49 |
| $TE_{02}$ | 2.92 | 2.02 | 1.63 |
| $EH_{12}$ | 3.53 | 2.39 | 1.93 |
| $HE_{13}$ | 3.70 | 2.56 | 2.08 |

low-loss, high-dielectric-constant powders. Flexible guides with losses as low as 0.12 dB/cm were demonstrated at 94 GHz. These guides also exhibited negligible bending loss for radii of curvature greater than 4 cm. Fig. I-6 is a photograph of some samples of W-band flexible guide made by this technique.

## 1. 10 GHZ MODELING EXPERIMENTS

Initial efforts to make dielectric waveguides by filling flexible hollow tubes with dielectric powders were conducted at 10 GHz to avoid inaccuracies due to the small guide dimensions at 94 GHz. In addition, the dielectric properties of the powders were known at 10 GHz, so the guides could actually be 'designed' and compared with theory.

The powders used were Emerson and Cumming ecco-flo powder, Trans-Tech D-30 nickel-aluminum titanate, and Trans-Tech D-38 barium tetratitanate. The particles of the D-30 and D-38 powders ranged in size from 43 μm to 100 μm. Trans-Tech gives $\varepsilon_r = 31$ and $\tan\delta < .0002$ for solid D-30 at 10 GHz, and $\varepsilon_r = 37$ and $\tan\delta < .0005$ for solid D-38 at 6 GHz. They do not specify the dielectric properties of the powders. Ecco-flo powder is specified by Emerson and Cumming to have $\tan\delta = .0007$ at 10 GHz.

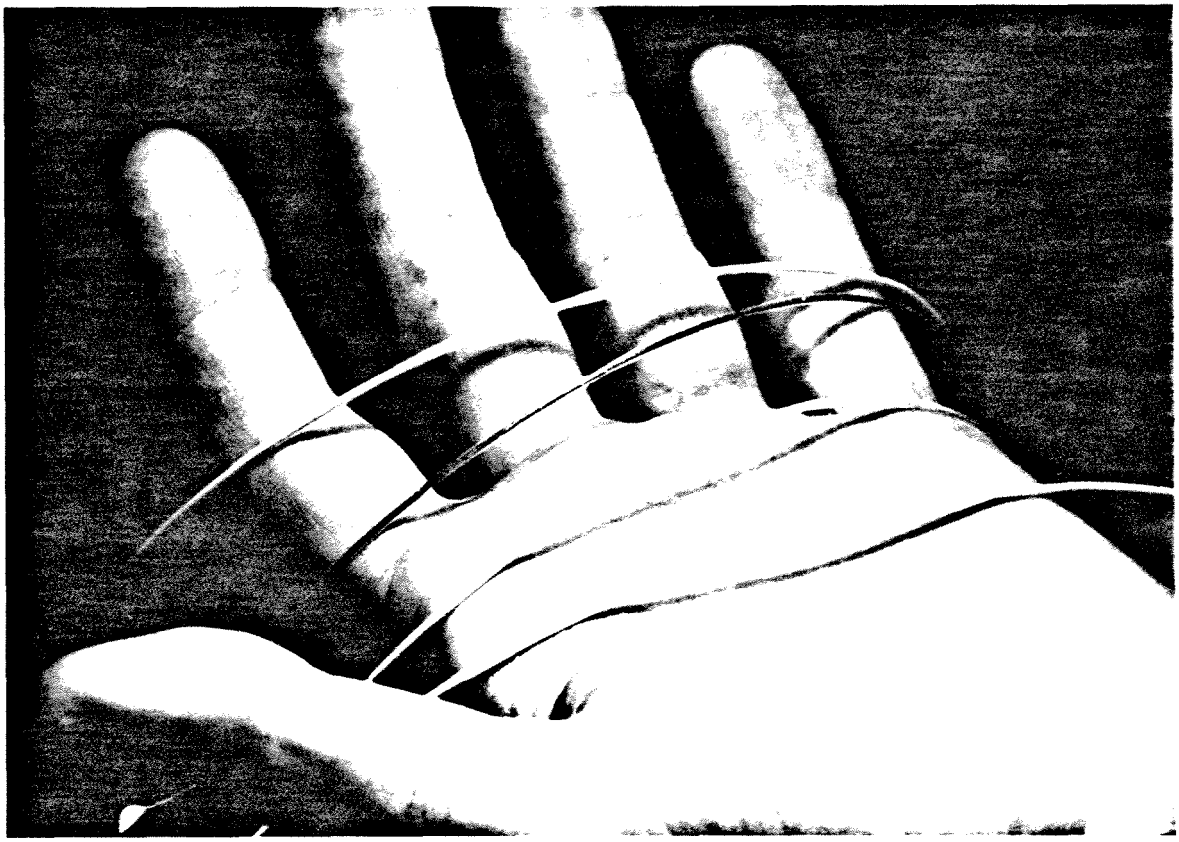

Figure I-6: Samples of W-band dielectric waveguide made by filling Teflon$^{R}$ spaghetti with various low-loss dielectric powders.

In order to design a dielectric waveguide with a powder core, it is necessary to know how the dielectric constant of the powder will vary with the packing density. This relationship was determined for each powder at 10 GHz by using the shorted waveguide technique (Ref. I-13) to measure dielectric constant. A typical plot of dielectric constant versus density (nickel-aluminum titanate) is given in Fig. I-7.

The cladding materials used were TFE Teflon$^{R}$, polyethylene, and Corning 7740 glass (Pyrex$^{R}$). The dielectric properties of these materials at 10 GHz as given by von Hippel (Ref. I-14) are shown in Table I-3. Although the Pyrex$^{R}$ tubes were inflexible, they were useful for making accurate guide wavelength and attenuation measurements.

Each waveguide was made by filling a tube with powder and plugging the ends with polyfoam. The inner diameter of the tube was chosen so that the $HE_{11}$ mode would propagate with a wavelength significantly smaller than the free space wavelength. Coupling was achieved by inserting one end of the tube into a flared section of rectangular metal waveguide (a $TE_{10}$ rectangular to $TE_{11}$ circular metallic waveguide transition). This metal waveguide transition was used since the transverse fields of the $TE_{11}$-circular mode of metal waveguide (Ref. I-15) are known to be similar to those of the $HE_{11}$ mode of a cylindrical dielectric rod. The waveguide was supported inside the

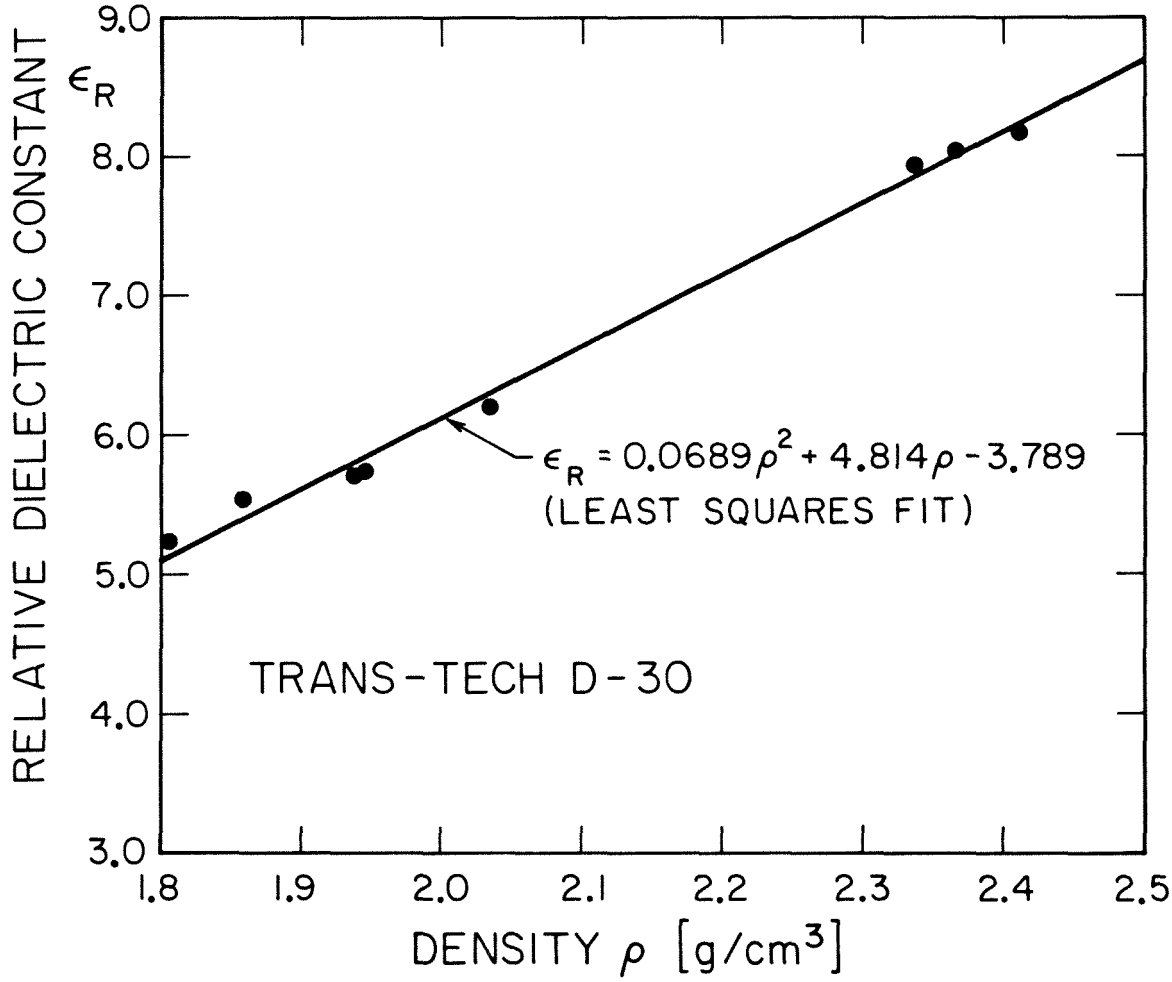


Figure I-7: Relative dielectric constant versus density for Trans-Tech D-30 powder. 70% of particles between 100 μm and 43 μm, 30% less than 43 μm.

TABLE I-3

Dielectric properties of tubing materials at 10 GHz

| Material | $\varepsilon_r$ | tan $\delta$ |
|---|---|---|
| TFE Teflon$^R$ | 2.08 | .0004 |
| polyethylene | 2.25 | .0004 |
| Corning 7740 Pyrex$^R$ glass | 4.52 | .0085 |

Data from A.R. Von Hippel, DIELECTRIC MATERIALS AND APPLICATIONS, John Wiley and Sons, Inc., pp. 301-370, New York, 1958.

flared section with a form-fitting polyfoam insert. With the waveguide inserted to the proper depth (determined by trial and error), the reflected power was more than 10 dB below the incident power. This amount of reflected power was sufficiently small for making guide wavelength measurements. In addition, there was no detectable radiation field away from the coupler and waveguide. A metal perturber placed a few mm away from the fiber, outside the volume of the ($HE_{11}$) guided mode caused no change in reflected power, which was already low. Finally, lossy foam was wrapped around the tube at the far end to prevent reflections.

Guide wavelength measurements were made by sliding a metal washer along the full length of the guide and observing the periodic variation in reflected power. Table I-4 shows that the measured guide wavelengths were in excellent agreement with those predicted by the theory of lossless 3-region cylindrical dielectric waveguide, as presented in section I-A. The values of $\varepsilon_{rcore}$ listed in Table I-4 were determined by using the $\varepsilon_r$ vs. density data and determining the density of the powder in the tube by precision weight measurement.

Rough estimates of transmission and bending loss were obtained for the powder-filled tubes by observing the exponential decay in the amplitude of the periodically varying reflected power as a metal washer was moved along the length of the guide (Fig. I-8). These

TABLE I-4

Comparison of measured and theoretical guide wavelengths for $HE_{11}$ mode of 3-region guide at X-band

| Core Radius (cm) | Cladding Radius (cm) | Freq. (GHz) | Core Mat'l. | Core $\varepsilon_r$ | Cladding Mat'l. | Cladding $\varepsilon_r$ | Guide Wavelength Meas. (cm) | Guide Wavelength Theo. (cm) |
|---|---|---|---|---|---|---|---|---|
| 0.33 | 0.45 | 10.000 | 1 | 7.62 | A | 4.52 | 2.05 | 2.06 |
| 0.25 | 0.35 | 10.000 | 2 | 13.45 | A | 4.52 | 2.30 | 2.19 |
| 0.26 | 0.30 | 10.000 | 2 | 11.40 | B | 2.08 | 2.88 | 2.86 |
| 0.26 | 0.30 | 11.311 | 2 | 11.40 | B | 2.08 | 2.14 | 2.09 |
| 0.30 | 0.40 | 10.940 | 2 | 13.02 | C | 2.25 | 1.38 | 1.32 |
| 0.32 | 0.47 | 9.794 | 2 | 12.39 | C | 2.25 | 1.71 | 1.65 |

Material 1 is nickel-aluminum titanate (Trans-Tech D-30).

Material 2 is Emerson and Cuming Ecco-flo powder.

Material A is Corning 7740 Pyrex$^R$ glass.

Material B is TFE Teflon$^R$.

Material C is polyethylene.

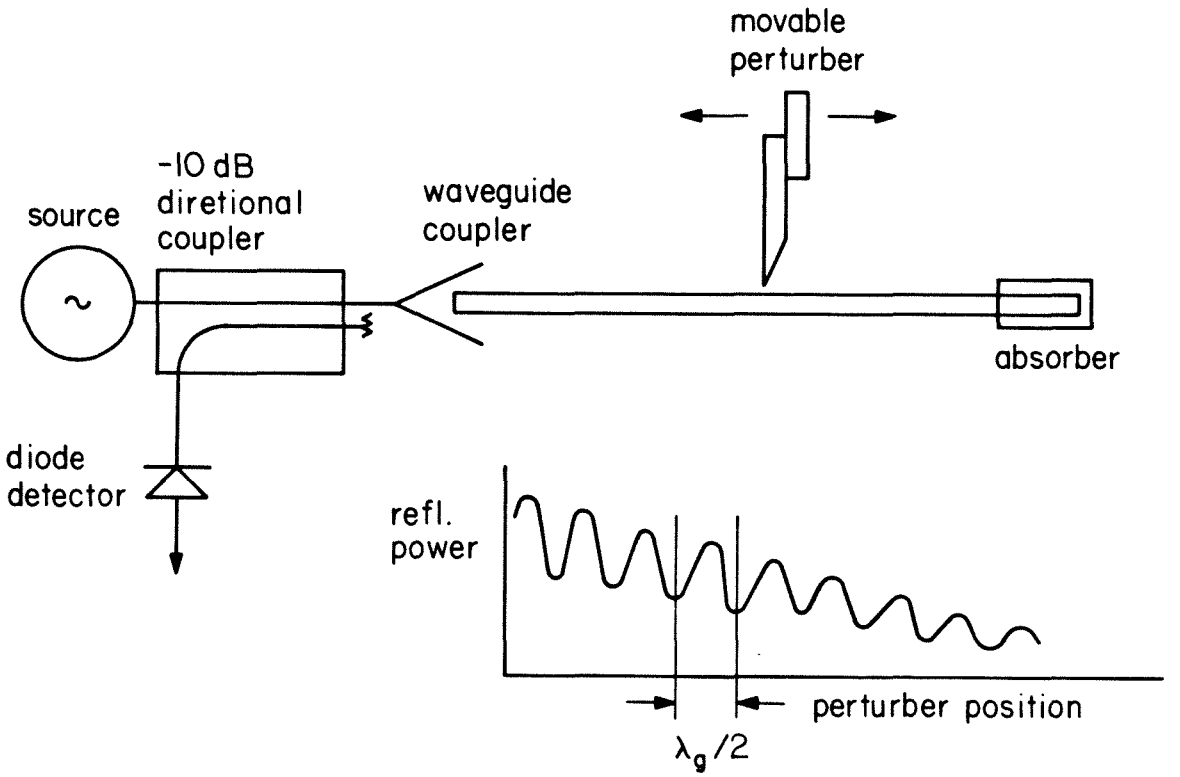


Figure I-8: Schematic of setup for guide wavelength measurement. Also shown is a curve of reflected power versus perturber position.

measurements indicated that the transmission and bending losses were low. Since we were primarily interested in millimeter-wave guides, we did not pursue this investigation far enough at 10 GHz to determine precisely the magnitude of these losses. Instead we began a program to build and test flexible 94 GHz powder-filled tube waveguides.

## 2. 94 GHZ EXPERIMENTS

94 GHz flexible dielectric waveguides were made by filling Teflon$^R$ tubes (18-23 AWG lightweight* electrical spaghetti) with dielectric powders. The guides were 'designed' using the theory of lossless 3-region cylindrical dielectric waveguide so that the $HE_{11}$ mode would be significantly slowed. In order to use the theory, the dielectric constant of the powders were needed. We used the values measured at 10 GHz because of the difficulty of controlling the length of a powder sample sufficiently accurately to measure its dielectric constant at 94 GHz with the shorted-waveguide technique. The dielectric constant of a powder composed of low-loss dielectric material should not vary

---

*Teflon$^R$ electrical spaghetti is available in 3 types, according to wall thickness. 'Standard wall' spaghetti has the thickest walls, followed in decreasing order of thickness by 'thin wall' and 'lightweight'.

much between 10 GHz and 94 GHz if the powder grains are small relative to wavelength at 94 GHz (for further explanation, see Appendix II.)

Coupling to metal waveguide was achieved by inserting the end of the tube into a slightly flared section of WR-10 metal waveguide. As before, guide wavelength measurements were made by sliding a metal perturber along the length of the waveguide and observing the periodic variation in reflected power.

The ecco-flo powder proved to be so lossy at 94 GHz that only surface waves would propagate along Teflon$^{R}$ tubes filled with this powder. These waves were the same kind of $v \sim c$ waves that were previously observed on KRS-5 guides (Ref. I-16.)

For tubes filled with the other powders used previously at X-band (D-30 and D-38 powders for which the particles ranged in size from 43 μm to 100 μm), we were unable to obtain meaningful measured values of guide wavelength. The measured wavelengths varied by as much as 100% with distance along the guide. We believe that one of the factors contributing to this wavelength variation was the random variation with length of the cross-sectional dimensions and circularity of the small (21,22,23 AWG), commercial grade spaghetti supporting these powders. Another source of error was that the small size of the tubes made them difficult to fill uniformly with powder. Finally, the

powder-filled tubes were so flexible they would bend during the measurement, making the length of a period difficult to measure accurately.

The foregoing difficulties were overcome by using three powders not received in time to be studied at X-band. These powders were Trans-Tech MCT-40 magnesium-calcium titanate, D-30 nickel-aluminum titanate, and D-8512, and improved barium tetratitanate. (Trans-Tech claims that D-8512 has lower loss than D-38 and also a smaller thermal coefficient of dielectric constant. Otherwise, we do not know the nature of the 'improvement'.) For each of these powders, all particles were less than 43 μm in size.

Since these powders had lower dielectric constants than the others, we were able to use larger-diameter spaghetti (18,19,20 AWG) while still allowing propagation of only the fundamental $HE_{11}$ mode. Thus, the problems associated with small tubing, dimensional imperfections, packing irregularities, and excessive flexibility, were all reduced significantly. In addition, the smaller particles of these powders also made it easier to pack them uniformly in the tubes. As a result of these improvements, the measured guide wavelengths agreed with the theoretical values for the $HE_{11}$ mode, as shown in Table I-5. For the guides represented in Table I-5, there were no beats in the pattern of reflected power versus perturber position, indicating that the guides

TABLE I-5

Comparison of measured and theoretical guide wavelengths for $HE_{11}$ mode of 3-region guide at W-band

| Powder | Core Radius (mm) | Freq. (GHz) | $\varepsilon_{r_{core}}$ | Guide Wavelength Meas. (mm) | Theo. (mm) |
|---|---|---|---|---|---|
| D-30 | .43 | 94.78 | 5.60 | 2.48 | 2.42 |
| D-8512 | .43 | 94.72 | 5.45 | 2.55 | 2.47 |
| D-8512 | .48 | 94.75 | 5.83 | 2.21 | 2.10 |
| D-8512 | .53 | 94.10 | 4.79 | 2.06 | 2.24 |

Cladding material is TFE Teflon$^R$, $\varepsilon_r = 2.08$.

Cladding thickness is .15 mm.

The free space wavelength is approximately 3.2 mm.

were single-mode as intended.

Attenuation measurements were made by measuring the power received with a diode detector at the far end of the waveguide. Power was coupled off the dielectric waveguide by inserting it into a flared section of metal waveguide connected to the detector. Another detector connected to a small horn was used as a movable probe to determine that there was an insignificant amount of radiation from the couplers and waveguide. Also the power reflected back into the metal waveguide from the feed coupler was approximately -20 dB down from the incident power. Thus, we concluded that there was very little power lost in coupling by reflection or radiation, so that the difference between the incident power and the power detected at the far end represented the true dielectric waveguide loss. The loss per unit length is then this loss divided by the length of the dielectric waveguide, typically 30 cm. Table I-6 gives the results of attenuation measurements on a few straight powder-filled teflon tubes.

Bending loss measurements were made using the same set-up as for attenuation measurements on straight guides. The plane of bending was perpendicular to the (vertical) plane of polarization of the $HE_{11}$ mode. A problem encountered during these measurements was that the ends of the teflon tubes tended to change position inside the flared metal waveguide couplers when the tubes were bent in arcs with radius

TABLE I-6

Attenuation of straight mm-wave guides

| Powder | Core Radius (mm) | Freq. (GHz) | $\varepsilon_{r_{core}}$ | Measured Guide Wavelength (mm) | Loss (dB/cm) |
|---|---|---|---|---|---|
| D-30 | .43 | 94.78 | 5.60 | 2.48 | .12 |
| D-8512 | .43 | 94.72 | 5.45 | 2.55 | .13 |
| D-8512 | .48 | 94.75 | 5.83 | 2.21 | .14 |
| MCT-40 | .53 | 94.08 | 4.48 | 2.12 | .26 |

Cladding material is TFE Teflon$^{R}$, $\varepsilon_r = 2.08$.

Cladding thickness is .15 mm.

Loss of silver WR-10 waveguide is approximately .05 dB/cm at 94 GHz.

less than about 4 cm. This movement changed the quality of the coupling between the dielectric waveguide and the metal waveguides, making it difficult to obtain accurate measurements of bending losses. When the tubes were bent into circles with curvature radius greater than or equal to 4 cm, bending losses were immeasurably small.

A straightforward comparison of our bending loss observations to theory is not possible because we know of no bending loss theory that applies to 3-region guides with thin cladding, large refractive index difference between layers, and curvature radius equal to about 20 guide wavelengths. In fact, all the theories with which we are familiar assume that the refractive index differences between layers are small. Keeping these limitations in mind, we have used the theory of Kuester and Chang (Refs. I-17 and I-18) for curved dielectric rods for rough comparison. To use the theory, the rod radius and dielectric constant were chosen equal to that of the core of the actual guide, and the surroundings of the rod were assumed to have a relative dielectric constant equal to one. The theoretical curvature losses were calculated for the vertically polarized $LP_{10}$ mode, which corresponds to the unapproximated vertically polarized $HE_{11}$ mode. Applied in this way, the theory predicted that a curvature radius of less than 2 cm would be necessary for our guides to exhibit bending losses comparable to our absorptive losses.

REFERENCES

I-1. D. Gloge, 'Weakly Guiding Fibers,' Applied Optics, vol. 10, pp. 2252-2258, October, 1971.

I-2. M.H. Kuhn, 'The influence of the refractive index step due to the finite cladding of homogeneous fibers on the hybrid properties of modes,' Archiv fur Elektronik und Ubertragungstechnik, vol. 28, pp. 393-401, October, 1974.

I-3. S. Ramo, J.R. Whinnery, and T. Van Duzer, FIELDS AND WAVES IN COMMUNICATION ELECTRONICS, Wiley, New York, 1966, Chapter 7.

I-4. H.G. Unger, PLANAR OPTICAL WAVEGUIDES AND FIBERS, Clarendon Press, Oxford, 1977, Chapter 4.

I-5. A. Safaai-Jazi and G.L. Yip, 'Classification of hybrid modes in cylindrical dielectric optical waveguides,' Radio Science, vol. 12, pp. 603-609, July-August 1977.

I-6. R.E. Beam, M.M. Astrahan, W.C. Jakes, H.M. Wachowski, and W.L. Firestone, 'Dielectric tube waveguides,' Rep. ATI 94929, chapter 5, Northwestern University, Evanston, Illinois, 1949.

I-7. E. Snitzer, 'Cylindrical dielectric waveguide modes,' J. Opt. Soc. Amer., Vol. 51, pp. 491-498, May 1961.

I-8. N.S. Kapany and J.J. Burke, OPTICAL WAVEGUIDES, Academic Press, New York, 1972, pp. 118.

I-9. P.J.B. Clarricoats, 'Propagation along unbounded and bounded dielectric rods,' Proc. Inst. Elec. Eng., vol. 108C, pp. 170-176, 1961.

I-10. S.P. Schlesinger, P. Diament, and A. Vigants, 'On higher-order hybrid modes of dielectric cylinders,' Transactions of the Institute of Radio Engineers, vol. MTT-8, No. 2, pp. 252, 1960.

I-11. D. Marcuse, LIGHT TRANSMISSION OPTICS, Van Nostrand Reinhold, New York, 1972, pp. 296-301.

I-12. A. Safaai-Jazi and G.L. Yip, 'Cutoff conditions in three-layer cylindrical dielectric waveguides,' IEEE Transactions on Microwave Theory and Techniques, vol. MTT-26, No. 11, pp. 898-903, November, 1978.

I-13. S. Roberts and A.R. von Hippel, 'A New Method for Measuring Dielectric Constant and Loss Tangent in the Range of Centimeter Waves,' J. Appl. Phys., Vol. 17, p. 610-616, July 1946.

I-14. A.R. von Hippel, DIELECTRIC MATERIALS AND APPLICATIONS, John Wiley and Sons, Inc., pp. 301-370, New York, 1958.

I-15. S. Ramo, J.R. Whinnery, and T. Van Duzer, FIELDS AND WAVES IN COMMUNICATION ELECTRONICS, Wiley, New York, 1966, pp. 432.

I-16. W.B. Bridges, 'Low loss flexible dielectric waveguide for millimeter-wave transmission and its application to devices,' Annual Technical Report SRO-0005-1, Chap. III, March, 1981.

I-17. D.C. Chang and E.F. Kuester, 'Radiation and propagation of a surface-wave mode on a curved open waveguide of arbitrary cross section,' Radio Science, Vol. 11, pp. 449-457, May 1976.

I-18. E.F. Kuester and D.C. Chang, 'Surface-wave radiation loss from curved dielectric slabs and fibers,' IEEE Journal of Quantum Electronics, Vol. QE-11, pp. 903-907, Nov. 1975.

# II. CHANNEL GUIDES

## Introduction

Difficulties in measuring bending loss for spaghetti guide and the desire to obtain good agreement between theory and experiment at 94 GHz originally led us to explore rigid guide structures. We adopted a powder-filled open channel in a solid block of polymer for our measurements. This configuration satisfied both the requirement of rigidity so that we could make precise length measurements and the requirement of uniformity, since the powder was loaded from the side rather than the end of the guide. In addition, this structure appears to be interesting in its own right, particularly for low-cost mm-wave integrated circuits, especially if injection-molded substrates prove feasible. Experimental work on 94 GHz channel guides and the supporting theory are the subjects of this chapter.

## A. Theory of Channel Guides

### 1. Survey of theoretical approaches

The rectangular dielectric channel waveguide is shown in cross section in Fig. II-1. No analytical solution exists for the propagating modes of this guide. However, there are several numerical methods which yield approximate values of the propagation constants.

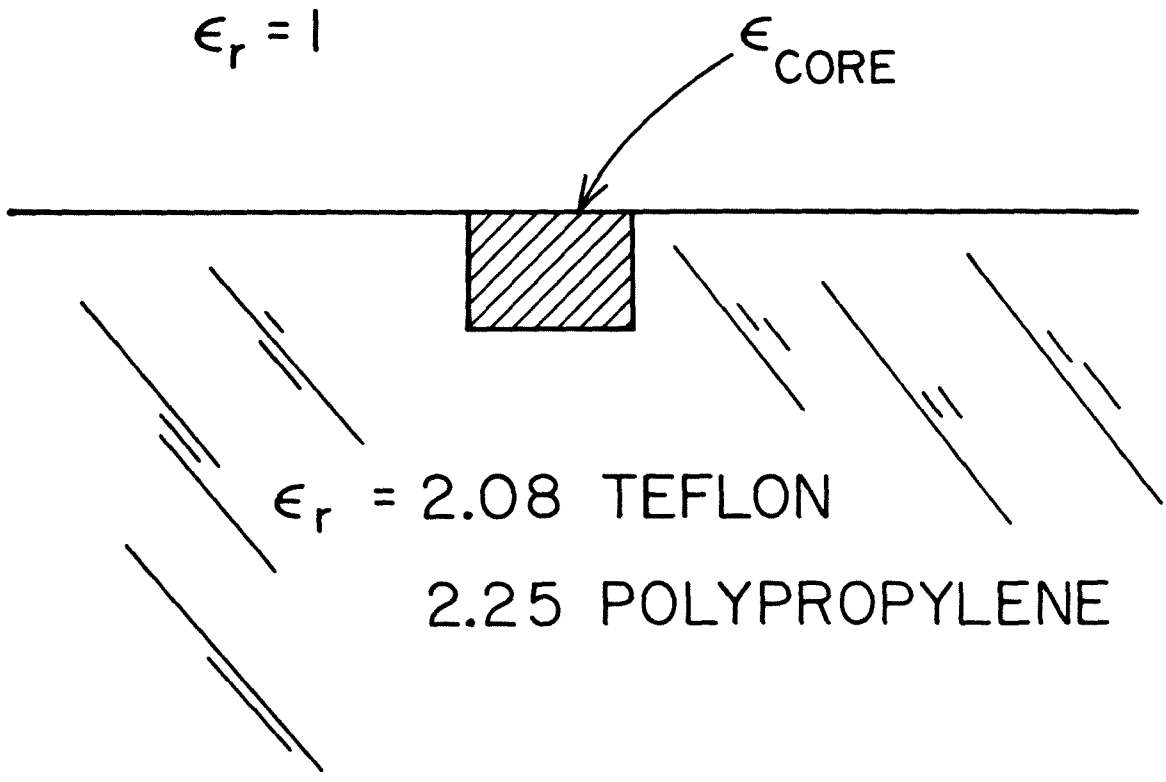


Figure II-1: Cross section of dielectric channel waveguide

Most of these techniques, such as those proposed by Goell (expansion in circular harmonics) (Ref.II-1), Yeh et al. (finite elements) (Refs. II-2, II-3), and Schweig and Bridges (finite differences) (Ref. II-4), require the use of large computers. Marcatili's approximate-mode method (Ref. II-5), on the other hand, is fairly easy to use since the computations involved are much simpler. Even though Marcatili's method uses an approximation that is not satisfied by our guide ($1 - n_{clad}/n_{core} \ll 1$), selected cases using other methods do seem to agree reasonably well with guide wavelengths calculated from Marcatili's theory (Refs. II-4, II-5). For these reasons, Marcatili's method was used here to predict propagation constants of guided modes of channel waveguides.

## 2. Marcatili's theory

The difficulty in obtaining a closed-form solution for a rectangular dielectric waveguide is contained in the mixed boundary conditions in the 'corner regions' shown shaded in Fig. II-2. Marcatili observes that, for a guided mode, a very small fraction of the power propagates in the corner regions. Hence it is reasonable to ignore the fields in these regions. Fields are assumed to exist only in regions 1-5 and these are matched only at the boundaries of region 1. Marcatili simplifies the problem further by assuming that the refractive index difference between region 1 and any other region is

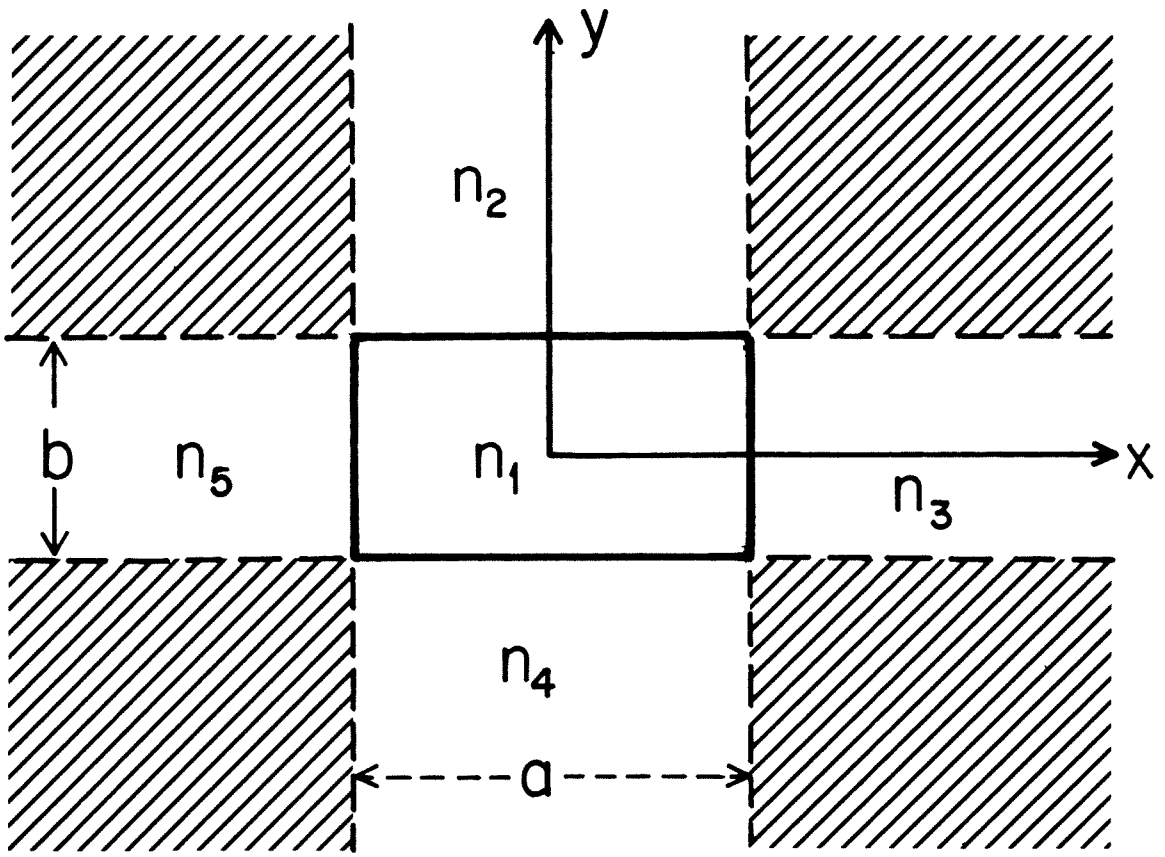


Figure II-2: Cross section of dielectric waveguide analyzed by Marcatili

small. (Stated precisely, Marcatili assumes that $1 - n_i/n_1 \ll 1$, $i = 2,3,4,5$. For our channel guides, the left-hand side of this inequality typically equaled 0.25 for $i = 3,4,5$ and 0.5 for $i = 2$.) As a result of these assumptions, the modes found by Marcatili have almost purely transverse fields (TEM) and can be grouped into two sets, $E^y_{pq}$ and $E^x_{pq}$. For both families of modes, the subscripts p and q indicate the number of extrema of the transverse field components in the x and y directions, respectively.*

For $E^y_{pq}$ modes, $H_x$ and $H_y$ are assumed to have the following form in each of the five regions:

$$H_{x1} = M_1 \exp(-ik_z z + i\omega t)\cos(k_x x + \gamma)\cos(k_y y + \delta)$$

$$H_{x2} = M_2 \exp(-ik_z z + i\omega t)\cos(k_x x + \gamma)\exp(-y/\eta_2)$$

$$H_{x3} = M_3 \exp(-ik_z z + i\omega t)\cos(k_y y + \delta)\exp(-x/\xi_3)$$

$$H_{x4} = M_4 \exp(-ik_z z + i\omega t)\cos(k_x x + \gamma)\exp(y/\eta_4)$$

$$H_{x5} = M_5 \exp(-ik_z z + i\omega t)\cos(k_y y + \delta)\exp(x/\xi_5)$$

$$H_{yj} = 0 \quad j = 1,2,3,4,5.$$

---

*We use Marcatili's notation here, despite the difficulty that the magnetic field associated with the '$E^y_{pq}$' mode is mainly x-directed and therefore cannot be designated '$H^y_{pq}$' without confusion. Marcatili solves this problem by rarely referring to the magnetic field. See also Ref. II-4 for an alternative way of naming modes.

The remaining field components are expressed in terms of $H_x$ and $H_y$ using Maxwell's curl equations. As a consequence of the assumption of small refractive index differences, $E_x$ is small enough to be neglected for the $E^y_{pq}$ mode. A similar procedure is used to find the fields of the $E^x_{pq}$ modes from assumed H components.

The propagation constant of a mode, $k_z$, is found by matching tangential field components at the edges of region 1 in two steps, equivalent to superposing two slab waveguides: $n_2$-$n_1$-$n_4$ and $n_3$-$n_1$-$n_5$. For $E^y_{pq}$ modes,

$$k_z^2 = k_1^2 - k_x^2 - k_y^2,$$

where $k_1 = n_1 k$, $k = 2\pi/\lambda$, and $\lambda$ is the free space wavelength. The constant $k_x$ is found by solving the transcendental characteristic equation for the $n_3$-$n_1$-$n_5$ slab,

$$k_x a = p\pi - \tan^{-1}(k_x \xi_3) - \tan^{-1}(k_x \xi_5),$$

in which

$$\xi_3 = ((\pi/A_3)^2 - k_x^2)^{-1/2} \qquad \xi_5 = ((\pi/A_5)^2 - k_x^2)^{-1/2}$$

and

$$A_3 = \lambda/(2(n_1^2 - n_3^2)^{1/2}) \qquad A_5 = \lambda/(2(n_1^2 - n_5^2)^{1/2}).$$

The constant $k_y$ is found by solving the transcendental characteristic equation for the $n_2$-$n_1$-$n_4$ slab,

$$k_y b = q\pi - \tan^{-1}((n_2/n_1)^2 k_y \eta_2) - \tan^{-1}((n_4/n_1)^2 k_y \eta_4),$$

in which

$$\eta_2 = ((\pi/A_2)^2 - k_y^2)^{-1/2} \qquad \eta_4 = ((\pi/A_4)^2 - k_y^2)^{-1/2}$$

and

$$A_2 = \lambda/(2(n_1^2 - n_2^2)^{1/2}) \qquad A_4 = \lambda/(2(n_1^2 - n_4^2)^{1/2}).$$

A similar procedure is used to find the propagation constants of the $E^x_{pq}$ modes.

## 3. Waveguide loss using Marcatili's theory

Marcatili's theory can be used to calculate waveguide loss as a function of material losses for rectangular dielectric channel waveguides in the standard way for small losses. We assume that the dielectric losses are so small in all regions that the transverse distribution of the fields is not changed. Losses due to dimensional imperfections (e.g., waveguide wall roughness) and to scattering from material inhomogeneities are not included in this analysis. We also note that for a rectangular dielectric channel guide (Fig. II-1), regions 3,4, and 5 in Marcatili's analysis (Fig. II-2) have identical material properties.

Since the material losses are assumed to be small, they can be taken into account by multiplying each of Marcatili's field components by the factor $\exp(-\alpha z)$. Here $2\alpha$ is given by the ratio of the average power dissipated per unit length to the average power flowing along the guide. These quantities, in turn, are found from the transverse field components given by Marcatili, assuming that the loss per unit volume is everywhere proportional to the square of the electric field.

For the $E^y_{pq}$ modes, $\alpha$ can be expressed as

$$\alpha = A/F, \qquad \text{(II-1)}$$

where

$$A = \omega\varepsilon_1'\tan\delta_1 P_1 + \omega\varepsilon_4'\tan\delta_4 P_4$$

$$P_1 = c_1^2 I_1 I_2(\pi/\omega) + c_2^2 I_1 I_3(\pi/\omega)$$

$$P_4 = (c_7^2 + c_8^2)(d_4)^2 I_1 I_6(\pi/\omega)$$

$$d_2 = \cos((k_y b/2) + \gamma)\exp(b/(2\eta_2))$$

$$d_3 = \cos(k_x a/2)\exp(a/(2\xi_3))$$

$$d_4 = \cos((-k_y b/2) + \gamma)\exp(b/(2\eta_4))$$

$$I_1 = (a/2) + \sin(k_x a)/(2k_x)$$

$$I_2 = (b/2) + \sin(k_y b)\cos(2\gamma)/(2k_y)$$

$$I_3 = (b/2) - \sin(k_y b)\cos(2\gamma)/(2k_y)$$

$$I_4 = (\eta_2/2)\exp(-b/\eta_2)$$

$$I_5 = (\xi_3/2)\exp(-a/\xi_3)$$

$$I_6 = (\eta_4/2)\exp(-b/\eta_4)$$

$$c_1 = (k_1^2 - k_y^2)/(\omega\varepsilon_0 n_1^2 k_z)$$

$$c_2 = k_y/(\omega\varepsilon_0 n_1^2)$$

$$c_3 = ((1/\eta_2)^2 + k_2^2)/(\omega\varepsilon_0 n_2^2 k_z)$$

$$c_5 = (k_3^2 - k_y^2)/(\omega\varepsilon_0 n_3^2 k_z)$$

$$c_7 = ((1/\eta_4)^2 + k_4^2)/(\omega\varepsilon_0 n_4^2 k_z)$$

$$c_8 = 1/(\eta_4\omega\varepsilon_0 n_4^2)$$

$$\gamma = \tan^{-1}(n_1^2/(n_2^2\eta_2 k_y) - k_y b/2$$

$$k_1 = n_1 k$$

$$k_2 = n_2 k$$

$$k_3 = n_3 k = k_4 = n_4 k.$$

The variable F can be expressed as

$$F = (W_1 + W_2 + W_3 + W_4 + W_5)(\pi/\omega),$$

where

$$W_1 = c_1 I_1 I_2$$

$$W_2 = c_3 I_1 I_4 d_2^2$$

$$W_3 = c_5 I_2 I_5 d_3^2$$

$$W_4 = c_7 I_1 I_6 d_4^2$$

$$W_5 = W_3.$$

In the equations above, $\varepsilon' = \mathrm{Re}(\varepsilon)$ and $\varepsilon_0$ is the permittivity of free space. Also, the subscripts 1,2,3 and 4 after the variables $k, \varepsilon, n$, and $\tan\delta$ associate them with the corresponding regions shown in Fig. II-2. In addition, we note that $\alpha$ depends implicitly on p and q through $k_x$ and $k_y$.

If the loss tangents of our powders had been known at 94 GHz, equation II-1 could have been used to predict the transmission losses of our channel guides. However, since the 94 GHz powder loss tangents were unknown, Equation II-1 was used to calculate them from the measured transmission losses of the $E^y_{11}$ mode. The results of these calculations are given later in this chapter.

## B. Experiments on channel guides

### 1. Guide wavelength and attenuation measurements

A rectangular groove was milled into the surface of a low-loss (TFE teflon or prolypropylene) substrate and was filled with a high-

dielectric constant powder to form the core of a dielectric waveguide (Fig. II-1). With this configuration, the powder could be packed from the top to assure a sufficiently uniform density along the length of the groove. Rectangular grooves with cross-sectional dimensions varying less than ± 0.001 inches or ± .025 mm from the specified values (typically 1 mm x 1 mm) could be milled with relative ease. This degree of dimensional accuracy was found to be sufficient at 94 GHz to produce a guide wavelength uniform within our measurement accuracy.

The guide wavelength and loss per unit length were measured for the fundamental vertically polarized ($E^{y}_{11}$) mode of various powder channel waveguides using the set-up shown in Fig. II-3. On each end of the substrate the dielectric-filled groove was extended with a thin-walled trough of substrate material. This trough fitted snugly into the end of a slightly flared section of WR-10 metal waveguide to couple to the dielectric guide. Lossy inserts made from Emerson and Cumming MF-110 absorber were placed at non-periodic intervals in the substrate 3 mm from the groove to attenuate any substrate modes (that is, propagation of energy through the substrate other than via the desired mode) that might have been excited at the coupling point and resulted in end-to-end coupling via the substrate.

To measure the guide wavelength, a metal perturber was held mechanically just above the surface of the powder. This perturber reflects a small fraction of the power travelling along the waveguide

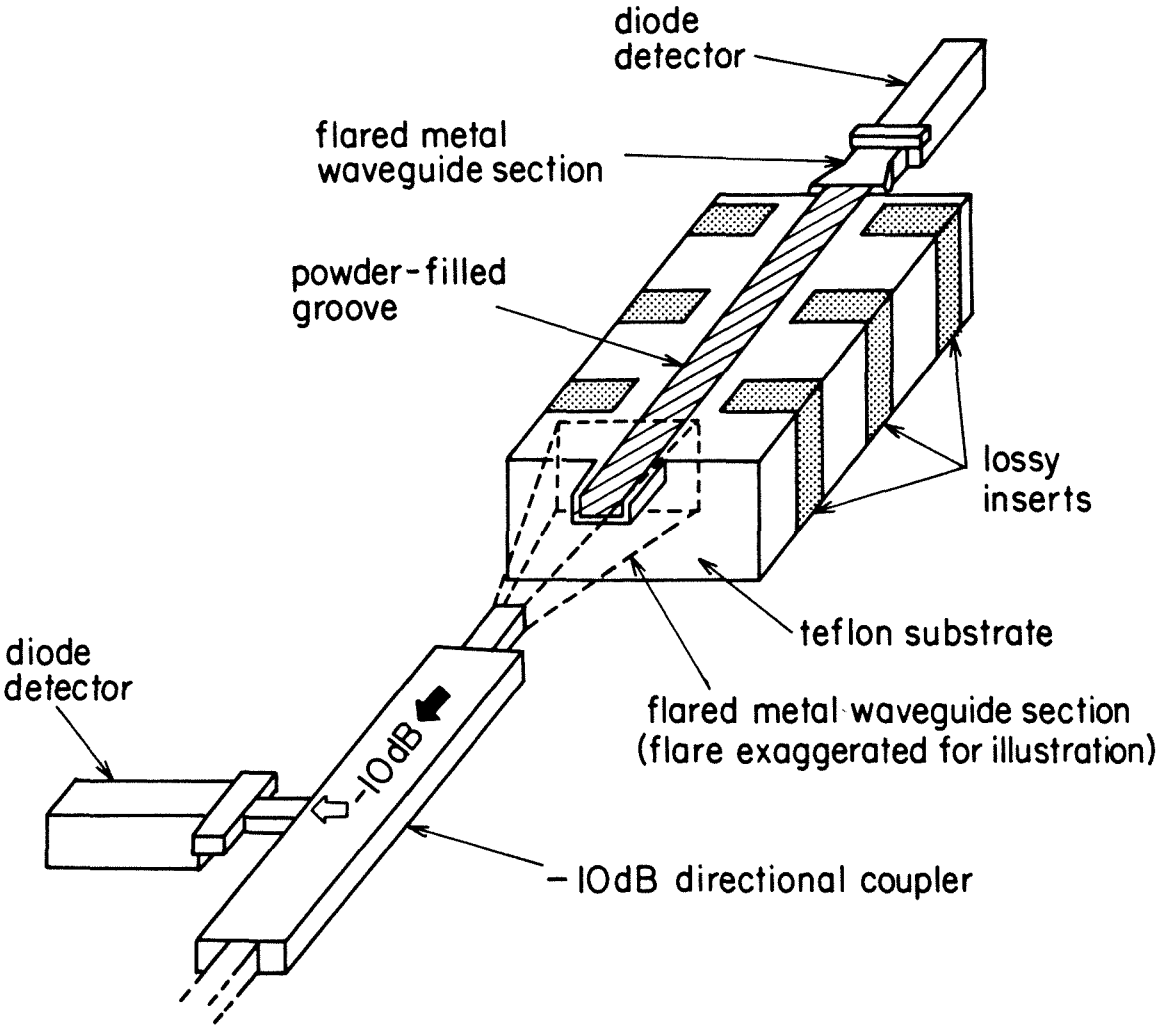


Figure II-3: Setup for measuring attenuation and guide wavelength

toward the feed, where it interferes with the reflection from the input coupler. The amplitude of this interference changes as the relative phase between these two signals changes. Thus, as the perturber was moved along the length of the groove, a sequence of maxima and minima in reflected power was sensed with a -10 dB directional coupler and a Schottky diode, as shown in Fig. II-4. The guide wavelength is twice the distance the perturber is moved between successive minima.

For various combinations of guide dimensions, dielectric powders, and substrate materials, the guide wavelengths were compared to the values predicted by Marcatili's approximate theory (Ref. II-5) for the fundamental vertically polarized mode. In order to use Marcatili's theory, the dielectric constants of the powders were needed. The density of the powder in the groove was determined by precision weight measurement, and previously measured curves of dielectric constant versus density were used to find the effective dielectric constant of the powder packed into the groove. The dielectric constants of the powders had been measured previously at 10 GHz using the shorted-waveguide technique. These measurements were made at 10 GHz because of the difficulty of controlling the length of a powder sample in a shorted WR-10 metallic waveguide sufficiently accurately to measure its dielectric constant at 94 GHz. The effective dielectric constant of a powder composed of low-loss dielectric material should not vary much between 10 GHz and 94 GHz if the powder grains are small

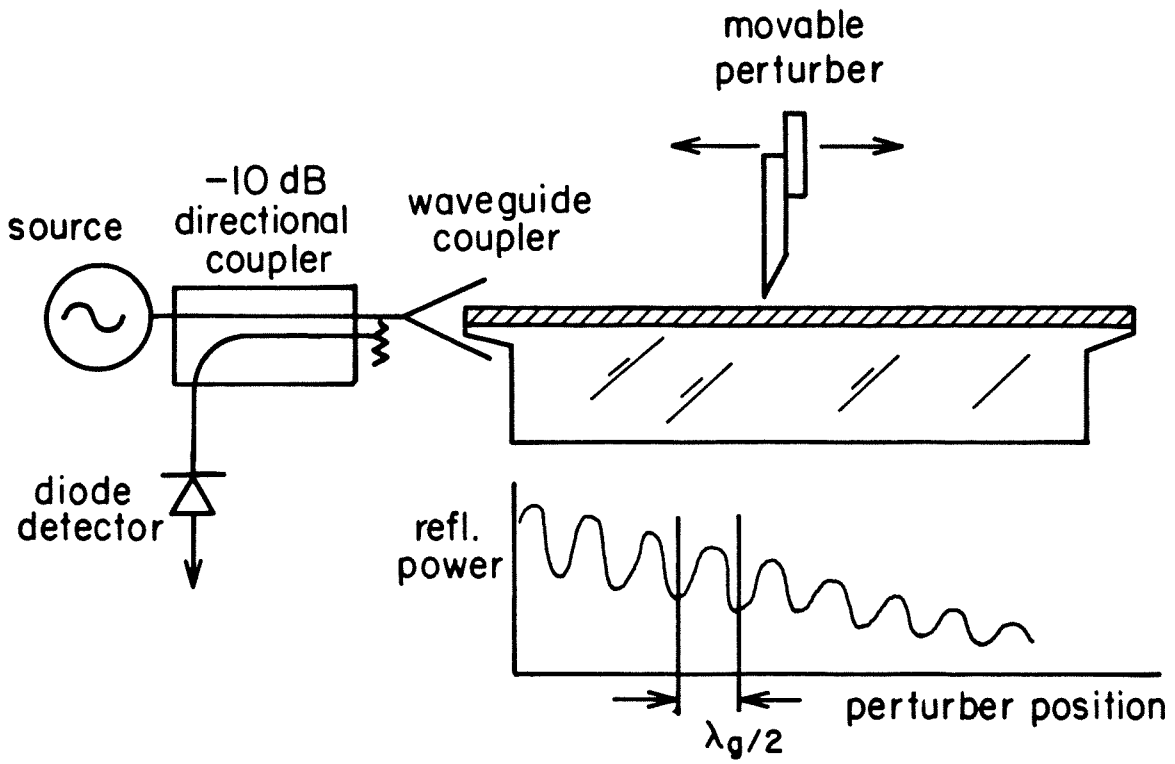


Figure II-4: Guide wavelength measurement

relative to wavelength at 94 GHz. (For further explanation, see Appendix II.)

The powders used were the same as for the flexible guide work described in Chapter I: Trans-Tech D-30 nickel-aluminum titanate, Trans-Tech D-38 barium tetratitanate, Trans-Tech MCT-40 magnesium calcium titanate, and Trans-Tech D-8512, an 'improved' barium tetratitanate. For D-8512, MCT-40, and for one batch of D-30, all particles were less than 43μm in size. For D-38 and for a second batch of D-30, 70% of the particles were between 100μm and 43μm and 30% were less than 43μm. Trans-Tech gives $\varepsilon' = 31$ and $\tan\delta < .0002$ for solid D-30 at 10 GHz, $\varepsilon' = 37$ and $\tan\delta < .0005$ for solid D-38 at 6 GHz, $\varepsilon' = 40$ and $\tan\delta < .002$ for solid MCT-40 at 6 GHz, and $\varepsilon' = 38.6$ and $\tan\delta < .0005$ for solid D-8512 at 6 GHz.

To determine the loss-per-unit length of a channel waveguide, the power transmitted from end-to-end was measured by a detector connected to the flared section of metal waveguide surrounding the trough on the far end of the substrate (Fig. II-3). Shorted stub ('E/H') tuners were added to match the coupling sections. The power detected at the far end could not be significantly increased by adding the E/H tuners, so we assume that the couplers are reasonably well matched by themselves. In addition, removing the lossy substrate inserts did not affect the power received at the far end, indicating that little power is lost to substrate modes. A third detector connected to a small horn antenna was used as a movable probe to determine that an insignificant amount

of power was radiated from the couplers or guide. Finally, the power reflected from the feed coupling was -15 dB down from the incident power even without the E/H tuners. Taken together, these observations indicate that almost all of the incident power was coupled into the dielectric waveguide, so that the difference between the incident power and the power detected at the far end represents dielectric waveguide loss. The loss per unit length is then this loss divided by the length of the dielectric waveguide.

A comparison between the measured values of the guide wavelength with those predicted for the $E^{y}_{11}$ mode by Marcatili's approximate theory is given in Table II-1 for various powders in plastic substrates at 94 GHz. Although Marcatili's theory assumes that the refractive index of the core is similar to that of the surrounding media and is thus only an approximation, the wavelengths it predicts for the $E^{y}_{11}$ mode (Table II-1) are in reasonable agreement with those measured. Hence, we conclude that the dielectric constants of the powders used were not too high for Marcatili's theory to be useful.

A selection of typical measured values of loss per unit length for straight powder-filled grooves in a plastic substrate are given in Table II-2. The measurements were made at 94 GHz. For given substrate material and channel dimensions, the transmission loss increased with powder density. This variation is consistent with a closer confinement of the mode energy to the core region, which has a higher material loss.

TABLE II-1

Comparison of measured guide wavelength with prediction of Marcatili

| Type of Powder | Substr. Type | Width of Groove (mm) | Depth of Groove (mm) | Powder Density ($g/cm^3$) | Dielectric Constant | $\lambda g$ (meas.) (mm) | $\lambda g$ (Marcatili) (mm) |
|---|---|---|---|---|---|---|---|
| 1 | T | 0.94 | 0.94 | 1.95±.07 | 5.78±.35 | 1.86 | 1.96±.08 |
| 2 | T | 1.12 | 1.12 | 1.77±.04 | 5.0 ±.4 | 2.06 | 1.9 ±.1 |
| 4 | T | 1.83 | 1.04 | 1.33±.02 | 3.77±.07 | 2.07 | 2.11±.02 |
| 3 | T | 1.27 | 1.10 | 1.55±.03 | 3.85±.07 | 2.16 | 2.18±.02 |
| 3 | T | 1.27 | 1.10 | 1.47±.02 | 3.55±.22 | 2.22 | 2.26±.06 |
| 3 | P | 1.47 | 1.10 | 1.55±.02 | 3.85±.08 | 2.04 | 2.09±.02 |

Powder 1 is nickel-aluminum-titanate (Trans-Tech D-30).

Powder 2 is barium tetra-titanate (Trans-Tech D-38).

Powder 3 is barium tetra-titanate (Trans-Tech D-8512).

Powder 4 is magnesium calcium titanate (Trans-Tech MCT-40).

Substrate T is TFE teflon.

Substrate P is polypropylene.

The uncertainty in the guide wavelength predicted by Marcatili's theory is estimated from the uncertainty in the dielectric constant of the powder.

TABLE II-2

Attenuation of powder-filled channel dielectric waveguides

| Type of Powder | Substrate Type | Width of Groove (mm) | Depth of Groove (mm) | Density of Powder ($g/cm^3$) | Loss (dB/cm) |
|---|---|---|---|---|---|
| D-30** | P | 1.17 | 1.13 | 1.75 | 0.34±.01 |
| MCT-40* | T | 1.50 | 1.05 | 1.26 | 0.14±.01 |
| D-8512* | T | 1.27 | 1.10 | 1.47 | 0.09±.01 |
| D-30* | P | 1.17 | 1.13 | 1.80 | 0.17±.01 |
| D-30* | P | 1.17 | 1.13 | 1.68 | 0.09±.01 |

** 70% of particles between 100μm and 43μm, 30% less than 43μm

* 100% of particles less than 43μm

Substrate T is TFE Teflon$^R$

Substrate P is polypropylene.

## 2. Effective loss tangents of powders

Using the measured transmission losses of our channel guides and literature values (Refs. II-6 and II-7) of the loss tangents of the substrate materials, the effective loss tangents of the powders themselves were calculated using Equation II-1. (The dielectric properties of heterogeneous media, such as powders, are often called 'effective' to distinguish them from the bulk properties of the constituent materials. In this thesis, the term 'effective' has been omitted when the properties being discussed are clearly those of powders.)

Some of the results are given in Table II-3. As shown there, the effective loss tangents increased with powder density, as expected. (See Appendix II.) This effect causes the waveguide loss to increase. However, the rise in waveguide loss accompanying increased powder density is not solely due to the increase in effective loss tangent. The effective dielectric constant of the powder also increases with density, causing a greater fraction of the power of the guided mode to travel in the core, rather than in the more low-loss substrate. (Even near cut-off, only a small fraction of the power travels in the air. The main effect of increasing the powder dielectric constant on the distribution of power among the various regions is to increase the fraction of power travelling in the core by reducing that in the substrate.)

TABLE II-3

Effective Loss Tangents of Powders

| Type of Powder | Substrate Type | Density of Powder ($g/cm^3$) | Powder Dielectric Constant | Waveguide Loss (dB/cm) | tanδ |
|---|---|---|---|---|---|
| D-30* | P | 1.68±.03 | 4.05±.08 | .09 | .0006 |
| D-30* | P | 1.80±.03 | 4.42±.11 | .17 | .0010 |
| D-8512* | T | 1.49±.02 | 3.62±.15 | 0.11 | .0009 |
| D-8512* | T | 1.63±.02 | 4.04±.08 | 0.17 | .0012 |
| D-8512* | T | 1.47±.02 | 3.55±.22 | 0.09 | .0007 |
| D-30** | P | 1.70±.03 | 4.59±.16 | 0.36 | .0021 |

* 100% of particles less than 43μm

** 70% of particles between 100μm and 43μm, 30% less than 43μm

tanδ = .0002 for TFE teflon (Ref. 6)

tanδ = .0002 for polypropylene (Ref. 7)

The uncertainty in the values of powder effective loss tangent is ± .0001.

As shown in Tables II-2 and II-3, waveguides made with 43 μm D-30 powder exhibited much lower losses than those using the larger grain D-30. As a result, the computed values of effective loss tangent for the 43 μm D-30 were smaller. The fact that higher losses were measured for the D-30 powder with larger particles suggests that the extra loss is due to scattering. However, the amount of power radiated from the guide was insignificant. In addition, the theory of scattering by powders (see Appendix II) predicts negligible scattering loss. Hence, absorption losses must be much greater for the coarse D-30 powder. We do not know why the coarse D-30 powder is more absorptive. The only known difference between the two batches of D-30 powder is in the distribution of particle sizes.

3. Embossed grooves

Powder channel dielectric waveguides offer the potential of low-cost fabrication, especially if an inexpensive process, such as injection molding, proves feasible for making dimensionally precise grooves in plastic. To check the feasibility of using molding processes, we developed a simple technique for embossing straight grooves in polypropylene with an aluminum die (Figs. II-5, II-6.)

After being sprayed with a dry Teflon lubricant, the die was heated to approximately 160 degrees Celsius. It was then pressed against a one-half inch thick slab of polypropylene. After 3 minutes, the

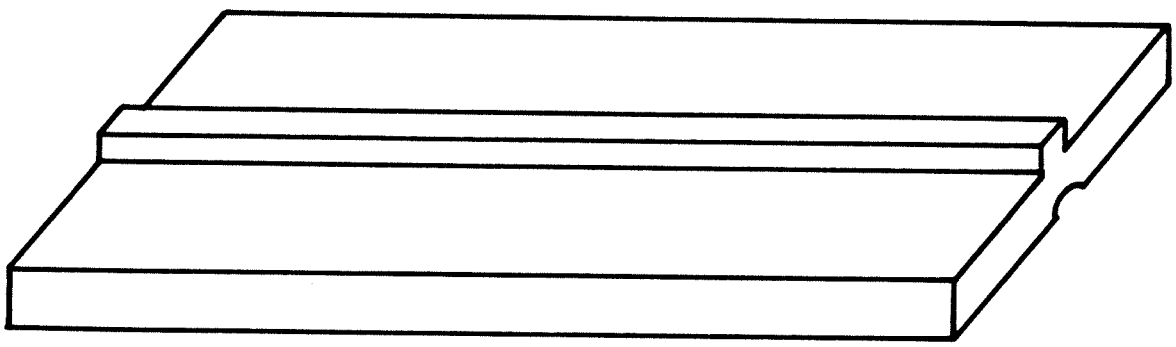

Figure II-5: Die used to emboss grooves in polypropylene

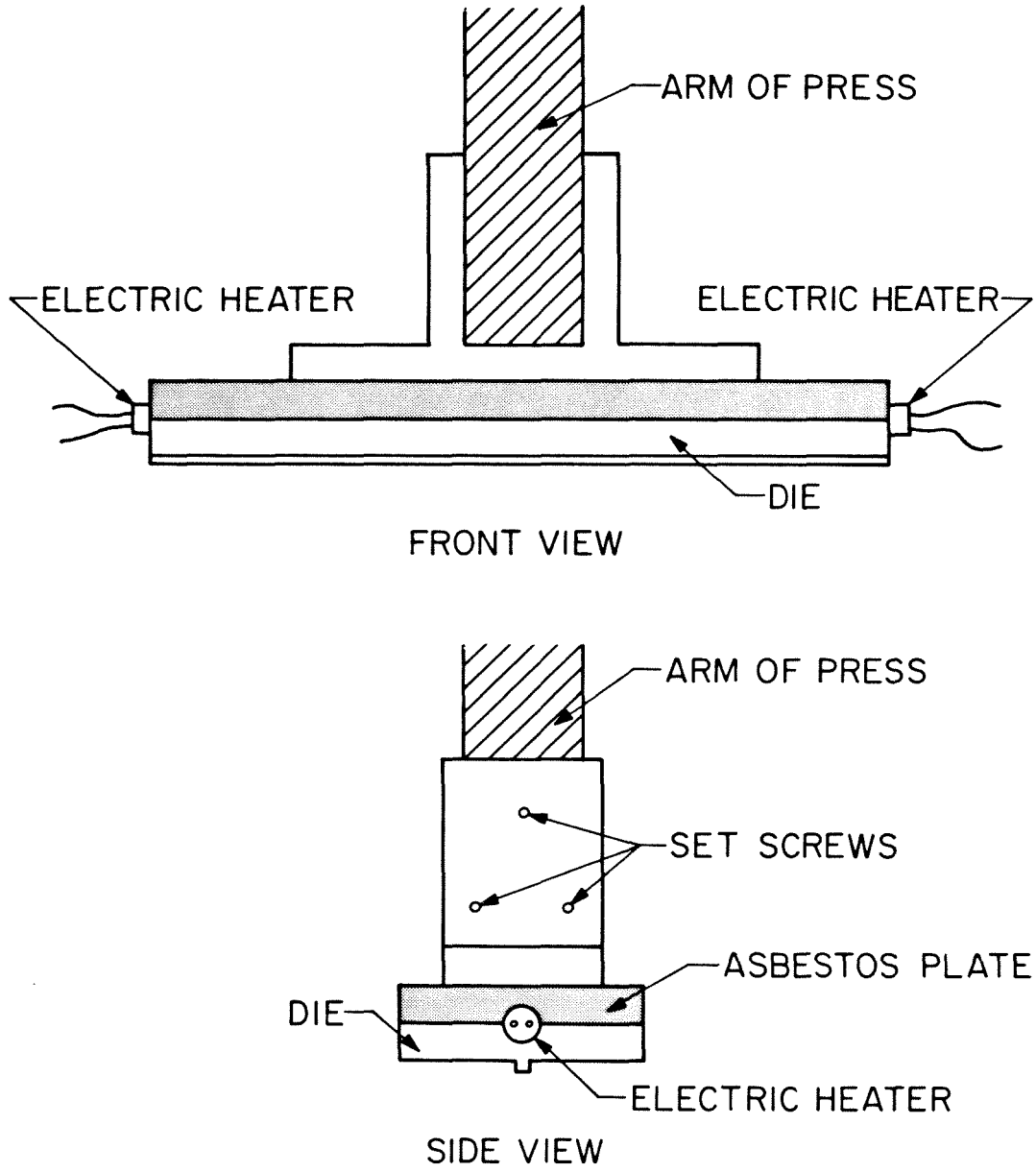


Figure II-6: Die assembly

heaters were turned off and air was blown across the die for cooling. Ten minutes later, the die was removed from contact with the plastic. Good quality grooves were formed by this technique, but after being pulled away from the die, the polypropylene slab would gradually become warped (about 1 cm in a 15 cm length). This effect could be significantly reduced by preheating the back side of the slab with a heat gun before embossing the groove.

This process was used to form straight grooves which were 6 inches long, 1.37 mm wide and 1.12 mm deep. The cross-sectional dimensions varied by less than 0.03 mm along the length of the groove. By filling one of these grooves with $1.57 \pm .05$ g/cm$^3$ of Trans-Tech D-8512 barium tetratitanate powder ($\varepsilon_r = 3.87 \pm .16$), a dielectric waveguide was obtained which had a loss of 0.10 dB/cm. The guide wavelength was measured to be 2.07 mm $\pm$ .01 mm. (Marcatili's theory predicted a guide wavelength of 2.10 mm $\pm$ .04 mm for the $E^y_{11}$ mode of this guide.) The good performance of this waveguide and the simplicity of the process by which it was made indicate that a molding technique would allow large-scale, low-cost production of powder core dielectric waveguides and components.

REFERENCES

II-1. J.E. Goell, 'A circular-harmonic computer analysis of rectangular dielectric waveguides,' Bell System Technical Journal, Vol 48, Sept. 1969, pp. 2133-2160.

II-2. C. Yeh, S.B. Dong, and W. Oliver, 'Arbitrarily shaped inhomogeneous optical fiber or integrated optical waveguides,' J. Appl. Phys., Vol. 46, May 1975, pp. 2125-2129.

II-3. C. Yeh, S.B. Dong, and W.P. Brown, 'Single-mode optical waveguides,' Applied Optics, Vol. 18, May 1979, pp. 1490-1504.

II-4. E. Schweig and W.B. Bridges, 'Computer analysis of dielectric waveguides: a finite-difference method.' IEEE Transactions on Microwave Theory and Techniques, Vol. MTT-32, No. 5, May 1984, pp. 531-541.

II-5. E.A.J. Marcatili, 'Dielectric rectangular waveguide and directional coupler for integrated optics,' Bell System Technical Journal, Vol. 48, Sept. 1969, pp. 2079-2132.

II-6. D. Jablonski, 'Attenuation characteristics of circular dielectric waveguide at millimeter wavelengths,' IEEE Transactions on Microwave Theory and Techniques, Vol. MTT-26, No. 9, Sept. 1978, pp. 667-671.

II-7. G.W. Chantry, J.W. Fleming, and G.W.F. Pardoe, 'Absorption spectra of polypropylene in the millimetre and submillimetre regions,' Infrared Physics, Vol. 11, 1971, pp. 109-118.

# III. RING RESONATORS

## Introduction

After demonstrating the efficacy of using powdered dielectric material to make waveguides, a natural step toward making more complex circuits is to build a simple passive component such as a resonator. Using our channel dielectric waveguides, one can imagine several possible resonator configurations. The simplest of these is a segment of straight waveguide (Fig. III-1a) with dielectric discontinuities at both ends. However, to maximize the reflection at the ends and minimize the radiation from the ends, the effective dielectric constant of the powder core would have to be much higher than that of the powders we have at our disposal. One might attempt to solve this problem by placing metal walls at the ends of the resonator (Fig. III-1b), but this approach is counter to our basic strategy of all-dielectric waveguide technology.

An alternative to these schemes would be to make reflective periodic structures at the ends of the resonator, such as shown in (Fig. III-1c). Each of the alternating sections would be one-quarter guide wavelength long (Ref. III-1). However, such designs are harder to fabricate by machining and suffer the additional disadvantage that the terminations are likely to radiate, thus resulting in lower Q.

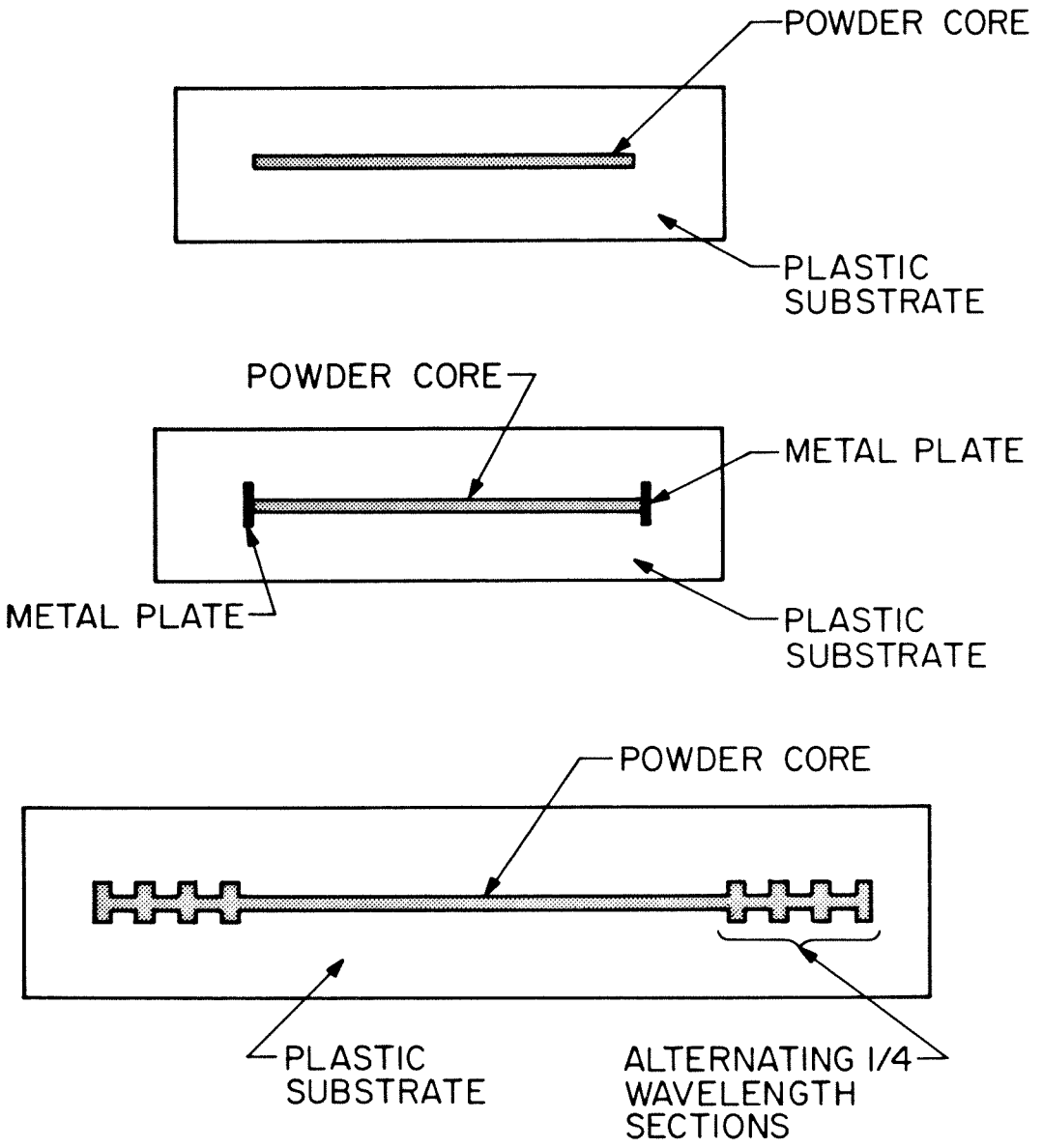


Figure III-1: (a) Segment of straight dielectric channel waveguide

(b) Segment of straight dielectric channel waveguide with metal reflecting plates at ends of channel

(c) Segment of straight dielectric channel waveguide with alternating 1/4 wavelength sections on ends to prevent radiation

A simple solution to the problems of the linear resonator of Fig. III-1 is to eliminate the ends by curving the guide into a ring, usually, but not necessarily, circular. The use of curved guides introduces the new problem of radiation induced by the curvature. The amount of radiation increases as the radius of curvature decreases. Hence, the radius of a circular ring resonator, for example, must be chosen large enough so that the amount of radiation is small or negligible compared to the other losses of the guide. On the other hand, the resonator should not be so large that it is unwieldy, so one should use the smallest possible radius of curvature for which radiation due to bending is insignificant.

## A. Design

To design a ring resonator, (henceforth assumed to be circular) a theory relating the bending loss to the waveguide parameters is required. The only such theory known to us which is applicable to dielectric channel waveguide is that of Marcatili (Ref. III-2). This theory is an extension of his approximate theory of propagation on a straight channel waveguide (Ref. III-3). Marcatili treats curvature as a perturbation, assuming that the radius of curvature is large compared to the wavelength. The field distributions of his modes of curved guide are thus only slightly different from those of straight

guide. Each mode of curved guide is given the name of the associated mode of straight guide. Like Marcatili's theory for straight channel guides, the theory of curved guide assumes that the differences in refractive index between the core and the surrounding media are small. However, since Marcatili's theory of straight channel guide seemed adequate for understanding our straight guides (Chp. II), we decided to try his theory of curved waveguides on ring resonators.

For our powders and substrate materials, Marcatili's theory predicts that, at 94 GHz, bending losses would be insignificant compared to the measured absorptive losses of straight guide for a radius of curvature greater than about 1 cm. We checked this prediction by measuring the transmission losses of guides machined in $180^{o}$ circular arcs. For 1 cm radius of curvature, the measured loss of the curved guide was found to be much higher than that of straight guide. On the other hand, the measured losses of guides with 4 cm and 5 cm radius of curvature were comparable to straight sections, so we decided to build one ring resonator with a 4 cm radius and another with a 5 cm radius.

Coupling to the ring resonators was achieved by placing a straight channel guide in proximity to the ring. No theory currently exists to analyze such a structure, Marcatili treats only the coupling between parallel straight guides (Ref. III-3). However, it is reasonable that

the coupling can be adjusted by changing the ring-to-straight guide spacing. The coupling for straight guides (Ref. III-3) is an approximately exponential function of the spacing. Thus, we used a technique that allowed this spacing to be adjusted easily.

Straight channel guides were positioned on opposite sides of the ring to couple power on and off. The resonator and the guides used for coupling were each built on individual substrates. Material was cut away from two opposing edges of the resonator substrate until each edge was only 0.38 mm from the channel. The substrate of each straight guide had an edge that was cut at an angle to the channel. For both of these substrates, the distance between the channel and the edge was 0.46 mm at one end and 4.32 mm at the other. When the three substrates were placed together as shown in Figure III-2, the separations between the resonator and the coupling guides could be adjusted by sliding the substrates with respect to one another.

Marcatili's theory of straight channel waveguides was used to design the guides used for coupling to the resonator so that only the $E^{y}_{11}$ mode would propagate. Since the substrate material had been chosen to be polypropylene ($\varepsilon_r$ = 2.25) and the dielectric constant of the core was constrained between 3.5 and 6 by the selection of low-loss powders, the design effort focused on choosing the best cross-sectional dimensions for the channel.

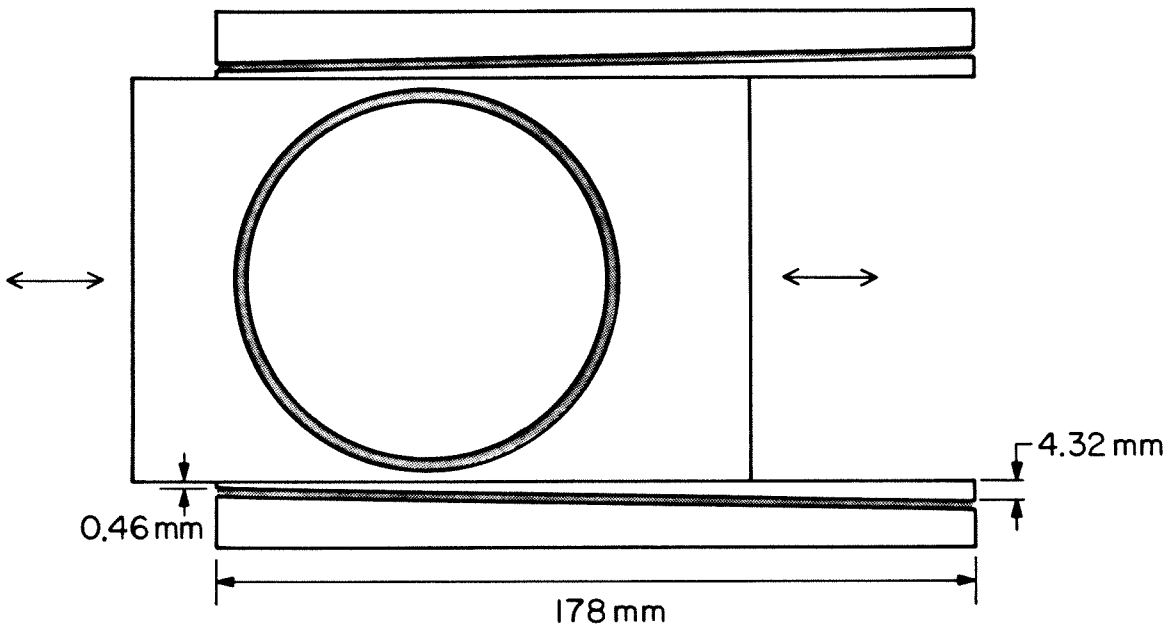


Figure III-2: Coupling scheme used to achieve adjustable distances between a ring resonator and two straight waveguides

Coupling occurs through the overlap in the substrate of the evanescent fields surrounding the rectangular core. To increase coupling, we may put the cores closer together or increase the penetration of the evanescent fields into the substrate. This increased penetration can be achieved by operating the guide closer to cut-off, that is, by decreasing the core dielectric constant or the channel width. The depth of the channel does not affect significantly the horizontal penetration (Ref. III-3), but the channel depth is limited to less than 1.06 mm by the inner dimensions of the flared WR-10 metal waveguide sections used for coupling to metal guide (Fig. III-3). Also, the area of the channel must exceed a minimum value of about 1.3 $mm^2$ in order for the $E^y_{11}$ mode to be guided. Hence, the width of the channel had to be larger than 1.2 mm. We picked 1.35 mm for the width and 1.05 mm for the depth. This choice fixed the penetration into the substrate and thus fixed the coupling obtained at a given distance.

The goal of the ring resonator design was to choose the optimum channel dimensions given the properties of the materials to be used. Marcatili's theory predicts that bending loss is independent of the channel depth when the plane of curvature is horizontal, so the depth was chosen equal to that of the straight coupling guides in order to enhance the coupling between these guides and the resonator.

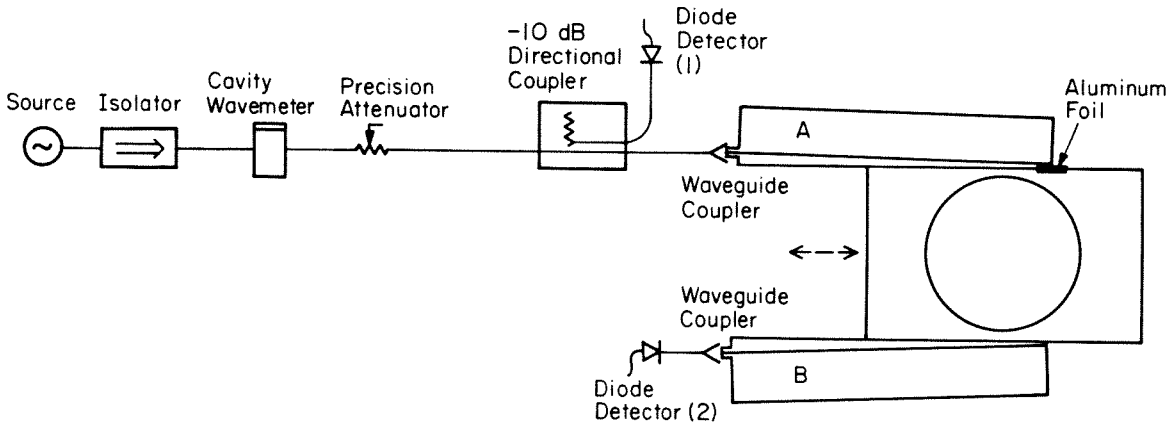


Figure III-3: Set-up for measuring Q's of ring resonators

Marcatili's theory also predicts that the bending loss of the $E^{y}_{11}$ mode decreases as the channel width increases. Consequently, we chose the width as large as possible without allowing propagation of higher-order vertically polarized modes.

B. Experiment

The experimental set-up is shown in Figure III-3. For the measurement of Q, the resonator was operated as a transmission filter. Since the loaded Q value of a resonator approaches the unloaded Q in the limit of zero coupling (Ref. III-4), we wanted the coupling between the resonator and the straight guides to be sufficiently weak that the difference between the loaded and unloaded Q's would be less than the other errors in the measurement. This was accomplished by sliding the substrates to decrease the coupling until further decreases yielded no measurable increase in Q. Data were taken with the filter operating with a 40 dB insertion loss, a value more than sufficient to make the loaded Q equal to the unloaded Q within the experimental uncertainty. The 40 dB insertion loss was obtained by setting the distance between the adjacent walls of the two channels to about 1.4 mm.

The Q was measured by varying the frequency of the source and observing the response of the resonator with the detector at (2). The

amount of power incident on waveguide A was monitored with the detector at (1) and the precision attenuator was used to keep this power level constant as the frequency was changed. The frequencies of the resonator's peak response and half-power response points were measured with the cavity wavemeter. The Q is the frequency of the peak response divided by the difference in frequency of the half-power points. Since the cavity wavemeter used to measure frequency had a Q comparable to that of the ring resonators, the uncertainties in our measured values of Q are relatively large.

We used several checks to determine that the measured Q was actually that of the ring and not the result of a spurious resonance elsewhere in the measurement set-up. First, with the frequency tuned to a resonance, the placement of a small piece of lossy ferrite over any portion of the ring caused a 10 dB drop in received powder at (2). Secondly, placing lossy ferrite inserts at various positions in or on the substrate of the resonator had no effect on the performance. These observations show that power was propagating through the ring's powder channel and not through the substrate. (The purpose of the aluminum foil shown in Figure III-3 was to prevent radiation from the end of waveguide A from entering the resonator's substrate.) Finally, the resonant frequency could be tuned by adjusting the height of a piece of polypropylene positioned over part of the ring.

## C. Conclusions

Using the results of our previous measurements on straight channel waveguide and applying the formula $Q = \beta/2\alpha$ (Ref. III-2), where $\beta$ and $\alpha$ are the propagation and attenuation constants of the straight guide, the predicted ring resonator Q's would be no larger than 1700 if bending losses were neglected. ($.09 \pm .01$ dB/cm loss and $\lambda_g = 2.04 \pm .02$ mm for the $E^y_{11}$ mode give $Q = 1500 \pm 200$.) Thus, we are surprised that some of the actual measured Q values (Table III-1 and Fig. III-4) exceed 1700. These results suggest that measurement of the Q of a ring resonator may be a better method for determining waveguide dissipative and scattering losses than end-to-end transmission on a straight guide.

Marcatili's theory predicts negligible bending loss for all of the resonators represented in Fig. III-4. If Marcatili's theory of curvature loss were accurate for these resonators, one would expect the Q's in Fig. III-4 to decrease with powder dielectric constant as a result of increased dielectric absorption in the channel (c.f. Chap. II). Instead, the Q's initially increased with powder dielectric constant until a maximum was reached and then declined as it was increased further. These observations and the poor prediction of the bending losses of semicircular arcs (described earlier), lead us to conclude that Marcatili's theory may not be completely reliable for

TABLE III-1

Measured Q of ring resonators

| Density of Powder ($g/cm^3$) | Dielectric Constant | Radius of Curvature (cm) | Frequency (GHz) | Measured Q |
|---|---|---|---|---|
| 1.76±.02 | 4.28±.07 | 4.0 | 94.39 | 1100±200 |
| 1.86±.02 | 4.65±.08 | 4.0 | 94.61 | 1300±200 |
| 1.88±.02 | 4.73±.09 | 4.0 | 94.24 | 2400±400 |
| 1.95±.02 | 5.06±.10 | 4.0 | 94.61 | 1600±200 |
| 2.10±.02 | 5.90±.13 | 4.0 | 94.31 | 1200±200 |
| 1.67±.02 | 4.02±.06 | 5.0 | 94.86 | 810±100 |
| 1.70±.02 | 4.10±.06 | 5.0 | 93.20 | 930±150 |
| 1.78±.02 | 4.35±.07 | 5.0 | 94.32 | 1300±200 |
| 1.83±.02 | 4.53±.08 | 5.0 | 94.28 | 1600±200 |
| 1.88±.02 | 4.73±.09 | 5.0 | 94.47 | 1900±200 |
| 1.89±.02 | 4.78±.09 | 5.0 | 94.44 | 1000±200 |

Powder: Nickel-aluminum titanate (Trans-Tech D-30).
All particles less than 43 μm.
Channel width: 1.83 mm
Channel depth: 1.09 mm for R = 5.0 cm
1.05 mm for R = 4.0 cm

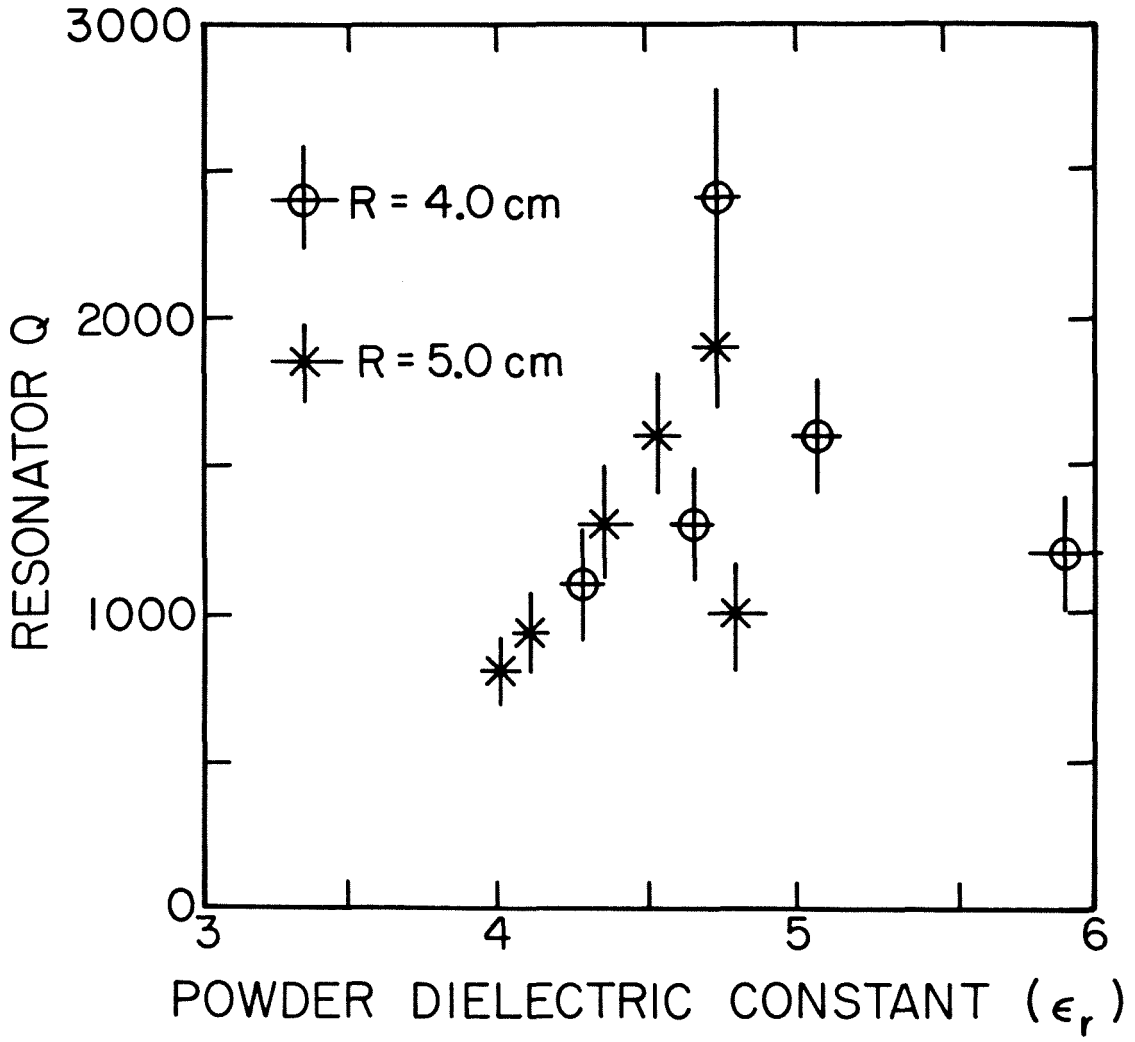


Figure III-4: Measured Q values of ring resonators versus the dielectric constant of the powder (Trans-Tech D-30 nickel aluminum titanate)

calculating the bending losses of channel guides with our large differences in dielectric constant.

We tentatively attribute the initial increase in Q with increasing powder dielectric constant to reduced bending loss. However, as powder dielectric constant increases, dielectric loss increases as the fields become more confined to the (relatively) lossy channel. Eventually this effect becomes dominant and the Q begins to decrease with increased powder dielectric constant. Propagation of a higher-order mode (or modes) may also have contributed to the eventual decrease in Q, particularly for the 5 cm radius ring for which the decrease in Q was abrupt.

REFERENCES

III-1. G.L. Matthaei, D.C. Park, Y.M. Kim, and D.L. Johnson, 'A study of the filter properties of single and parallel-coupled dielectric-waveguide gratings,' IEEE Transactions on Microwave Theory and Techniques, Vol. 31, pp. 825-835, Jan. 1983.

III-2. E.A.J. Marcatili, 'Bends in optical dielectric guides,' Bell Syst. Tech. J., Vol. 48, pp. 2103-2132, Sept. 1969.

III-3. E.A.J. Marcatili, 'Dielectric rectangular waveguide and directional coupler for integrated optics,' Bell Syst. Tech. J, Vol. 48, pp. 2071-2102, Sept. 1969.

III-4. E.L. Ginzton, MICROWAVE MEASUREMENTS, McGraw-Hill, New York, 1957, pp. 403-405.

# IV. ADJUSTABLE DIRECTIONAL COUPLER

## Introduction

Since directional couplers are a useful part of many millimeter-wave systems, we were interested in building a directional coupler using our powder-core channel waveguides. We decided to build one consisting of two straight channel waveguides in parallel because an approximate analysis (Ref. IV-1) existed for this structure. In order to better investigate the degree of coupling between the two waveguides, an experiment was devised wherein the distance between them could be varied.

## A. Design

Well-established formulas have been derived by Miller (Ref. IV-2) which describe the the propagation of waves on any pair of coupled parallel waveguides for which the coupling is small per wavelength and uniform along the direction of propagation. We expected these conditions to apply for our directional coupler. Assuming that a single mode on one of the waveguides is coupled to one mode of the other, Miller's formulas give the power carried by each of these modes, denoted as 1 and 2, as a function of distance, z, along the

mutually parallel extent of the two guides (Fig. IV-1). If, as expected for our directional coupler, the individual guides have equal attenuation constants, then $P_1(z)$ and $P_2(z)$, which represent the power carried by modes 1 and 2, respectively, are given by Miller as

$$P_1(z) = P_1(0)\ (\Delta\beta^2/(c^2 + \Delta\beta^2))\exp(-2\alpha z)(\sin^2((c^2 + \Delta\beta^2)^{1/2}z) + \cos^2((c^2 + \Delta\beta^2)^{1/2}z)) \qquad \text{(IV-1)}$$

and

$$P_2(z) = P_1(0)((c^2/(c^2 + \Delta\beta^2))\exp(-2\alpha z)\sin^2((c^2 + \Delta\beta^2)^{1/2}z)), \qquad \text{(IV-2)}$$

where

$$\Delta\beta = (\beta_1 - \beta_2)/2.$$

Here $\beta_1$ and $\beta_2$ are the propagation constants of modes 1 and 2, respectively, in the absence of coupling between the two waveguides. The amplitude attenuation constant of each guide in the absence of coupling is represented by $\alpha$. Finally, it was assumed in the derivations of Equations 1 and 2 that all the power is initially in guide 1 ($P_2(z=0) = 0$).

Thus, given the propagation and attenuation constants of the individual waveguides and the length over which they are parallel (quantities which can be controlled by design for our powder-core channel waveguides), these formulas predict the coupling in terms of a parameter called the coupling coefficient. The coupling coefficient, in turn, depends upon the fields of the two coupled waveguide modes and the relative positioning of the waveguides.

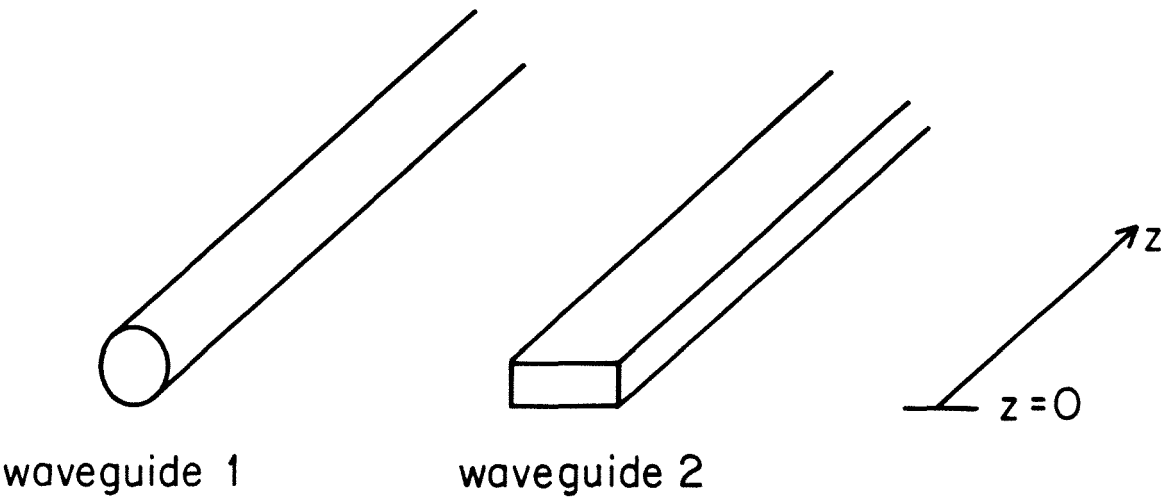


Figure IV-1: Schematic of coupled waveguides analyzed by Miller

Although Miller's formulas apply to a wide variety of parallel waveguide pairs, the coupling coefficient must be determined individually for each pair, since it depends on the fields. Unfortunately, there is no unapproximate analytical theory which gives the coupling coefficient for a pair of parallel channel waveguides. In fact, the only theory we know which predicts this coupling coefficient is the approximate theory of Marcatili (Ref. IV-1). (The directional coupler analyzed by Marcatili is shown in Fig. IV-2). This is the same theory that was shown in Chapter II to be reasonably accurate for predicting the guide wavelengths of the $E^{y}_{11}$ mode of our straight dielectric channel guides. If it also could predict accurately the coupling coefficient, it would be useful for designing directional couplers. Unfortunately, we knew of no experimental data confirming Marcatili's prediction of the coupling coefficient. In addition, for our powder-core channel guides, the refractive index differences between the core and the surrounding media are large enough to push the validity of Marcatili's approximation (c.f. Chap. II) to its limits. As a result, we were unsure of the accuracy that could be expected from Marcatili's predicted values of the coupling coefficient.

Since, for the reasons just stated, we were uncertain of how the coupling coefficient would depend upon the separation between the two waveguides, we devised an experiment in which the spacing between the

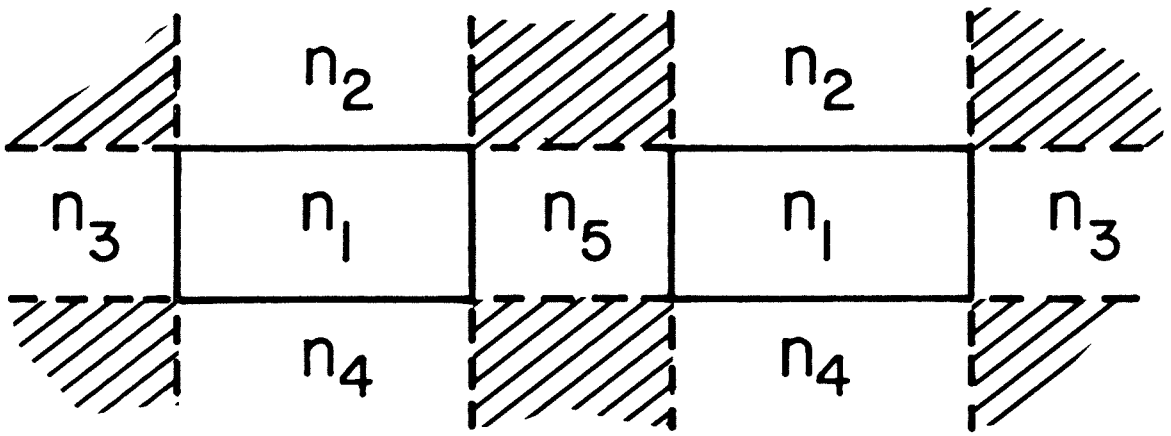


Figure IV-2: Cross-section of the directional coupler analyzed by Marcatili

two parallel channel guides could be varied. To do this, each of the two waveguides would be built on individual plastic substrates (Fig. IV-3). A wedge made from the same material as the substrates would be lowered or raised in order to change the spacing between the channels. Thick plastic plates made of the substrate material would be placed directly above and below the waveguide substrates. These plates would be sufficiently thick that, for purposes of analysis, one could assume that the two channel waveguides were immersed in an infinitely thick plastic medium. Thus, the geometry of our coupler would be the same as that analyzed by Marcatili (with $n_2 = n_3 = n_4 = n_5$), so we could compare its measured performance to predictions based on his theory.

Since, in general, the fields of a guided mode of a dielectric waveguide decrease approximately exponentially with distance away from the guiding medium (core), we suspected that the coupling coefficient would decrease rapidly as the separation between the channels increased. Thus, we wanted our experimental setup to allow fine adjustments in the channel separation and also to permit close spacing of the two channels. In order to make fine adjustments, the wedge would need to be tall and thin. To permit a small separation, the groove for the channel of each waveguide would have to be very close to the edge of its substrate nearest the wedge. If the experiment were to be done at W-band, for example, the nearest edge of the groove

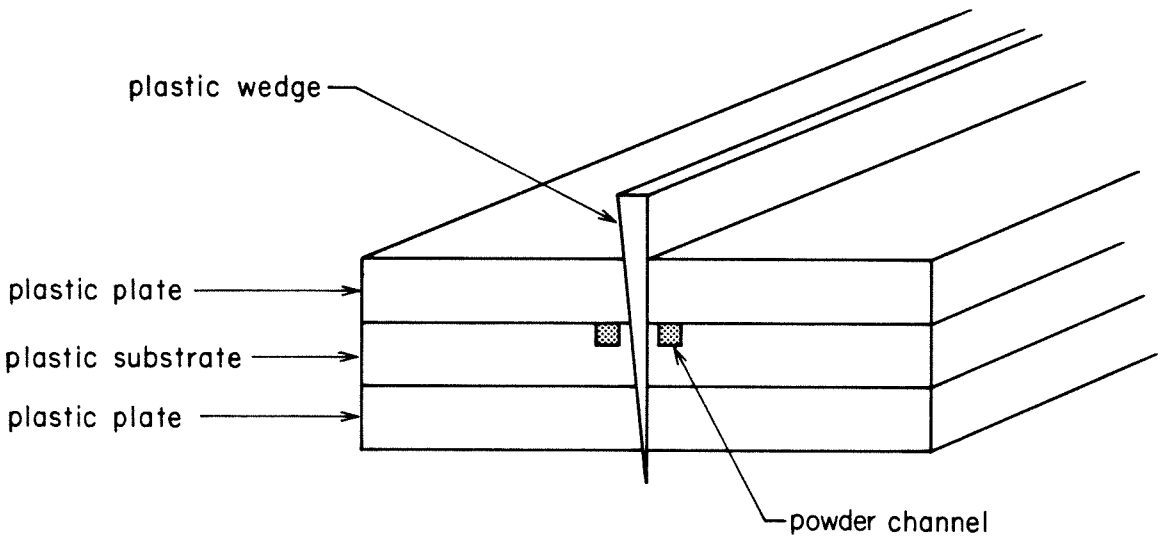


Figure IV-3: Method of achieving variable spacing between two parallel channel waveguides

would need to be within a few tenths of a millimeter of the edge of the substrate. Since it was prohibitively difficult to machine plastic with sufficient precision to meet such requirements at millimeter-wave frequencies, we decided to conduct the experiment at 10 GHz.

The next step in the design was to choose a substrate material. We decided to use Rexolite$^{R}$ (a cross-linked polystyrene sold specifically as a low-loss microwave dielectric material by C-LEC Plastics) rather than other low-loss, machinable materials that we possessed, such as polypropylene, TFE teflon, and polyethylene, mainly because Rexolite$^{R}$ has the largest dielectric constant at 10 GHz. For Rexolite$^{R}$, $\varepsilon_r = 2.56$, as compared to 2.25 for polypropylene and polyethylene (Ref. 3), and 2.08 for TFE teflon. The values of $\varepsilon_r$ listed here for Rexolite$^{R}$, polypropylene, and TFE teflon were measured using the shorted-waveguide technique (Ref. 4) and are in good agreement with values quoted in the literature.

We wanted the relative dielectric constant of the substrate to be as close as possible to that of the powder core, which was expected to be approximately 4, since we intended to compare our results with Marcatili's theory. Additionally, the smaller difference in dielectric constant between the core and a Rexolite substrate would cause the fields to be more loosely confined to the core and thus

would likely result in a less rapid decline of the coupling coefficient with increasing separation between the waveguides. Finally, Rexolite$^{R}$ is easier to machine than most of the aforementioned alternative plastics.

Again, to minimize the difference in dielectric constant between the core and the substrate, we chose Trans-Tech D-8512 (barium tetratitanate) as the powder material because it had the lowest effective dielectric constant of any powder available in the lab. The powder was to be packed just enough so that inadvertent jarring of the experimental setup would cause minimal settling. Thus, the powder density was chosen to be 1.74 g/cm$^{3}$, giving a relative effective dielectric constant of 4.4.

We next picked the channel dimensions for the two waveguides using Marcatili's theory as a design tool, since it had already been shown (c.f. Chap. II) to be reasonably accurate for predicting the guide wavelength of the $E^{y}_{11}$ mode of straight channel waveguides. For simplicity, it was desired that each waveguide be able to propagate only the fundamental vertically polarized ($E^{y}_{11}$) mode. (We expected to excite only vertically polarized modes.) Secondly, since for a given value of coupling coefficient the power transferred between the two waveguides is maximized over $\Delta\beta$ when $\Delta\beta$ equals zero (c.f. Eqs. 1 and 2), we wanted the channel dimensions for the two waveguides to

be identical. Thirdly, the guided $E^{y}_{11}$ mode was to be near cut-off so that the fields would extend farther into the substrate. We were able to satisfy all these constraints by picking the channel depth and width both equal to 1.20 cm. With these dimensions and with the relative effective dielectric constant of the powder equal to 4.4, the guide wavelength for the $E^{y}_{11}$ mode was predicted by Marcatili's theory to be 1.72 cm at 10 GHz. (For comparison, the cut-off wavelength was 1.88 cm and $\lambda_0/(4.4.)^{1/2}$ = 1.43 cm.)

In our experiment, we planned to excite the $E^{y}_{11}$ mode at an end of one of the parallel channel waveguides (hereafter, to be referred to as the 'primary' channel waveguide) and measure the power received at the other end of both guides as a function of the distance between them. To do so, a means would be required of coupling power between channel guide and rectangular metal waveguide. We intended to couple between these two different types of waveguide by way of an intervening section of rectangular dielectric rod upon which the $E^{y}_{11}$ mode would propagate. Fortunately, we already possessed two 30 cm lengths of Stycast$^{R}$ dielectric rod with cross-sectional dimensions similar to those chosen for the channel guide. For one of these rods, the width was 1.26 cm and the height was 1.02 cm. For the other, the width and height both equaled 1.30 cm. The Stycast$^{R}$ material was specified by the manufacturer, Emerson and Cuming, to have $\varepsilon_r = 3.0 \pm 3\%$ and $\tan\delta < .002$ at 10 GHz.

According to Marcatili's theory, both of these rods could propagate only the fundamental vertically polarized ($E^{y}_{11}$) mode at 10 GHz. The guide wavelength of the $E^{y}_{11}$ mode was predicted to be 2.73 cm for the rod with smaller cross-sectional area and 2.40 cm for the other. Also, the cross-sectional field distribution of the $E^{y}_{11}$ mode of each of these rods was predicted to be similar to that of the $E^{y}_{11}$ mode of the channel guide, so one would expect to get good coupling between these two types of waveguide by butting them together end-to-end. Since the field distribution of the $E^{y}_{11}$ mode of each rod was also fairly similar to that of the dominant $TE_{10}$ mode of the rectangular metal guide, we would try to couple between these two types by inserting the rod into the metal guide.

Two detectors could have been used to determine simultaneously the power transmitted to the far ends of both of the parallel channel waveguides comprising the directional coupler. However, to preclude the calibration problems inherent in obtaining two identical detectors, a single detector would be switched between the two guides. The far end of one of the channel guides would be terminated in a matched load while the power transmitted to the far end of the other guide would be coupled first onto a Stycast$^{R}$ rod and then into a segment of metal waveguide containing a detector. The matched load would consist of a Stycast$^{R}$ rod with pieces of Emerson and Cuming MF-110 absorber placed above and below the rod. This switched

detector scheme was also necessary in order to provide the minimum possible separation between the channel guides without being limited by the width of a metal waveguide flange. However, it introduced the potential problem of unwanted coupling between the two dielectric rods emerging in parallel from the far ends of the channel waveguides (Fig. IV-4). If the amount of power transferred between the rods was significant compared to that between the channel guides, the experimental results would be more difficult to interpret.

Unfortunately, for a given separation distance, the coupling coefficient for the two parallel rods would be similar to that for the channel guides, according to Marcatili's theory. Thus, in order to reduce the power transferred between the rods, we wanted the difference in their propagation constants for the $E^y_{11}$ mode to be large (c.f. Eqns. 1 and 2). To achieve this goal, the two rods were chosen to have cross-sectional dimensions that would assure different $\beta$'s. The one chosen to couple to metal waveguide would be a segment of the rod with height equal to 1.02 cm because this height more closely matched the inner height of the metal guide. The rod used for making the matched load would be a piece of the one which had both width and height equal to 1.30 cm. Thus, the value of $\Delta\beta$ for the $E^y_{11}$ modes of these two rods would be about 0.16 $cm^{-1}$, according to Marcatili's theory. We hoped that this value of $\Delta\beta$ would be sufficiently large that the power transferred between the rods would

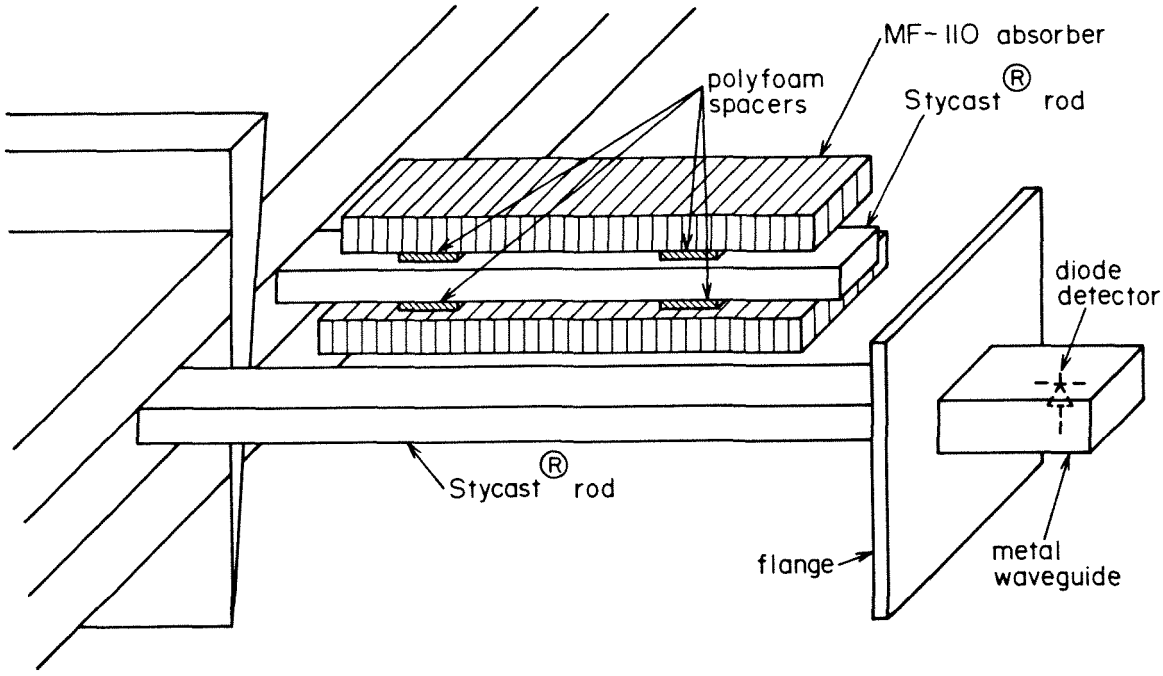


Figure IV-4: Space-saving scheme for terminating one channel guide in a matched load while measuring the power transmitted to the end of the adjacent guide

be negligible compared to that between the channel guides over the entire range of separation distances possible with the experimental setup. However, we could not be confident of this outcome because we were uncertain of the accuracy of the values of coupling coefficient given by Marcatili's theory. In addition, we were unsure of how the coupling coefficient between the rods would be affected by the presence of the pieces of MF-110 absorber used to attenuate the wave travelling on one of them.

There would also be two dielectric rods in parallel at the near end of the directional coupler. One each of these would emerge from the near end of each of the parallel channel waveguides. Here again, the rods were chosen to have different cross-sectional dimensions to reduce the power transferred between them. The purpose of one of these rods would be to feed power onto the primary channel. This rod would be cut from the 30 cm length which had a height of 1.02 cm. The other rod, which would be used to make a matched load for the near end of the other channel guide (hereafter to be referred to as the 'secondary' channel waveguide), would be a segment of the rod which had both width and height equal to 1.30 cm.

The thickness of the substrates for the channel guides would be 2.5 cm, using our thickest Rexolite$^{R}$ sheet stock. The plates to be placed directly above and below these substrates would also be 2.5 cm thick.

Although we did not really know what thickness for these plates would be sufficient to simulate Marcatili's geometry, our experience with dielectric waveguides led us to believe that 2.5 cm would be enough because the field strength at 2.5 cm from the core probably would be negligible. Indeed, Marcatili's theory predicted that the penetration depth of the fields into the substrate would be only about 0.4 cm. (The penetration depth is the distance from the channel in which the fields decay by a factor of 1/e.) In any case, more plates could be added during the experiment if tests indicated that they were necessary. We also intended to put a layer of 1.3 cm thick Emerson and Cuming MF-110 absorber underneath the lower plates (Fig. IV-5) to absorb any stray power that might escape from the dielectric waveguides, thus preventing reflection from the metal jacks used for support. MF-110 is specified by Emerson and Cuming to have a relative dielectric constant of 2.9 at 10 GHz.

Another important part of the design was to pick the shape and size of the wedge. First, one side of the wedge (viewed in cross section) was chosen to be vertical so that Rexolite$^{R}$ plates could be added next to it (Fig. IV-5) to increase the range of separation distances possible with the experiment. Since we possessed a large number of plates, the separation distance could be made quite large with this scheme. The proportions of the wedge were picked so that a given vertical displacement would result in a much smaller change in

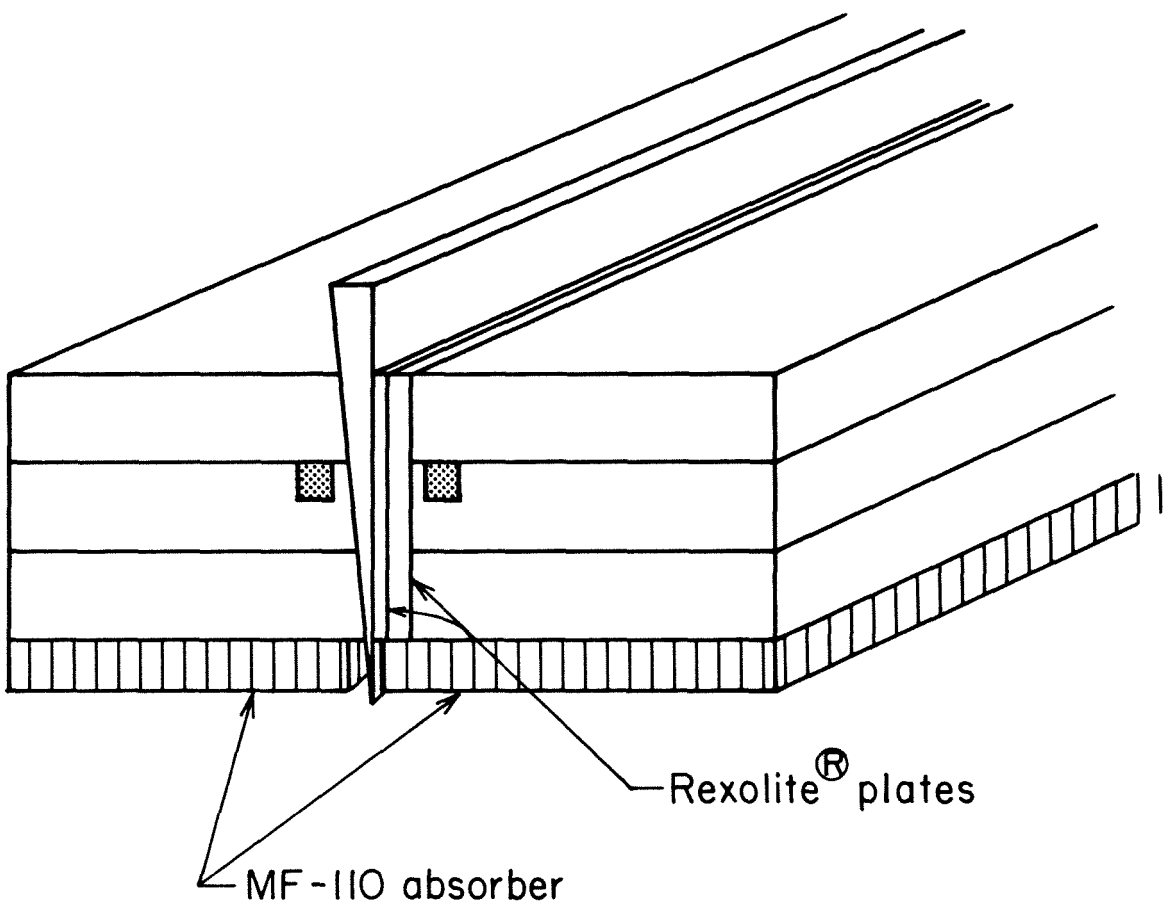


Figure IV-5: Diagram of coupled channel guides showing Rexolite® plates used to increase the range of separation distance possible with the experiment. Supporting structures (metal jacks) not shown.

separation distance (in the ratio 12:1). In particular, the height of the triangular wedge was to be 12.0 cm and the base was to be 1.0 cm.

The wedge would be supported and guided from above by a metal frame (Figs. IV-6). A long, finely threaded (40 threads/inch) screw attached to the frame would be used to push the wedge downward to increase the separation distance. Because of the fine threads of the screw and the gradual slope of the wedge, it would be possible to adjust the separation distance in increments of less than one-tenth of a millimeter. This degree of adjustment was judged to be adequate since the penetration depth of the fields into the substrate was expected to be a few millimeters.

In order to be able to achieve the smallest possible separation between the two coupled channel guides, it was desirable for each channel to be put as close as possible to the edge of its substrate nearest to the wedge. However, the closer the channels were to the edge, the more fragile would be the substrates. They would also become harder to fabricate. As a compromise, each channel was put 0.20 cm away from the edge of its substrate nearest the wedge (Fig. IV-5). Thus, the minimum possible separation distance between the two channels would be 0.82 cm, occurring when the point of the wedge was extended just to the bottom of the Rexolite$^{R}$ plates underneath the substrates.

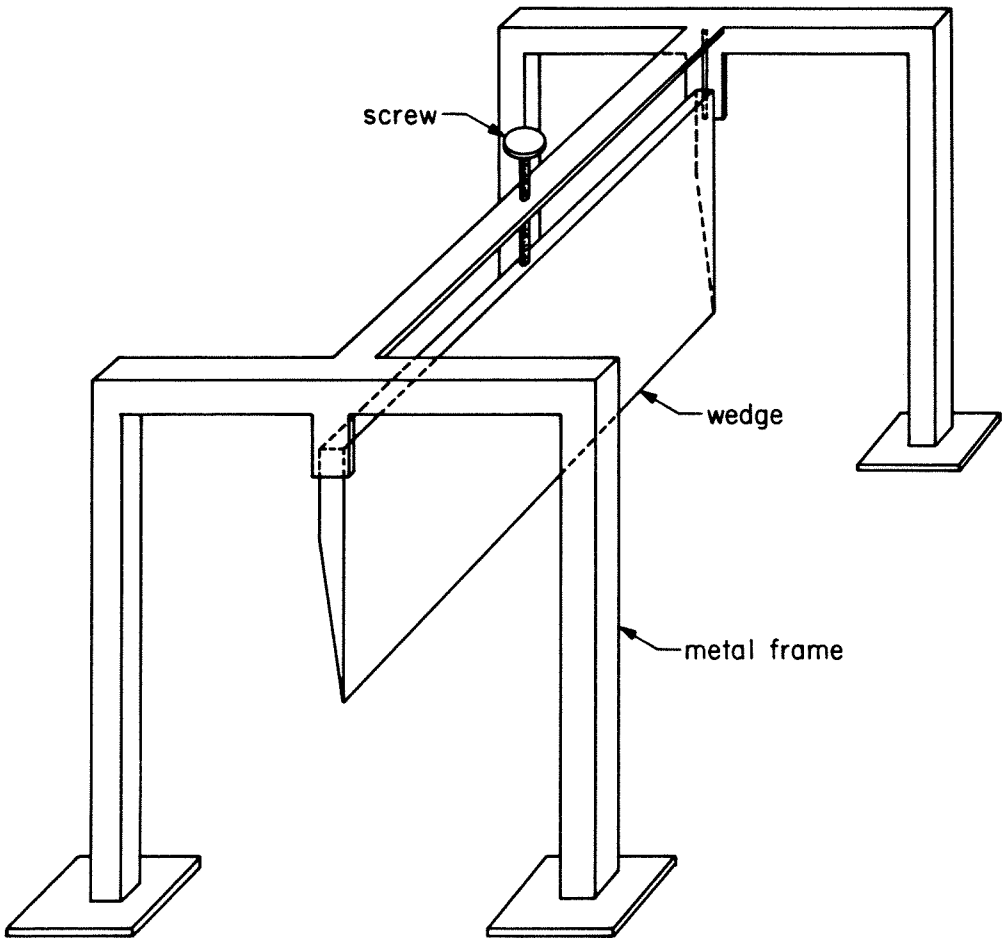


Figure IV-6: Metal frame used to support and guide the Rexolite$^{R}$ wedge

To choose the length of the coupler, Miller's equations (Eqns. IV-1 and IV-2) were used. For our application, $P_1(z)$ and $P_2(z)$ in these equations represent the power carried in the positive z direction by the $E^y_{11}$ modes in the two parallel waveguides at distance z from the end at which power is introduced onto the primary waveguide. From Eqns. IV-1 and IV-2, we observed that the longer the length of the directional coupler, the greater would be the number of oscillations of $P_1$ and $P_2$ as c is varied over the range possible with the setup. However, we were limited to a maximum length of about 30 cm by our supply of D-8512 powder. Also, according to Marcatili's theory, the coupling coefficient, c, would reach a maximum value of only .053 when the separation distance equaled its minimum value of 0.82 cm. Thus, we chose 30 cm for the length of the coupler so that if Marcatili's predicted value of coupling coefficient were too small, we might begin to observe the first oscillation of the sinusoidal terms in Eqns. IV-1 and IV-2 as the separation distance approached the minimum value possible with the setup. (Assuming that $\Delta\beta$ for the two channel guides equaled zero.) On the other hand, if Marcatili's values were accurate or too large, the argument of the sinusoids would never become appreciably greater than $\pi/2$.

B. Experiment-Preliminaries

The first experimental step was to investigate the coupling at 10 GHz between rectangular metal waveguide and the Stycast$^{R}$ rod with height equal to 1.02 cm. This experiment, and all the ones described below, were done with the X-band test equipment configured as shown in Fig. IV-7. Since the rod's height was a little too large to allow an end to fit into the metal guide, which had an inner height of 1.00 cm, the top and bottom sides of the rod were sanded near one end until the height there was reduced to 0.95 cm. This end of the rod was then inserted into the feed (an open-ended section of metal waveguide) and the standing wave ratio was measured with the slotted line for several insertion depths less than 4.0 cm. The ratio of reflected power to incident power was calculated from the standing wave ratio.

To prevent reflections from the far end of the 30 cm long rod, a piece of MF-110 absorber which was 2.0 cm wide, 1.3 cm high and 16 cm long was placed parallel to the dielectric rod about 2 mm from its upper surface as shown in Fig. IV-8. The 2 mm distance between the rod and the absorber was small enough to allow sufficient absorption, but large enough that there was negligible reflection caused by the absorber. Indeed, as long as the 2 mm distance was maintained, the value of the standing wave ratio measured with the slotted line was independent of the precise position of the absorber along the length

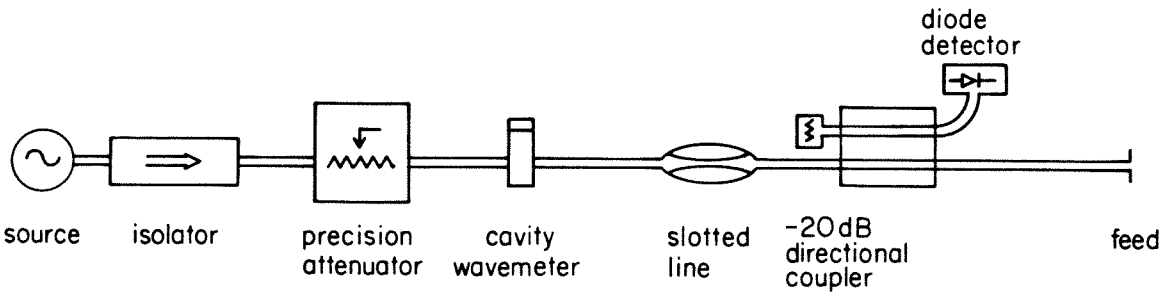


Figure IV-7: Setup of the X-band test equipment

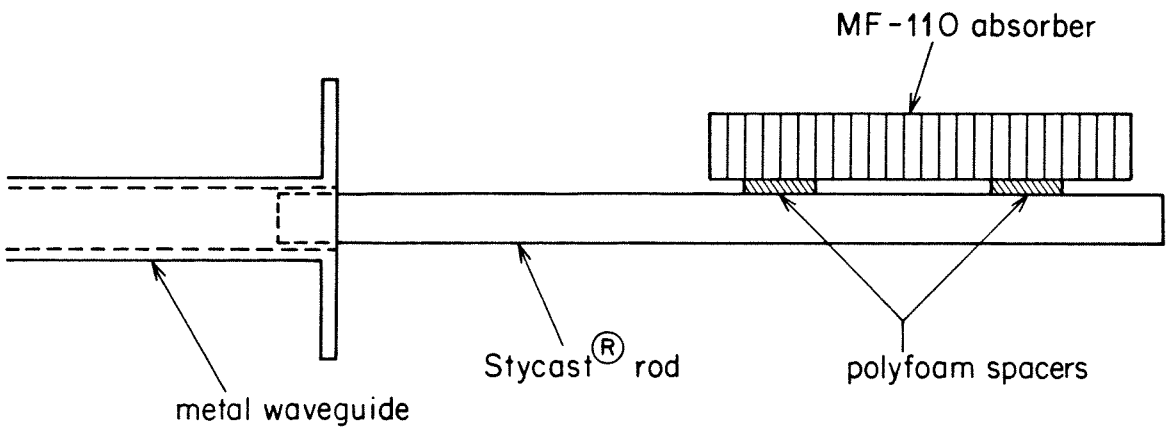


Figure IV-8: Setup for testing coupling between metal guide and dielectric rod

of the rod. Moreover, with the absorber present, probing the space around the end of the rod with a metal perturber had no effect on the reflected power. Without the absorber, however, the perturber had a pronounced effect. Thus, we concluded that with the absorber in position, the only significant source of reflected power was the imperfect coupling between the metal waveguide and the dielectric rod.

As the dielectric rod was inserted into the metal waveguide, the reflected power varied periodically with insertion depth with a period of 1.0 cm. At the minima, the reflected power (calculated from the SWR) was 21 dB down from the incident power. Minima were recorded at insertion depths of 0.7 cm, 1.7 cm, 2.7 cm, and 3.7 cm. With the rod at each of these depths, a detector connected to a short length of rectangular metal waveguide was used as a movable probe to determine that the amount of radiation emanating from the feed was small. In each case, the detected radiation was more than 25 dB below the incident power, no matter where the probe was positioned. (The incident power was monitored with the detector connected to the directional coupler shown in Fig. IV-7.) Hence, we concluded that virtually all of the power that was not reflected was coupled onto the dielectric rod, rather than radiated.

After removing the absorber, guide wavelength measurements were conducted by moving a metal perturber along the length of the

dielectric rod and observing the periodic variation of reflected power as a function of perturber position. As expected, no beats were detected in this pattern, indicating that a single mode was propagating on the rod. The guide wavelength was determined to be 2.70 cm ± .02 cm, in reasonable agreement with Marcatili's prediction of 2.63 cm for the $E^{y}_{11}$ mode.

Next, the rod's height at its other end was reduced slightly by sanding so that it could fit into metal guide. As a check, the procedure described above for determining the optimal insertion depths (in terms of minimum reflected power) for coupling to metal waveguide was repeated for the newly sanded end of the rod. Not surprisingly, the results were the same as for the other end. Then, knowing how to couple to both ends of the rod, we were able to determine its transmission loss using the setup shown in Fig. IV-9. Since the power lost in coupling was so small, the difference between the incident power and that detected at the far end of the rod equaled its transmission loss to within our measurement precision of 0.2 dB. The transmission loss of the rod was thus determined to be 1.0 dB ± 0.2 dB. Using this value in the extension of Marcatili's theory described in Chapter II, the loss tangent of the Stycast$^{R}$ material was calculated to be .0025 ± .0005 at 10 GHz. Since this number is close to that specified by the manufacturer (.002), we were confident in the accuracy of the loss measurement.

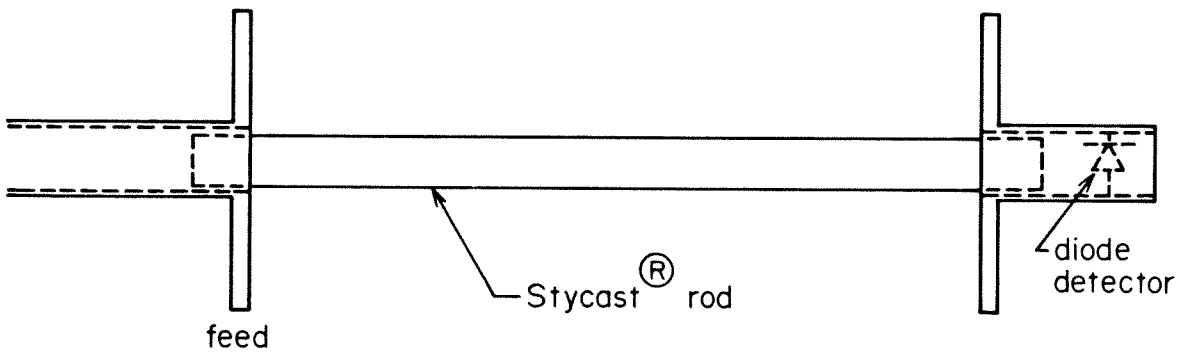


Figure IV-9: Setup for measuring the transmission loss of a dielectric rod

The Stycast$^{R}$ rod with height equal to 1.02 cm was now cut in half to make two 15 cm lengths to be used to couple power between metal guide and the channel guides of the directional coupler. The sides of each of these segments were sanded slightly at one end to allow it to fit into the channel guide. The other end of each segment had been sanded earlier on the top and bottom and would be inserted into metal waveguide.

To determine the depth to which these dielectric rods needed to be inserted into the channel guide for best coupling, the appropriate end of one of them was first inserted into the metal feed to a depth of 3.7 mm. (This depth was one of those which yielded optimal coupling to the metal guide.) The other end of the rod was then inserted into the near end of the primary channel waveguide (Fig. IV-10). The channel of this guide had a width of 1.22 cm $\pm$ .01 cm, a depth of 1.20 cm $\pm$ .01 cm, and a dielectric constant, due to the D-8512 powder, of 4.19 $\pm$ .03. While testing the coupling between the Stycast$^{R}$ rod and this channel guide, a Rexolite plate was butted against the edge of its substrate which would be adjacent to the wedge during testing of the directional coupler (Fig. IV-10). Otherwise, there would have been a substrate-air boundary very close to the channel.

To prevent reflections from the far end of the channel guide, a piece of MF-110 absorber 2.0 cm wide, 1.3 cm high and 16 cm long was

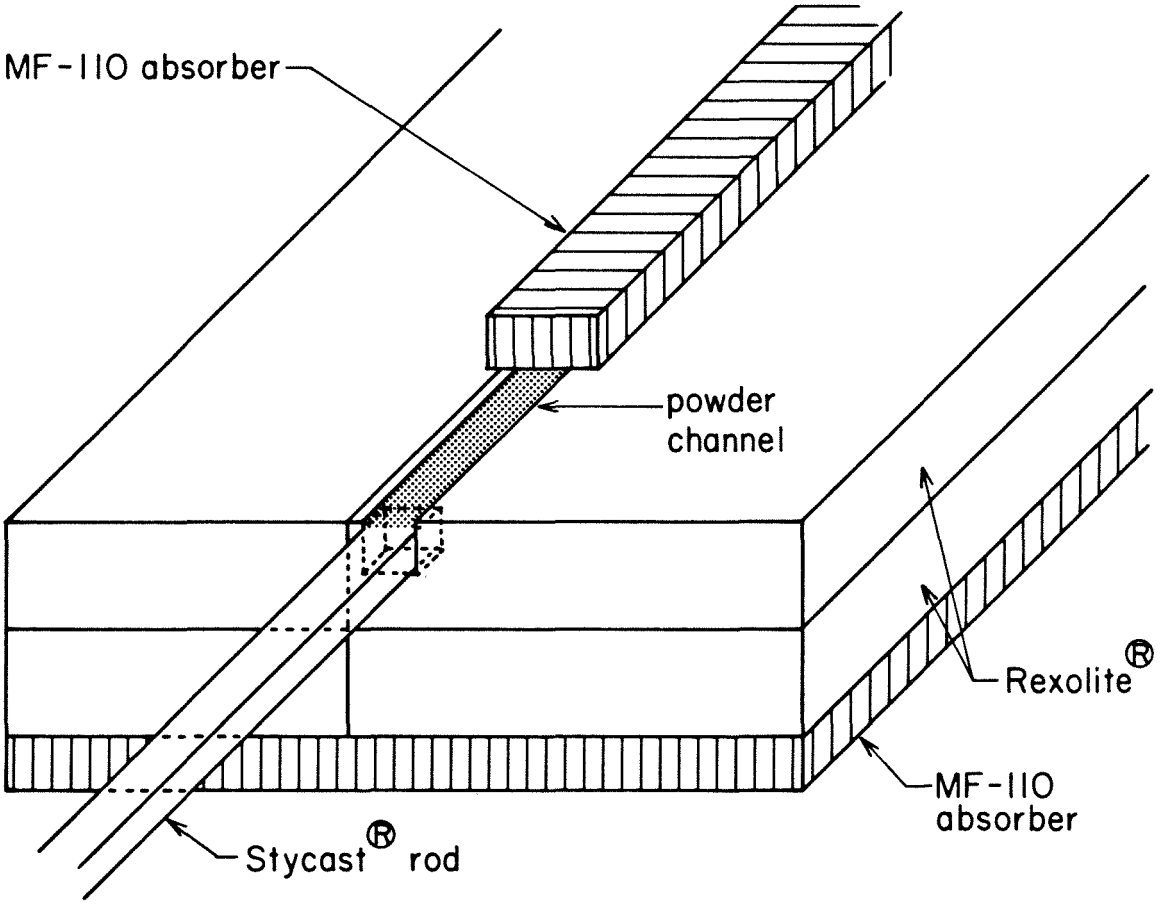


Figure IV-10: Setup for testing coupling between a Stycast® rod and a channel guide

placed directly over the channel, several centimeters from the near end (Fig. IV-10). The standing wave ratio measured with the slotted line was independent of the position of this absorber along the length of the channel, indicating that any reflection caused by its presence was negligible compared to those caused by the imperfect coupling of the dielectric rod to the metal guide and to the channel guide. In addition, since no measurable change in reflected power could be caused by probing the region around the far end of the channel guide with a metal perturber, the absorber provided adequate attenuation. Without the absorber, however, the perturber caused a large reflection.

With the dielectric rod inserted 5 mm into the near end of the channel, the reflected power, as calculated from the standing wave ratio, was negligibly different from that arising from the junction of the dielectric rod with the metal waveguide. Hence, we concluded that the power reflected from the junction of the rod with the channel guide could be ignored because it was much smaller than that from the junction of the metal guide with the rod. Next, a movable probe (as described earlier) was used to determine that the amount of power radiated from the junction of the rod with the channel guide was small. No matter where in the vicinity of the junction the probe was placed, the measured radiation emanating from it was at least 24 dB below the incident power. Hence, virtually all the power available

from the far end of the rod was coupled onto the channel guide.

The next step was to investigate the coupling between channel guide and the Stycast$^{R}$ rod which was to be used to make matched loads. (This rod was the one which had both width and height equal to 1.30 cm.) Two 10 cm lengths were cut from the original 30 cm long rod, and the sides of each of these were sanded near one end to allow them to just fit into the channel guide. Then, after removing the absorber which earlier had been placed over the channel, the sanded end of one of the rods was inserted into the far end of the channel.

To prevent reflections from the far end of this rod, pieces of MF-110 absorber, each 2.0 cm wide, 1.3 cm high, and 9 cm long, were placed parallel to the top and bottom of the rod as shown in Fig. IV-11. This configuration was the same as was to be used to make matched loads for the channel guides of the directional coupler. Thin polyfoam spacers were inserted between the rod and the pieces of MF-110 to insure that the distance between them would be 2 mm. (From our earlier experience with the other rod, we estimated that a 2 mm separation between the rod and the absorbers would yield adequate absorption and negligible reflection.) By the same methods used previously, we determined that the presence of the absorbers and polyfoam caused a negligible reflection and that the absorbers provided sufficient attenuation.

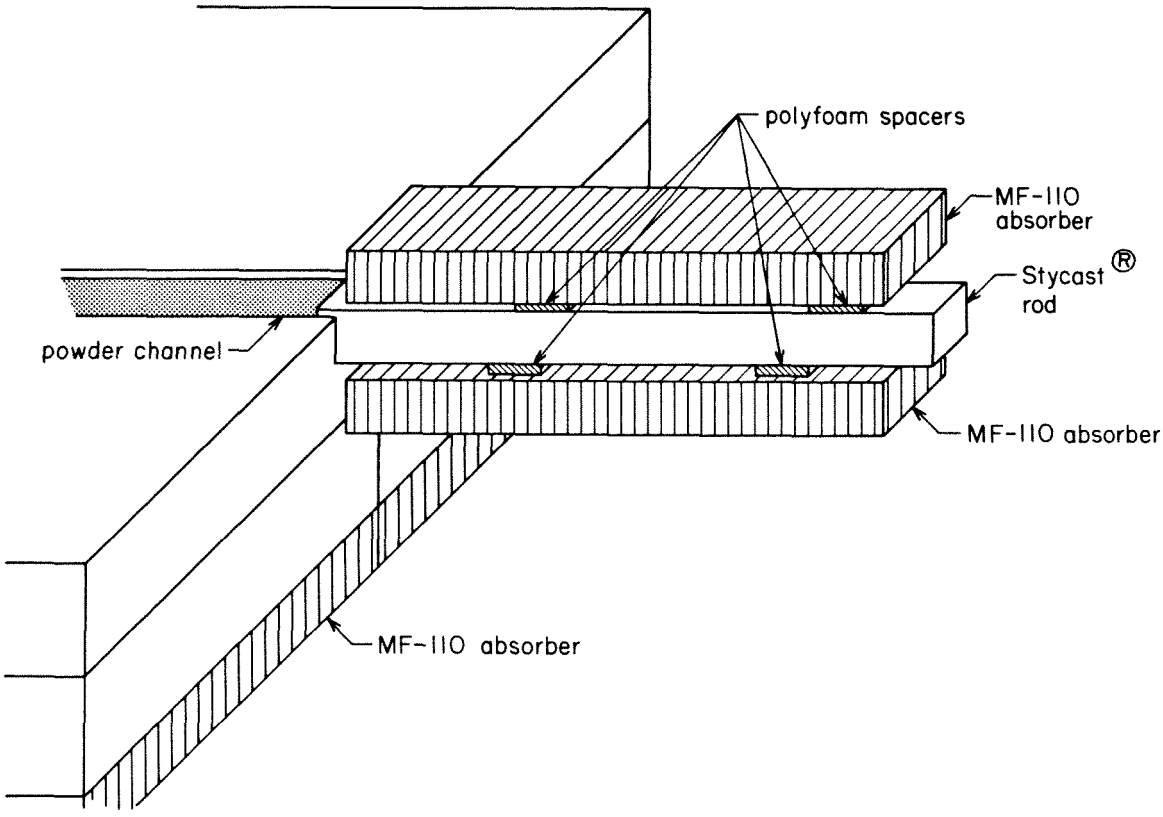


Figure IV-11: Matched termination for a channel guide

An insertion depth of 6 mm was found to be the one for which the standing wave ratio measured by the slotted line changed minimally (0.3 dB) from the value resulting from the reflection from the feed. With the rod inserted to this depth, the reflected power calculated from the standing wave ratio was 19 dB below that available from the feed, so we concluded that the power reflected from the junction at the far end of the channel guide was sufficiently small. In addition, the amount of power radiated from this junction was also small. No matter where the movable probe was positioned, the detected power was more than 24 dB below that available from the feed. Thus, almost all of the power incident on the rod at the far end of the channel was coupled onto it and then absorbed by the pieces of MF-110.

With the combination of rod and absorbers acting as a matched load at the far end of the channel guide, the guide wavelength of the channel guide was measured by moving a metal perturber along the length of the channel and observing the periodic variation of the reflected power as a function of perturber position. As expected from Marcatili's theory, no beats were observed in this variation, indicating that only one mode was propagating. The guide wavelength was measured as 1.77 cm $\pm$ .02 cm, in reasonable agreement with the value of 1.81 cm given by Marcatili's theory for the $E^{y}_{11}$ mode of this guide.

Up to this point, all the experiments on this channel waveguide (i.e., learning how to couple it to dielectric rods and measuring its guide wavelength) had been conducted without covering the channel with a Rexolite$^{R}$ plate, as would be done for the experiments on the directional coupler. We now needed to add this plate and determine whether a change would occur in the degree of coupling between the Stycast$^{R}$ rods and the channel guide. Consequently, a Rexolite$^{R}$ plate which was 2.5 cm thick, 15 cm wide, and 30 cm long was placed directly over the channel. Since the top of the rod used for the matched load rose slightly above the top of the channel (the height of this rod was 1.0 mm greater than that of the channel), the plate's position was offset 6 mm toward the feed to allow it to lie flat against the channel guide's substrate. With the plate in this position, the standing wave ratio measured with the slotted line equaled 1.5 dB. It was thus different by only 0.4 dB from its value of 1.9 dB without the plate. In addition, probing the regions around the ends of the channel guide with a movable detector showed that the radiation from the junctions with the rods was not significantly greater than when the channel was uncovered. Hence, the addition of the Rexolite$^{R}$ covering plate did not significantly affect the coupling between the rods and the channel guide.

To check whether the thickness of the plate covering the top of the channel was large enough to be considered infinite for comparison to

Marcatili's theory, the space immediately above the plate was probed with a metal perturber. The presence of the perturber caused no measurable change in the standing wave ratio, indicating that the field strength of the mode guided by the channel was negligible at the top of the plate. As another check on the field strength at the top of the plate, the matched load was removed from the far end of the channel guide and a segment of Stycast$^{R}$ rod with height equal to 1.02 cm was inserted 5 mm into he channel to couple power between it and a piece of metal guide containing a detector. The power measured by this detector was 3.0 dB $\pm$ .2 dB below that available from the feed. Placement of a piece of MF-110 absorber which was 30 cm long, 30 cm wide, and 1.3 cm thick over the top of the covering plate had no measurable affect on the power observed with the detector. Hence, the thickness of the covering plate was deemed to be sufficiently thick to be considered infinite.

To check whether the Rexolite$^{R}$ plate underneath the channel guide's substrate (Fig. IV-11) was sufficiently thick, an additional 2.5 cm thick Rexolite$^{R}$ plate was inserted below it next to the layer of MF-110, and the power transmitted through the channel guide and coupling rods was remeasured. If the field strength of the guided mode of the channel were significant at the bottom of the original plate, the transmission loss would be expected to decrease when the extra layer of dielectric was inserted above the absorber. Instead,

it was still equal to 3.0 dB. Consequently, we concluded that the original plate underneath the substrate could be considered infinitely thick.

So far, all of the foregoing experiments had involved the channel waveguide which was to be the primary guide of the directional coupler. We now repeated these tests on the channel waveguide which was to be the secondary guide. The channel of this guide had both width and depth equal to 1.19 cm $\pm$ .01 cm and dielectric constant (due to the D-8512 powder) of 4.44 $\pm$ .04. The same insertion depths were found to be best for coupling between this channel guide and the Stycast$^{R}$ rods as for the other channel guide. The quality of the coupling was also essentially the same. The guide wavelength was measured as 1.73 $\pm$ .02 cm in the absence of the Rexolite$^{R}$ covering plate, in reasonable agreement with the value of 1.77 cm predicted for the $E^{Y}_{11}$ mode by Marcatili's theory. This measured value equaled that for the primary guide to within the experimental uncertainty, as desired. With the covering plate, the power lost in transmission through the combination of the channel guide and the two Stycast$^{R}$ rods was measured as 3.3. dB $\pm$ 0.2 dB. Again, this value equaled that for the other channel guide to within the experimental uncertainty.

By subtracting the losses due to the Stycast$^{R}$ rods (1.0 $\pm$ 0.2 dB), the transmission losses of the two channel guides were calculated as

2.0 dB ± .4 dB and 2.3 dB ± .4 dB. These values correspond to attenuation constants equal to .0077 $cm^{-1}$ ± .0015 $cm^{-1}$ and .0088 $cm^{-1}$ ± .015 $cm^{-1}$, respectively. Thus, for computing the theoretical performance of the directional coupler, $2\alpha$ in Equations IV-1 and IV-2 would be taken as .017 $cm^{-1}$ ± .003 $cm^{-1}$. (Twice the average of $\alpha$ for the two guides.)

As the last preliminary step before testing the directional coupler, we conducted a crude measurement of the power transferred between the rod which would be used to couple power to the near end of the primary channel guide and the assembly of rod and absorbers which would be used as a matched load for the near end of the secondary channel guide. First, the rod to be used for coupling to the primary channel guide (this rod will be called 'rod A') was inserted 3.7 cm into the feed. This depth was one of those which yielded the best coupling between rod A and metal guide. Next, the other rod (rod B) and the pieces of MF-110 were placed parallel to rod A as shown in Fig. IV-12. A segment of metal waveguide containing a detector was then butted against the far end of rod A to measure the transmitted power as a function of the distance between the rods. (The height of the far end of rod A was too large for it to be inserted into the metal guide for better coupling.)

The power measured at the far end of rod A is plotted in Fig.

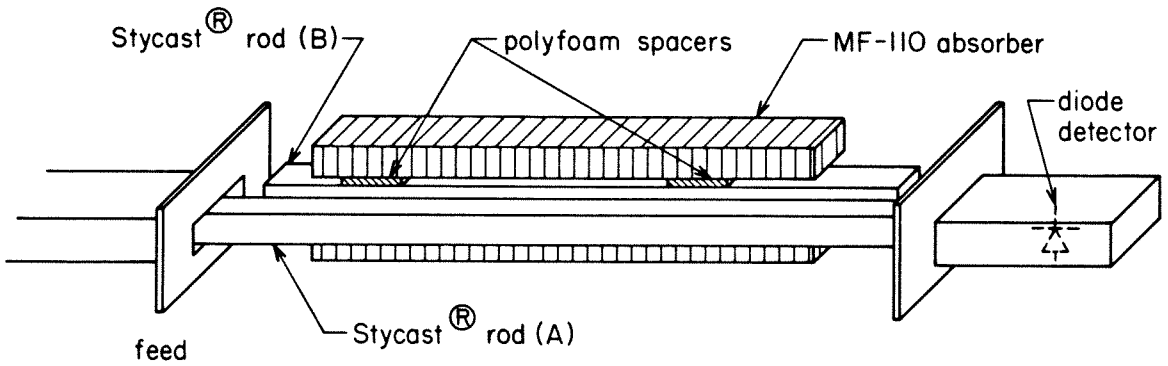


Figure IV-12: Setup for measuring the power transferred between the rod (A) to be used to couple power onto the near end of the primary channel guide and the assembly of the rod (B) and absorbers forming a matched load for the near end of the secondary guide.

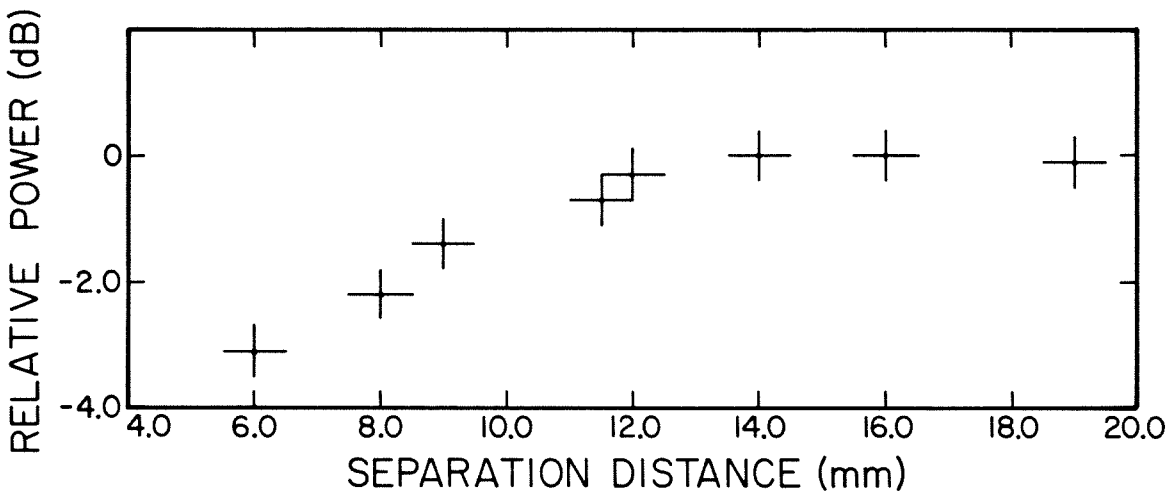


Figure IV-13: Power detected at the far end of the rod A relative to the amount detected in the absence of rod B and its accompanying absorbers

IV-13, normalized to the amount detected in the absence of rod B and its accompanying absorbers. As shown there, this power decreased measurably as the distance from rod B and its accompanying absorbers decreased below 12.0 mm. This decrease, which presumably represents power transferred to rod B and the absorbers, could be expected to affect the measured performance of the directional coupler.

We next attempted to learn how much power transferred from rod A was available from the far end of rod B because, during testing of the directional coupler, this power (or virtually all of it) could be expected to couple onto the near end of the secondary channel guide, in violation of the desired condition that $P_2(z=0) = 0$. To make this measurement, the far end of rod B was inserted 6 mm into the near end of the channel guide which was to be the secondary guide of the directional coupler (Fig. IV-14). A small metal plate was placed at the far end of rod A to prevent it from radiating in the direction of the channel guide. Another Stycast$^R$ rod with the same cross-sectional dimensions as rod A was inserted into the far end of the channel guide to couple power to a segment of metal guide containing a detector.

The measured power decreased rapidly as the distance between the rods increased and, fortunately, was very small over the entire range of separation distances which would be used in testing the directional coupler. For instance, when the distance between the rods was only 8

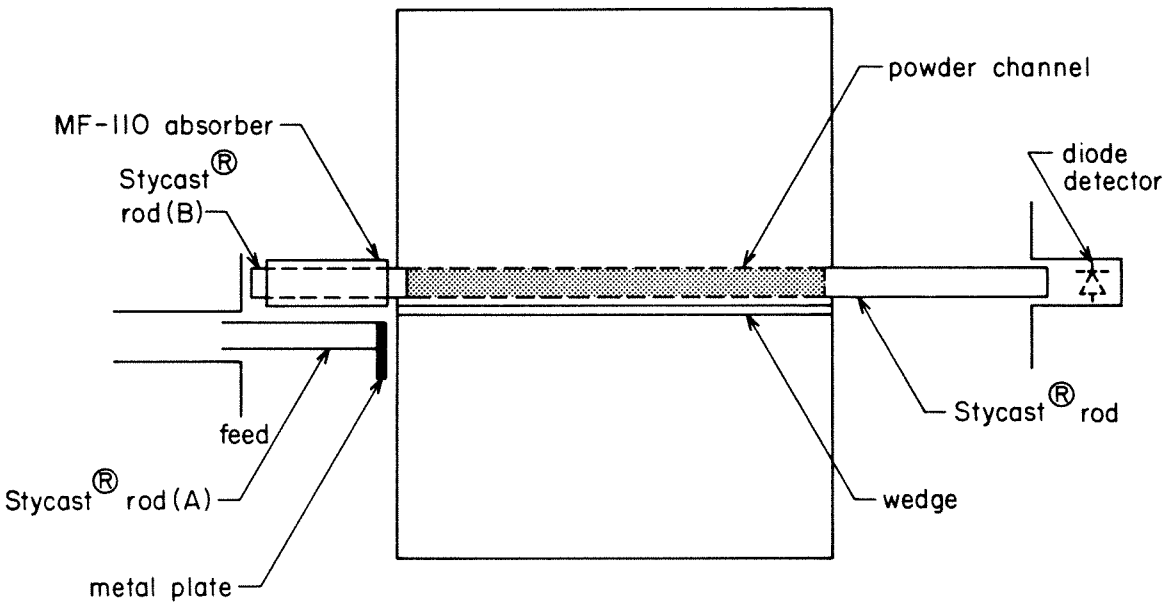


Figure IV-14: Top view schematic of setup for determining the power coupled onto the near end of the secondary channel guide

mm, the detected power was 32 dB below that available from the feed. Since, over the range of separation distances to be used, the detected power was much smaller than that expected at the far end of the secondary guide of the directional coupler as a result of coupling between the two channel guides, we concluded that a sufficient amount of the power transferred from rod A to rod B had been dissipated by the absorbers. Thus, the condition $P_2(z=0) = 0$ would apply for our experiment.

C. Experiment - Coupler Measurement

We were now ready to begin testing the directional coupler. Our goals were to learn the dependence of the coupling, insertion loss, and directivity on the distance between the parallel channel guides. (Coupling is defined as $10\log(P_2(z = 30\ \text{cm})/P_1(z = 30\ \text{cm}))$, insertion loss is defined as $-10\log((P_1(z = 30\ \text{cm}) + P_2(z = 30\ \text{cm}))/P_1(z = 0))$, and directivity is defined as $10\log(P_2(z = 30\ \text{cm})/P_2(z = 0))$.) The power transmitted to the far ends of the channel guides, relative to that coupled onto the near end of the primary guide, would be measured as a function of the separation distance to determine the coupling and insertion loss. The directivity would be determined by measuring the relative available power at the near end of the secondary guide. Unfortunately, our coupling scheme required placing Stycast$^R$ rods of identical cross section in parallel at the near ends of the channel

guides in order to make this measurement, so we were skeptical of the outcome.

To test the directional coupler, the primary and secondary channel guides, wedge, covering plates, etc., were configured according to the design. Matched loads were placed on the far end of the primary guide and the near end of the secondary guide, and the relative power transmitted to the far end of the secondary guide was determined by adding 1.0 dB to that measured with the detector in Fig. IV-15. The 1.0 dB correction accounted for the losses of the Stycast$^{R}$ rods used to couple power between metal and channel guide. (Recall that the loss of a 30 cm length of this rod had been determined previously to be 1.0 dB $\pm$ 0.2 dB and that the two rods used for coupling between metal guide and channel guide were each 15 cm long.) Using the same correction, the relative power transmitted to the far end of the primary guide was determined with a matched load on the far end of the secondary guide.

For both of the above measurements, the distance between the channel guides was varied from 12.0 mm to 16.4 mm and from 19.6 mm to 24.6 mm. The first range of separation distances was obtained by putting a 5.0 mm thick Rexolite$^{R}$ plate next to the vertical side of the wedge. A 12.9 mm thick plate was used to obtain the second range. Separation distances smaller than 12.0 mm were not used since coupling

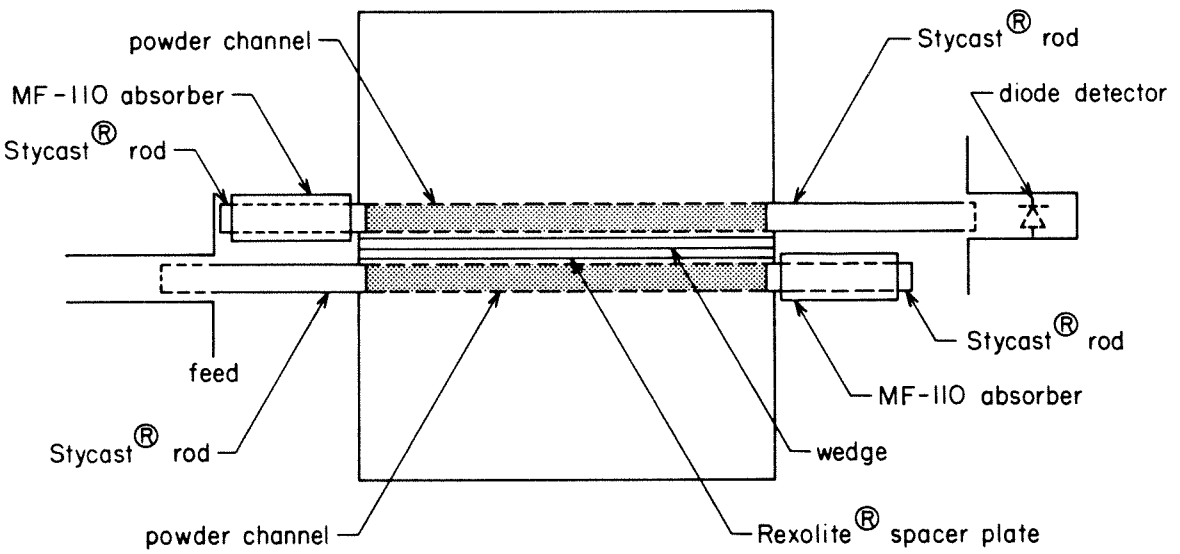


Figure IV-15: Top view schematic of setup for testing the channel guide directional coupler

between the Stycast$^{R}$ rods was significant when they were less than 12.0 mm apart.

We attempted to determine the directivity of the coupler, even though it was predicted to be greater than 30 dB by coupled mode theory. We measured the relative available power at the near end of the secondary guide with the far ends of both channel guides terminated in matched loads. Only the set of larger separation distances was used in order to allow sufficient clearance between the Stycast$^{R}$ rod inserted into the near end of the secondary guide and the flange of the metal waveguide feed (Fig. IV-16). The power measured with the detector in Fig. IV-16 was 30 dB below that available from the feed and, surprisingly, was independent of the distance between the channel guides. This result suggested that most of the power reaching the detector had arrived via a spurious path. Indeed, when the Stycast$^{R}$ rod coupling the near end of the secondary guide to the detector was removed entirely from the setup and the end of the channel was covered with a small piece of metal, the detected power was unchanged. By probing with a piece of MF-110 absorber, we determined that the detected power had been radiated from the feed and then reflected by the substrates of the channel guides. Thus, we knew only that the power from the near end of the secondary guide was more than 30 dB below that in the primary guide for separation distances

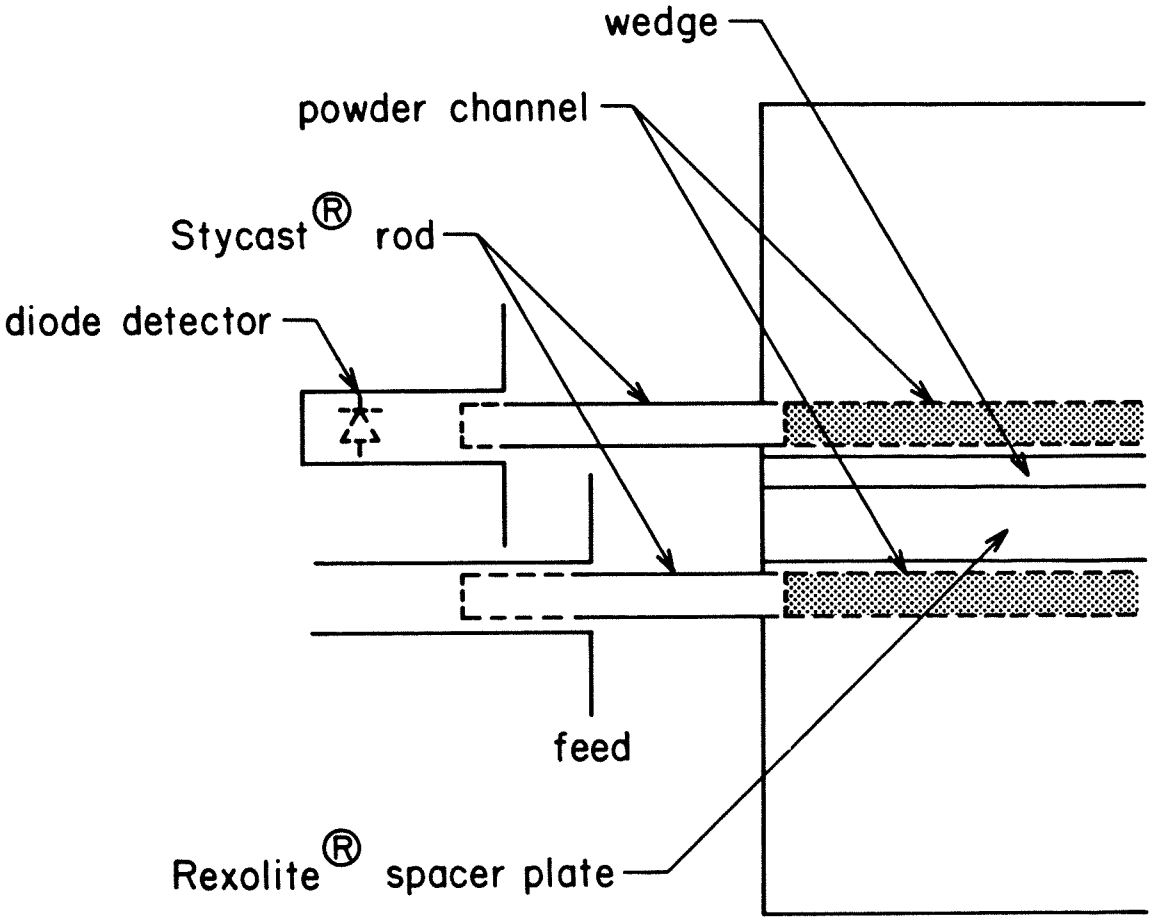


Figure IV-16: Top view schematic of the near end of the channel guide coupler during testing of the directivity

between 19.6 mm and 24.6 mm. This measurement is consistent with the theoretical prediction of directivity greater than 30 dB.

D. Analysis of results

Marcatili's theory predicts the coupling coefficient between a pair of identical parallel channel waveguides. We attempted to make the channel guides in the coupler as identical as possible by precision machining and powder packing. However, there were small differences in actual dimensions (1.22 cm x 1.20 cm versus 1.19 cm x 1.19 cm) and powder dielectric constant (4.19 versus 4.44), and we observed a small difference in $\beta$. To apply Marcatili's theory to our directional coupler, the dimensions and dielectric constants of the cores of the two channel waveguides were averaged to produce an 'average' channel waveguide. The coupling coefficient was then computed for a pair of parallel 'average' waveguides as a function of their separation distance. These values of coupling coefficient were then used in Miller's equations along with values of $2\alpha$ and $\Delta\beta$ to compute $P_1(z=30\text{ cm})$ and $P_2(z=30\text{ cm})$. As explained earlier, the value of $2\alpha$ used in Miller's equations equaled .017 $cm^{-1}$. The uncertainty in $2\alpha$ ($\pm$ .003 $cm^{-1}$) caused an uncertainty of $\pm$ 0.4 dB in the computed values of $P_1$ and $P_2$.

There was also uncertainty in the experimental value of $\Delta\beta$ used in Miller's equations. From the values of the propagation constants measured for the two channel guides in the absence of the Rexolite$^{R}$ covering plates (3.55 $cm^{-1}$ ± .04 $cm^{-1}$ and 3.63 $cm^{-1}$ ± .04 $cm^{-1}$), the true value of $\Delta\beta$ must have been between 0 and 0.08 $cm^{-1}$ for the uncovered guides. Since the addition of the plates was predicted by Marcatili's theory to cause virtually equal changes in the propagation constants of the two guides, the value of $\Delta\beta$ for the covered guides of the directional coupler was probably between 0 and 0.08 $cm^{-1}$.

Since $P_1(z=30cm)$ and $P_2(z=30cm)$ are quite sensitive to errors in $\Delta\beta$, curves of $P_1(z=30cm)$ and $P_2(z=30cm)$ versus the distance between the waveguides were plotted for several values of $\Delta\beta$ between 0 and 0.08 $cm^{-1}$ (Figs. IV-17 and IV-18). As shown, the theoretical $P_2$ curves (Fig. IV-18) did not coincide with the measured one to within the experimental error for any of the values of $\Delta\beta$. In particular, there is a clear difference in slope between the theoretical and measured $P_2$ curves. Since Miller's equations are well established, the discrepancy between the theoretical and measured results probably stems from inaccuracies in the theoretical values of the coupling coefficient. An error in the coupling coefficient had been anticipated because Marcatili's theory neglects coupling in the regions between the guides shown shaded in Figure IV-2. In addition, Marcatili's requirement of small refractive index differences was only

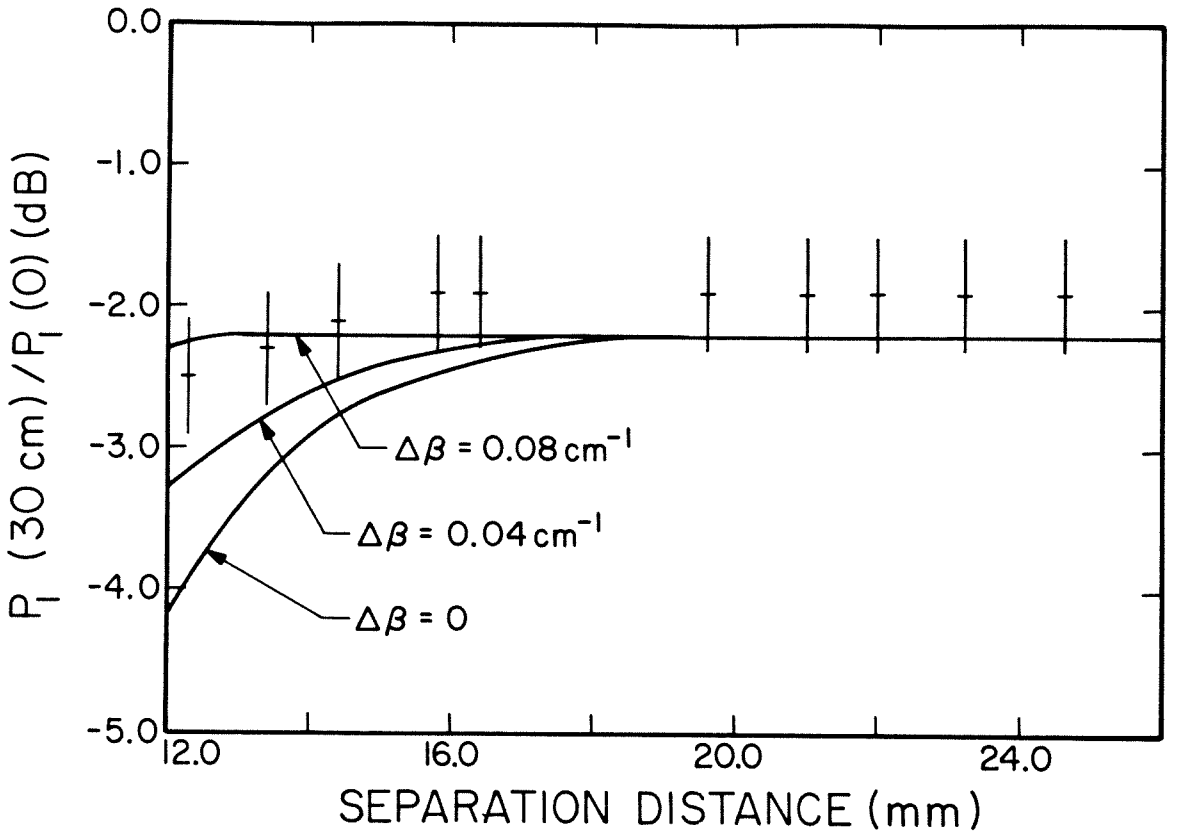


Figure IV-17: Power transmitted to the far end of the primary channel guide (relative to that coupled onto the near end) versus separation distance. The solid curves are theoretical results. The measured points have corrected for the 1 dB loss of the Stycast$^{R}$ rods

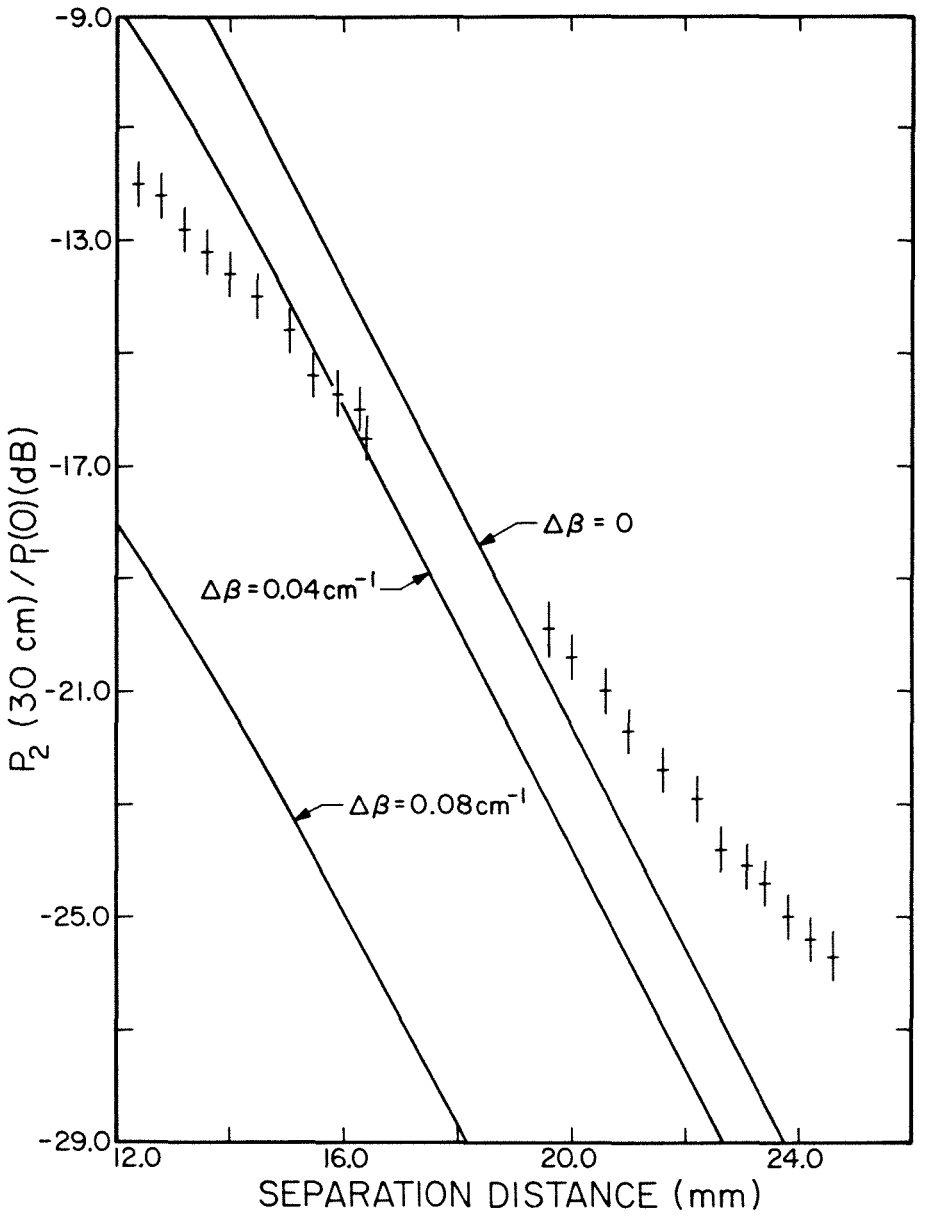


Figure IV-18: Power transmitted to the far end of the secondary channel guide (relative to that coupled onto the near end of the primary guide) versus separation distance. The solid curves are theoretical results. The measured points have been corrected for the 1 dB loss of the Stycast$^{R}$ rods.

marginally satisfied for our channel guides.

According to Marcatili's theory, the coupling coefficient, c, varies with the distance, d, between the guides as

$$c \propto \exp(-d/\xi_5).$$

(See page 51 for Marcatili's definition of $\xi_5$.)

This exponential dependence of the coupling coefficient on the inter-guide spacing results from the fact that the fields in Marcatili's analysis decrease exponentially with distance from the core. Since, for loose coupling, $c^2 << \Delta\beta^2$, Eqn. IV-2 for the theoretical value of $P_2$ reduces to

$$P_2(z)/P_1(0) = c^2\exp(-2\alpha z)\sin^2(\Delta\beta z)/\Delta\beta^2,$$

the theoretical $P_2$ values decrease exponentially with distance between the guides as

$$P_2 \propto \exp(-2d/\xi_5).$$

The measured $P_2$ values also decrease exponentially with distance between the guides, but the decay constant is only about half the theoretical value. The measured decay constant for $P_2$ is $2.60 \pm 0.16$ $cm^{-1}$ and the theoretical one is $4.56$ $cm^{-1}$. Thus, the coupling coefficient for our channel guide coupler decreased exponentially with guide spacing with only about half the decay constant predicted by Marcatili's theory.

As is apparent from Figs. IV-17 and IV-18, the parallel channel guides functioned as a coupler with adjustable coupling. As the

separation distance was increased from 12.0 mm to 16.4 mm, the coupling decreased from -8.5 dB ± 0.8 dB to -14.6 dB ± 0.8 dB. For separation distances from 19.6 mm to 24.6 mm, the coupling decreased from -18.0 ± 0.8 dB to -23.8 ± .08 dB. The insertion loss remained within 0.2 dB of the value of 1.9 dB ± 0.8 dB over both ranges of separation distance.

As discussed earlier, the power available from the near end of the secondary channel guide was not determined, so the directivity of the coupler is unknown. From our measurements, we can give only a lower bound on the directivity, equal to 9 dB for a separation of 19.6 mm and decreasing to 3 dB at 24.6 mm. However, since $\Delta\beta$ would be large for two oppositely directed waves, the true directivity was probably much greater than these limiting values.

REFERENCES

IV-1. E.A.J. Marcatili, 'Dielectric rectangular waveguide and directional coupler for integrated optics,' Bell System Technical Journal, Vol. 48, Sept. 1969, pp. 2079-2132.

IV-2. S.E. Miller, 'Coupled wave theory and waveguide applications,' Bell System Technical Journal, Vol. 33, No. 3, May 1954, pp. 661-719.

IV-3. A.R. von Hippel, DIELECTRIC MATERIALS AND APPLICATIONS, John Wiley, New York, 1958, pp. 327-328.

IV-4. Roberts and A.R. von Hippel, 'A new method for measuring dielectric constant and loss tangent in the range of centimeter waves,' J. Appl. Phys., Vol. 17, July 1946, pp. 610-616.

# APPENDIX I. SOLIDS WITH LARGE DIELECTRIC CONSTANT AND LOW LOSS AT MILLIMETER WAVE FREQUENCIES

The first step toward making powder-core millimeter wave dielectric waveguides is to find a suitable powder. Since millimeter wavelengths are comparable to the physical dimensions of the guides, the effective dielectric constant of the powder core must be significantly greater than that of the cladding for the fields to be tightly confined. Since our cladding materials were TFE Teflon$^{R}$ and polypropylene, powders were required to have effective dielectric constants much larger than 2 to serve as practical core materials. Such powders are obtained from solid materials with dielectric constants of roughly 20 or more. The solid must also have moderately low loss. Unfortunately, the number of materials whose millimeter wave dielectric properties have been measured is relatively few (Ref. AI-1 gives an index to the literature on millimeter wave properties of materials as of 1982) and none of these appeared to be suitable for our purposes. This appendix describes our search for suitable materials.

There are three different mechanisms which can contribute to electric polarization in a homogeneous solid:

(1) The tendency of molecules possessing permanent dipole moments to align with the direction of an applied electric field results in dipolar polarizability.

(2) Relative displacement of ions results in ionic polarizability.

(3) Displacement of electrons relative to the nucleus results in electronic polarizability.

In most cases, the dipolar and ionic polarizabilities are not both large in the same substance (Ref. AI-2).

Each of the polarization mechanisms is frequency-dependent. For sufficiently low frequency, a particular mechanism can easily follow the applied field. It thus contributes to the real part of the dielectric constant but not to the imaginary part. At higher frequencies it begins to lag the applied field, resulting in dielectric loss. At even higher frequencies, the field alternates too fast for the mechanism to respond and there is no contribution to either the real or the imaginary part of the dielectric constant. The electronic and ionic mechanisms typically respond up to the ultraviolet and infrared regions, respectively (Ref. AI-2). Dipolar relaxation in solids occurs at lower frequencies. Often there are several different dipolar relaxation mechanisms present in a single polar material, giving rise to absorption over a wide range of frequencies (Refs. AI-3 and AI-4). Nylon, for example, has a broad absorption band which extends from below 100 Hz up to microwave frequencies (Refs. AI-5 and AI-6).

Since the frequencies typically characterizing dipolar relaxation in polar solids were too low, we focused our search on solids with large ionic and electronic polarizabilities. We found that several ionic compounds possessing structures of the perovskite family have very large dielectric constants and low loss at microwave frequencies (Refs. AI-5 and AI-7). Most perovskites have the chemical formula $ABO_3$ (Refs. AI-8 and AI-9). Some examples are: $SrTiO_3$, $SrZrO_3$, $BaZrO_3$, $BaTiO_3$, $KTaO_3$, and $CaTiO_3$. Many of them are ferroelectric in certain temperature regions (Refs. AI-8 through 10).

The extreme dielectric properties of the perovskites are related to their crystal structures. In particular, they possess one or more optical branch vibrational modes which can be very strongly excited by an applied electric field (Ref. AI-10). The amplitude of vibration of these modes is large because the local electric field caused by the electric polarization counteracts the harmonic restoring forces on the ions. Such large motion(s) accounts for the high polarizability of the perovskites (Refs. AI-10 and AI-11). In strontium titanate ($SrTiO_3$), for example, the crystal structure contains lines of alternating $Ti^{4+}$ and $O^{2-}$ ions. An electric field applied parallel to these lines excites a strong vibration of the $Ti^{4+}$ ions against the $O^{2-}$ ions (Ref. AI-10). In some perovskites, at sufficiently low temperature, the forces on the ions due to the polarization are stronger than the harmonic restoring forces. The crystal then becomes

distorted, giving rise to a spontaneous electric polarization (i.e., ferroelectricity) (Refs. AI-10 through 12).

We became curious whether there might be simple metal oxides other than perovskites which could be useful to us. We found that Trans-Tech sells several metal oxide ceramics in solid form as high dielectric constant, low-loss microwave materials. Some of these materials, barium tetratitanate ($BaTi_4O_9$), magnesium-calcium titanate, and nickel-aluminum titanate, were acquired in powder form and tested. Their effective dielectric constants were sufficiently high and their losses sufficiently low at 94 GHz to serve as core materials for dielectric waveguides.

In the future, it would be interesting to try paraelectric perovskites such as strontium titanate as core media for 94 GHz dielectric waveguides. Since their microwave dielectric constants (Refs. AI-5 and AI-7 ) are much larger than those of the materials we obtained from Trans-Tech, they could be advantageous for waveguide applications requiring tight field confinement, provided their dielectric absorption is not too high. The loss tangent of solid strontium titanate ceramic has been reported to be .0028 at 10 GHz (Ref. AI-5), not greatly different from that of solid magnesium-calcium titanate, which Trans-Tech gives as 0.002 at 6 GHz.

REFERENCES

AI-1. G.J. Simonis, 'Index to the literature dealing with the near-millimeter wave properties of materials,' International Journal of Infrared and Millimeter Waves, Vol. 3, No. 4, July 1982, pp. 439-469.

AI-2. C. Kittel, INTRODUCTION TO SOLID STATE PHYSICS, John Wiley, New York, 1956, Chapter 7.

AI-3. R.H. Cole, 'Theories of dielectric polarization and relaxation,' in PROGRESS IN DIELECTRICS, Vol.3, ed. J.B. Birks, John Wiley, New York, 1961, pp. 47-99.

AI-4. R.J. Meakins, 'Mechanisms of dielectric absorption in solids,' in PROGRESS IN DIELECTRICS, Vol. 3, ed. J.B. Birks, John Wiley, New York, 1961, pp. 151-202.

AI-5. A.R. von Hippel, DIELECTRIC MATERIALS AND APPLICATIONS, John Wiley, New York, 1958, pp. 301-370.

AI-6. G.W. Chantry, J.W. Fleming, and G.W.F. Pardoe, 'Absorption spectra of polypropylene in the millimetre and submillimetre regions,' Infrared Physics, Vol. 11, 1971, pp. 109-118.

AI-7. R.C. Kell, A.C. Greenham, G.C.E. Olds, 'High-permittivity temperature-stable ceramic dielectrics with low microwave loss,' Journal of the American Ceramic Society, Vol. 56, No. 7, July 1973, pp. 352-354.

AI-8. H.D. Megaw, FERROELECTRICITY IN CRYSTALS, Methuen, London, 1957, pp. 83-123.

AI-9. F. Jona and G. Shirane, FERROELECTRIC CRYSTALS, MacMillan, New York, 1962, pp. 216-261.

AI-10. A.S. Barker, 'Infrared dielectric behavior of ferroelectric crystals,' in FERROELECTRICITY, ed. E.F. Weller, Elsevier, New York, 1967, pp. 213-250.

AI-11. A.S. Barker and M. Tinkham, 'Far-infrared ferroelectric vibration mode in $SrTiO_3$,' Physical Review, Vol. 125, No. 3, March 1962, pp. 1527-1530.

AI-12. C. Kittel, INTRODUCTION TO SOLID STATE PHYSICS, John Wiley, New York, 1956, pp. 192-194.

# APPENDIX II. EFFECT OF GRANULARITY ON PLANE WAVE PROPAGATION

## Introduction

Since the central theme of this thesis is that dielectric materials in powder form are useful as core materials for low-loss dielectric waveguides, a discussion of electromagnetic wave propagation in granular materials is appropriate. These theories fall roughly into two groups. Those in the first group attempt only to find the effective dielectric constant of the powder (assumed to be real). The other group of theories is more comprehensive and attempts to determine the scattering and absorption coefficients for plane wave propagation as well. The discussion here treats these two groups separately. Theories which predict only the effective dielectric constant are discussed in Part A. Those which also deal with scattering and attenuation losses are the subject of Part B.

## A. Effective dielectric constant

### Introduction

The group of theories which attempt to find only the effective dielectric constant of a powder share in common the assumption that the frequency is zero (Refs. AII-2 through AII-9 and AII-12 through

AII-18). However, under certain conditions discussed later, they can be applied when the frequency is not zero.

To find the effective dielectric constant, the powder is visualized as filling the space between the plates of an infinitely large parallel plate capacitor. A uniform dc electric field is maintained between the plates. The average polarization (average dipole moment per unit volume) of the powder is then found in terms of the electric field between the plates.

A rigorous derivation is difficult because the polarization of any individual particle depends not only on the imposed field, but also on the polarization of all the other particles. In order to account for these mutual polarization effects, the positions, shapes, sizes, and orientations of all particles must be known. In every theory it is assumed that all the particles have an identical ellipsoidal or spherical shape and identical size. Nevertheless, since their orientations and positions are not known, the mutual effects must be treated either by using simplifying assumptions (Refs. AII-2 through AII-8, AII-17, AII-18) or statistical methods (Refs. AII-9, AII-12 through AII-16, AII-19, AII-21 through AII-26). The simpler theories will be discussed first.

## 1. Simple theories of effective dielectric constant

The simple theories treat a powder composed of particles of a homogeneous, isotropic, lossless dielectric material (referred to hereafter as material 1) by focusing on an individual particle of that material. The particle is visualized as being surrounded not by other particles, but by a homogeneous, isotropic, and lossless dielectric medium. Various authors ascribe different values to the dielectric constant of the hypothetical surrounding medium, but it is always assumed to be between that of empty space ($\varepsilon_r = 1$) and the effective dielectric constant of the powder. The next step is to find the local electric field at the position of the particle in terms of the average, or macroscopic, electric field. Authors disagree on how to express the local electric field in terms of the average field, but the local field is always assumed to be uniform over the volume of the particle. After deriving an expression for the local electric field in terms of the average field, the particle's polarization is found in terms of the average electric field using a well-known formula (Ref. AII-1) for an ellipsoidal dielectric in a uniform static applied field. Since the polarization of every particle is assumed to be equal, the average polarization of the powder is given by multiplying the polarization of a single particle by the volume fraction of material 1. Having finally found the average polarization in terms of the average electric field, the effective dielectric constant is

obtained using

$$D = \varepsilon_0 E + P \qquad \text{and} \qquad D = \varepsilon_0 \varepsilon_r E.$$

Many theories have been proposed which use the basic argument given above. The more widely known ones will be discussed here. Some of these, such as the formula of Clausius and Mossoti (Ref. AII-2), work well for dilute mixtures like non-polar gases, but are of limited value when the inhomogeneities are densely packed, as in a powder. Many such theories which work only for dilute mixtures make the assumption that the hypothetical homogeneous surrounding medium used in the derivation of the polarization of a typical particle has a dielectric constant equal to that of empty space. On the other hand, several of the theories which are useful for dense mixtures assume that the dielectric constant of the hypothetical surroundings is equal to the effective dielectric constant of the mixture.

A few of the more well-known formulas for the effective dielectric constant of a powder are given below. Throughout, the volume fraction occupied by the particulate matter (material 1) is denoted by f, the relative effective dielectric constant of the mixture by $\varepsilon_r$, and the relative dielectric constant of solid material 1 by $\varepsilon_1$.

The formula of Clausius and Mossoti is probably the first one to be used for random heterogeneous media (examples of such are gases,

liquids, and powders). For spherical particles, the formula is

$$(\varepsilon_r - 1)/(\varepsilon_r + 2) = f(\varepsilon_1 - 1)/(\varepsilon_1 + 2).$$

It can be derived in the way described above by assuming that the dielectric constant of the hypothetical surroundings is equal to that of empty space.

Bottcher (Ref. AII-3) has proposed that the effective dielectric constant of a powder composed of spherical particles is given by

$$(\varepsilon_r - 1)/(3\varepsilon_r) = f(\varepsilon_1 - 1)/(\varepsilon_1 + 2\varepsilon_r).$$

He assumes that the dielectric constant of the hypothetical surroundings is equal to the effective dielectric constant of the powder.

Another formula, derived by Bruggeman (Ref. AII-4), for a powder composed of spherical particles is

$$(\varepsilon_r)^{1/3}(1 - f) = (\varepsilon_1 - \varepsilon_r)/(\varepsilon_1 - 1).$$

In his derivation, Bruggeman initially assumes that f is very small and that the dielectric constant of the hypothetical surroundings is equal to that of free space. He then calculates the effective dielectric constant for larger values of f by the imaginary process of gradual addition of particles of material 1.

Using a derivation very similar to Bruggeman's, Landau and Lifshitz (Ref. AII-6) and also Looyenga (Ref. AII-7) have obtained yet another

formula for a powder composed of spherical particles. The difference between their derivation and Bruggeman's is the theoretical increase in $\varepsilon_r$ caused by an infinitesimal increase in f (i.e., the form of $d\varepsilon_r/df$ used in the two derivations is different.) The Landau-Lifshitz, Looyenga formula is

$$f(\varepsilon_1^{1/3} - 1) = \varepsilon_r^{1/3} - 1.$$

Figure AII-1 shows theoretical curves of effective dielectric constant versus the volume fraction of particulate matter for particles composed of a material with a relative dielectric constant of 9.0 ($Al_2O_3$). The formulas of Clausius and Mossoti, Bottcher, Bruggeman, and Looyenga for spherical particles are each represented.

Several authors have also proposed formulas for powders composed of ellipsoidal particles. The formula of Polder and Van Santen (Ref. AII-8) is valid for randomly oriented ellipsoidal particles of general shape. For randomly oriented, prolate ellipsoids (needles), van Beek (Ref. AII-5) has derived the following formula:

$$\varepsilon_r = 1 + f(\varepsilon_1 - 1)(5\varepsilon_r + \varepsilon_1)/(3(\varepsilon_r + \varepsilon_1)).$$

Finally, Bruggeman (Ref. AII-4) has derived a formula for randomly oriented, oblate ellipsoids by the same method he used for spherical particles. Known as Bruggeman's equation for 'disks', it is

$$\varepsilon_r = \varepsilon_1(3 + 2f(\varepsilon_1 - 1))/(3\varepsilon_1 - f(\varepsilon_1 - 1)).$$

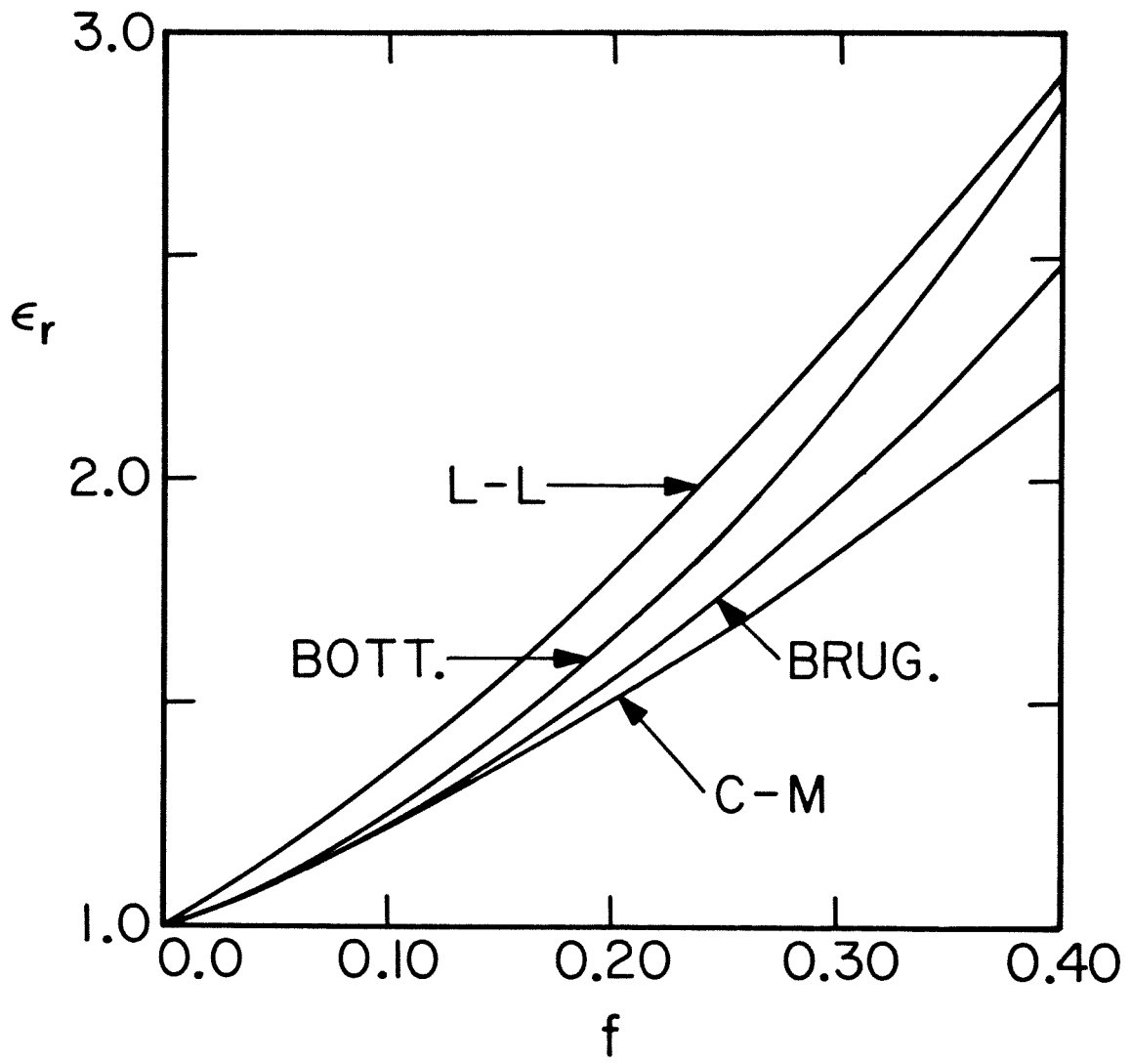


Figure AII-1: Theoretical curves of power effective dielectric constant versus volume fraction for particles composed of a material with a dielectric constant of 9.0 ($Al_2O_3$). The formulas of Clausius and Mossoti, Bottcher, Bruggemann, and Looyenga for spherical particles are each represented.

## 2. Statistical theories of effective dielectric constant

A few authors have attempted more sophisticated treatments of mutual polarization effects using statistical correlation functions to describe the relative positions of the particles. The correlation functions are found using the methods of statistical mechanics. One of the first such attempts was made by Kirkwood (Ref. AII-9). Although Kirkwood's theory was originally intended for dense gases and liquids, it can also be applied to powders. Successive authors have tried to improve upon it in various ways (Refs. AII-12 through 17), but the value of these modifications has not yet been demonstrated. Hence, Kirkwood's remains the best known of the statistical theories of effective dielectric constant of random heterogeneous media. A brief description of Kirkwood's method is given below.

The polarization, $p_i$, of molecule i is expanded in an infinite series.

$$p_i = p_{0i} + p_{1i} + p_{2i} + \cdots$$

$p_{0i}$ represents the contribution to $p_i$ due to the applied electric field and $p_{1i}$ is that due to the polarizations $p_{0j}$ induced in the other molecules by the applied field. $p_{2i}$ is the contribution from the polarizations $p_{1j}$ in the other molecules, etc. $p_i$ is then averaged over all possible configurations of the N molecules, yielding

$$\langle p_i \rangle = \langle p_{0i} \rangle + \langle p_{1i} \rangle + \langle p_{2i} \rangle + \cdots$$

In order to find $\langle p_{1i} \rangle$, $\langle p_{2i} \rangle$, ..., the 2-particle, 3-particle, etc., correlation functions are needed. An approximate expression for the 2-particle correlation function is found using the dilute gas approximation (Ref. AII-10), treating the molecules as hard spheres. Next, the superposition approximation (Ref. AII-11) is used to express the 3-particle correlation function in terms of the 2-particle function. Terms in the expansion of $\langle p_i \rangle$ involving correlations between more than 3 particles are dropped. Finally, assuming $\langle p_i \rangle$ to be the same for any i, the polarization of the medium and hence the effective dielectric constant are readily found.

Felderhof et al. (Refs. AII-15 and 16) have also given an expansion for the effective dielectric constant of a powder composed of spherical particles. As in Kirkwood's theory, successive terms in the expansion involve particle correlation functions of successively higher order. Felderhof retains one less term in the expansion than Kirkwood, dropping those which include correlations of three or more particles. The 2-particle correlation function is the same as that used by Kirkwood.

Felderhof (Refs. AII-12 through 14) has also calculated bounds on the effective dielectric constant of a powder composed of spherical particles. The bounds are expressed as expansions, and again successive terms involve correlation functions of successively higher

order. Terms containing correlation functions of order 3 or less are retained. The correlation functions used here are more sophisticated than those obtained with the dilute gas approximation.

## 3. Comparison of the theories to experiment

In this section the previously discussed theories of effective dielectric constant are compared to experiment in order to assess their respective ranges of validity. The measured values of effective dielectric constant used in the comparisons come both from the literature and from our own measurements. All of these empirical data were measured at non-zero frequencies.

Although the theories of effective dielectric constant presented above were derived assuming static fields, they hold at all frequencies for which certain conditions are satisfied. The first condition is that the dielectric material of which the particles are composed must be low-loss. The second condition is that the particles must be small compared to the wavelength in the dielectric material ($(n_1 kd/2) \ll 1$, where $n_1$ is the refractive index of the material, k is the free space wavenumber, and d is a typical dimension of the particle.). This requirement insures that the polarization throughout the particle will be in phase with the excitation and that the incident electric field is uniform over the extent of the particle.

The utility of the various formulas for predicting the effective dielectric constant of powders depends on the volume fraction (f) and on the dielectric constant of the material of which the particles are composed ($\varepsilon_1$). For loosely packed powders (f < .3) of material with low dielectric constant ($\varepsilon_1$ < 5), all the theories give reasonably accurate results. As $\varepsilon_1$ and f increase, the theories begin to disagree with experiment. For tight packing and high dielectric constant material, none are accurate.

The formulas of Kirkwood, Felderhof, and Clausius and Mossoti give very similar values. As f and $\varepsilon_1$ increase, these theories disagree with experiment sooner than the others. As shown in Table AII-1, they are significantly in error for $\varepsilon_1$ = 9. The range of agreement of Bruggeman's formula is slightly better than these. Bottcher's formula is more reliable at higher volume fractions and dielectric constants than Bruggeman's, while the Landau-Lifshitz, Looyenga formula is the best of all. Unfortunately, none of the formulas are accurate for tightly packed, high dielectric constant powders such as the ones we have used for making millimeter wave dielectric waveguides (see Table AII-2).

Each material shown in Tables AII-1 and AII-2 is low-loss at the frequency at which the effective dielectric constant was measured. The condition ($(n_1 kd/2) << 1$) is also satisfied for all the powders at

TABLE AII-1

Comparison of experimental values of effective dielectric constant to theoretical values predicted by the Clausius-Mossoti, Bottcher, and Landau-Lifshitz formulas.

| Material | Volume Fraction | $\varepsilon_1$ | $\varepsilon_{rmeas.}$ | $\varepsilon_{C-M}$ | $\varepsilon_{Bott.}$ | $\varepsilon_{L-L}$ |
|---|---|---|---|---|---|---|
| KCl | .253 | 4.84 | 1.65 | 1.50 | 1.57 | 1.62 |
| KCl | .350 | 4.84 | 1.89 | 1.73 | 1.88 | 1.92 |
| KCl | .522 | 4.84 | 2.46 | 2.24 | 2.54 | 2.52 |
| $Z_nO$ | .095 | 8.7 | 1.34 | 1.22 | 1.24 | 1.33 |
| $Al_2O_3$ | .296 | 9.0 | 2.33 | 1.82 | 2.15 | 2.30 |
| $Al_2O_3$ | .380 | 9.0 | 2.86 | 2.15 | 2.72 | 2.81 |
| $S_rO$ | .313 | 13.30 | 3.21 | 2.01 | 2.64 | 2.92 |
| $S_rO$ | .344 | 13.30 | 3.51 | 2.15 | 2.95 | 3.18 |

Data were taken from references AII-17 and AII-18 except for $Z_nO$. The effective dielectric constant of $Z_nO$ powder was measured at 10 GHz by the shorted-waveguide technique. The bulk dielectric constant, $\varepsilon_1$, for $Z_nO$ is from Ref. AII-28.

The values of $\varepsilon_1$ and $\varepsilon_{rmeas.}$ were measured at frequencies between 9.4 and 10 GHz, except for $\varepsilon_1$ of $Z_nO$ for which the precise (microwave) frequency of measurement is unknown.

For every powder except $Z_nO$, the particles ranged in size from 50 μm to 150 μm. The size of the $Z_nO$ particles is estimated to be less than 50 μm.

TABLE AII-2

Comparison of experimental values of effective dielectric constant to theoretical values predicted by the Clasius-Mossoti, Bottcher, and Landau-Lifshitz formulas.

| Material | Volume Fraction | $\varepsilon_1$ | $\varepsilon_{rmeas.}$ | $\varepsilon_{C-M}$ | $\varepsilon_{Bott}$ | $\varepsilon_{L-L}$ |
|---|---|---|---|---|---|---|
| D-30 | .396±.005 | 31.0 | 3.76 | 2.69 | 5.93 | 6.31 |
| D-8512 | .400±.005 | 38.6 | 4.47 | 2.77 | 7.01 | 7.44 |
| MCT-40 | .318±.003 | 40.0 | 3.28 | 2.26 | 4.28 | 5.54 |
| MCT-40 | .470±.003 | 40.0 | 5.43 | 3.32 | 10.42 | 9.76 |

The listed values of $\varepsilon_1$, the relative dielectric constant of the bulk material, were measured at various frequencies between 6 GHz and 10 GHz by Trans-Tech. Trans-Tech gives the uncertainty in these measurements as 5% for D-30 and MCT-40 and 1.5% for D-8512.

The empirical values of powder effective dielectric constant, $\varepsilon_{rmeas.}$, were measured at 10 GHz by the shorted-waveguide technique. The uncertainty in these values is ± .03.

the measurement frequency. The powders were composed of particles with roughly spherical shapes.

Microscopic examination showed that for each of the powders in Table AII-2, the majority of the particles were about the same size (43 μm). However, most of the powders represented in Table AI-1 contained particles of various sizes in the range 50-150 μm and the distribution of sizes within this range was different for each powder. Nevertheless, the accuracies of the formulas (for spherical particles) for effective dielectric constant appear to depend mainly on the bulk dielectric constant, $\varepsilon_1$, and the volume fraction, f, of these powders, as shown in Table AII-1 (see also Refs. AII-17 and AII-18). The validity of the formulas appears to be independent of the particle size distribution, provided all particles are small. This behavior is to be expected from the theories for spherical particles since they calculate the polarization (dipole moment per unit volume) of a single particle and then multiply by the volume fraction to obtain the average polarization of the powder. The polarization of a sphere in a uniform field is independent of its diameter.

## 4. Summary

Since theoretical guide wavelengths of dielectric waveguides calculated with the dielectric constant data measured by the

shorted-waveguide technique for our powders agreed well with measured values (c.f. Chap. I and Chap. II), we are confident of the accuracy of the shorted-waveguide technique for measuring the dielectric constants of powders. Moreover, since none of the theoretical values of effective dielectric constant agreed with our measured values for tightly packed, high dielectric constant powders, we conclude that the theories are not useful for such powders.

## B. Scattering and absorption

### Introduction

In this section we discuss the theories which treat scattering and absorption in granular material. Propagation of electromagnetic waves in random heterogeneous media is an old subject, dating back to Rayleigh's paper on scattering by gas molecules (1871). However, theories concerning propagation in powders are relatively new. The reason for their late development is that propagation in a powder is a complex problem involving multiple and dependent scattering.

Dependent scattering occurs when the positions of the scatterers are correlated, causing a systematic phase relationship to exist between the waves scattered from different particles. To calculate

the total scattering, the amplitudes of the individual scattered waves must be added, taking phases into account. In contrast, most theories treat dilute concentrations of scatterers where the particles are so far apart that their positions can be considered uncorrelated. In these cases, no systematic phase relationship exists between the individual scattered waves, and their intensities can be added to give the total scattered intensity. Wave propagation in powders must be treated as a dependent scattering problem because the particle positions show short-range order.

Multiple scattering occurs when the particle excitation contains a significant contribution from waves scattered by other particles and is thus not equal to the incident wave excitation alone. If these scattered waves add incoherently, the problem is one of independent multiple scattering, often called radiative transfer. If they add coherently, as in a powder, the scattering is both dependent and multiple.

Most scattering theories concern dilute, weakly scattering media for which a single scattering treatment is appropriate. In single scattering, the total scattered intensity is found by multiplying the scattered intensity of one particle by the total number of particles. Only a relatively few theories treat the more difficult case of dependent multiple scattering appropriate to powders.

## 1. Theories for powders

Recently, attempts have been made to derive formulas predicting propagation constants for electromagnetic waves in powders consisting of identical particles (Refs. AII-19 through 25). The various theories are quite similar, and an outline of their general approach is given below.

The powder medium is viewed as filling an infinite half-space with a plane wave normally incident upon it. The total field inside the powder is given by the incident wave plus the sum of all waves radiated by individual particles. The field exciting a given particle is the sum of the incident wave and the waves radiated from the other particles. Thus, the radiation from each particle depends on that from every other particle. In order to find the wave scattered by any one particle, the positions and orientations of every other particle must be known. However, for a real powder, the particle positions and orientations are uncertain.

The problem of not knowing the particle positions and orientations can be overcome by averaging the fields over all possible configurations of the particles. To do this, however, one needs the joint probability density describing the positions and orientations of all the particles. Knowledge of this joint density function is

equivalent to possessing the N-particle correlation functions of all orders. Unfortunately, methods for finding correlation functions of more than 3 particles do not exist currently. As a result, authors use the quasi-crystalline approximation (Ref. AII-26) to allow calculation of approximate averages with knowledge of only the 2-particle correlation function. The two particle correlation function is often found using the Percus-Yevick equation (Ref. AII-27), treating the particles as hard spheres.

To find the effective propagation constant, the quasi-crystalline approximation is used to write an integral equation for the configurational average of the field exciting an individual particle. Next, the exciting field is expanded in vector spherical wave functions. The expansion is truncated after an arbitrary, but large, number of terms. A trial solution is assumed and after much simplification a system of linear homogeneous equations is generated for the unknown coefficients in the expansion. An implicit equation for the effective propagation constant is found by setting the secular determinant of this system to zero.

The equation yielding the effective propagation constant is quite cumbersome and requires numerical solution. However, when the particles are small compared to the wavelength ($n_1'ka \ll 1$, where $n_1'$ is the real part of the refractive index of the particle material, k

is the free space wave number, and a is the particle radius), the equation for the effective propagation constant reduces to a much simpler form given by both Twersky (Ref. AII-20) and Tsang and Kong (Ref. AII-22).

For small spherical particles, the real part of the effective propagation constant is

$$\beta = n_{eff}k,$$

where

$$n_{eff} = (1 + 2\xi_0/(1 - 2\xi_0/3))^{1/2} \qquad \text{(AII-1)}$$

and

$$\xi_0 = (3/2)f((n_1')^2 - 1)/((n_1')^2 + 2).$$

The imaginary part of the propagation constant, $\alpha$, can be decomposed into a contribution from scattering and a contribution from absorption.

$$\alpha = \alpha_s + \alpha_a.$$

The term due to scattering, $\alpha_s$, is

$$\alpha_s = SW/(2n_{eff}(1 - 2\xi_0/3)^2), \qquad \text{(AII-2)}$$

where

$$S = 2fk^4a^3((n_1')^2 - 1)^2/((n_1')^2 + 2)^2$$

and

$$W = (1 - f)^4/(1 + 2f)^2.$$

Note that the scattering loss $\alpha_s$ varies as the cube of the particle

radius, as in Rayleigh scattering. The contribution to $\alpha$ due to absorption is

$$\alpha_a = A/(2n_{eff}(1 - 2\xi_0/3)^2), \qquad \text{(AII-3)}$$

where

$$A = 18fkn_1'n_1''/((n_1')^2 + 2)^2.$$

Here $n_1''$ is the imaginary part of the refractive index of the particle material. Note that $\alpha_a$ is independent of the particle radius, a.

The differences between values predicted with Equations AII-2 and AII-3 and those obtained with the full equation for particles of arbitrary size remain small until $n_1'ka$ approaches $\pi/2$. When this condition occurs, the particles are about one-half wavelength long and can support internal standing waves. As a result, absorption losses become much larger than predicted by Equations AII-2 and AII-3.

## 2. Comparison to experiment

The loss predictions of the theory presented above show good agreement with experiment for low ($\varepsilon_1 = 2.5$) dielectric constant particles (Ref. AII-24). However, as far as we know, the predicted losses have never been compared to experiment for powders with large $\varepsilon_1$ such as we have used for making dielectric waveguides. The theoretical values of effective dielectric constant will agree with

experiment only when the dielectric constant of the bulk material ($\varepsilon_1$) is low because the effective dielectric constant predicted by these scattering theories is identical to that given by the Clausius-Mossoti formula for spherical particles (discussed in Sec. A). We know that formula is inadequate for large $\varepsilon_1$, so it is reasonable to conclude that the theoretical attenuation constants $\alpha_s$ and $\alpha_a$ will likewise be inaccurate when $\varepsilon_1$ is large. Nevertheless, these theories are all we have, so we attempt to use them to predict the losses of our powders due to scattering.

To calculate the theoretical scattering losses, the particle sizes were needed. For the D-8512 and MCT-40 powders and for one batch of D-30 powder, the manufacturer (Trans-Tech) specified that all particles were less than 43 μm in size. Microscopic examination of these powders showed that most of the particles were the same size, presumably about 43 μm wide. For the other batch of D-30 powder used in our experiments, 70% of the particles were between 100 μm and 43 μm, and the rest were smaller than 43 μm. Since the theory assumes that all particles of a powder are the same size, the theoretical scattering predictions were computed using 43 μm and 100 μm as the respective particle diameters of the two sets of powders. These choices give the most pessimistic (largest) values of $\alpha_s$. Even so, the theoretical values of $\alpha_s$ at 94 GHz were less than $10^{-4}$ $cm^{-1}$ for the smaller grain powders and $10^{-3}$ $cm^{-1}$ for the coarse D-30 powder for

all appropriate values of f. These values of $\alpha_s$ are negligible compared to the measured attenuation constants of our 94 GHz powder core guides, which were greater than or equal to $10^{-2}$ $cm^{-1}$.

The question of accuracy notwithstanding, we are unable to use the scattering theory to make estimates of $\alpha_a$ values expected for powder core dielectric waveguides since the loss tangents of the materials of which the powders are composed are unknown at 94 GHz. However, the reverse process is possible. Estimates of the bulk loss tangents of these materials can be obtained from the theory using measured losses for powder core waveguides. These estimates are crude, not only because of the expected inaccuracy of the theory for large $\varepsilon_1$, but also because the theory applies to plane waves, not modes of dielectric waveguides.

Estimates of the loss tangent values at 94 GHz of bulk D-8512, MCT-40, and D-30 are given in Table AII-3. The waveguide loss data used to compute these estimates were measured for the $E^y_{11}$ mode of rectangular powder core dielectric waveguide far from cut-off. The powder effective loss tangents are also given in Table AII-3 for comparison. These values were obtained from the measured waveguide losses using the extension of Marcatili's theory explained in Chapter II.

TABLE AII-3

Bulk Loss Tangent Values

| Material | Waveguide Loss (dB/cm) | Powder Effective Loss Tangent | Estimated Bulk Loss Tangent at 94 GHz | Manufacturer's Values of Bulk Loss Tangent |
|---|---|---|---|---|
| D-8512 | 0.17 | .0012 | .018 | < 0.0005 |
| MCT-40 | 0.18 | .0016 | .020 | < 0.002 |
| D-30* | 0.17 | .0010 | .010 | < 0.0002 |
| D-30** | 0.49 | .0023 | .025 | < 0.0002 |

*100% of particles smaller than 43 μm.

**70% of particles between 43 μm and 100 μm, 30% less than 43 μm.

The manufacturer's values of bulk loss tangent were quoted at 6 GHz for D-8512 and MCT-40, and at 10 GHz for D-30.

The most noteworthy point about these estimates is that the loss tangents predicted for the bulk materials are much higher than the effective loss tangents of the respective powders. This relationship indicates that low-loss dielectrics can be obtained by grinding moderately lossy materials into powders. Of course, the effective dielectric constant of the powder will be lower than that of the original bulk material.

Another interesting result is that two quite different values of loss tangent were predicted for bulk D-30 based on waveguide loss measurements using two different batches of powder. Since we have already seen that theory predicts that scattering accounts for a negligible fraction of the total measured propagation loss, the difference in the measured propagation losses associated with the two batches of D-30 must be attributed to greater absorption for the coarser powder, as evidenced by the higher computed value of loss tangent for the bulk D-30 material. (It could be that the bulk D-30 from which one batch was made was substantially more lossy than for the other batch.) Contamination is a possibility. We do not know of any reasons by which the large range of particle size present in the coarser powder could be expected to cause the extra absorption.

## 3. Summary

In Chapter II, effective loss tangents of powders were computed using an extension of Marcatili's theory. The computed values increased as the packing fraction increased. The theories reviewed above predict this same behavior. For powders with particle size, $\varepsilon_1$, and f similar to those used in our waveguide experiments, theoretical scattering losses decrease with increasing f and should be negligible, but absorption losses increase. For practical high dielectric constant powders (i.e., ones obtained from bulk materials with loss tangents greater than .001 at 94 GHz), absorption dominates, causing the effective loss tangent to increase as the packing fraction increases.

References

AII-1. J.A. Stratton, ELECTROMAGNETIC THEORY, McGraw-Hill, New York, 1941.

AII-2. C.J.F. Bottcher, THEORY OF ELECTRIC POLARIZATION, Elsevier Publishing Company, New York, 1952, pp. 199-212.

AII-3. C.J.F. Bottcher, THEORY OF ELECTRIC POLARIZATION, Elsevier Publishing Company, New York, 1952, pp. 417.

AII-4. D.A.G. Bruggeman, 'Berechnung Verschiedener Physikalischer Konstanten von Heterogenen Substanzen,' Annalen Der Physik, Vol. 24, Dec. 1935, pp. 636-664.

AII-5. L.K.H. van Beek, 'Dielectric behaviour of heterogeneous systems,' in PROGRESS IN DIELECTRICS, ed. J.B. Birks, Heywood Books, London, 1967, pp. 69-114.

AII-6. L.D. Landau and E.M. Lifshitz, ELECTRODYNAMICS OF CONTINUOUS MEDIA, Pergamon Press, London, 1960, pp. 46.

AII-7. H. Looyenga, 'Dielectric constants of heterogeneous mixtures,' Physica, Vol. 31, 1965, pp. 401-406.

AII-8. D. Polder and J.H. van Santen, 'The effective permeability of mixtures of solids,' Physica, Vol. 12, Aug. 1946, pp. 257-271.

AII-9. J.G. Kirkwood, 'On the theory of dielectric polarization,' Journal of Chemical Physics, Vol. 4, Sept. 1936, pp. 592-601.

AII-10. D.L. Goodstein, STATES OF MATTER, Prentice-Hall, Englewood Cliffs, New Jersey, 1975, pp. 265.

AII-11. D.L. Goodstein, STATES OF MATTER, Prentice-Hall, Englewood Cliffs, New Jersey, 1975, pp. 286.

AII-12. B.U. Felderhof, 'Bounds for the effective dielectric constant of disordered two-phase materials,' Journal of Physics C, Vol. 15, 1982, pp. 1731-1739.

AII-13. B.U. Felderhof, 'Bounds for the effective dielectric constant of a suspension of spherically symmetric particles,' Journal of Physics C, Vol. 15, 1982, pp. 3943-3951.

AII-14. B.U. Felderhof, 'Bounds for the effective dielectric constant of a suspension of uniform spheres,' Journal of Physics C, Vol. 15, 1982, pp. 3953-3966.

AII-15. B.U. Felderhof, G.W. Ford, and E.G.D. Cohen, 'Cluster expansion for the dielectric constant of a polarizable suspension,' Journal of Statistical Physics, Vol. 28, Jan. 1982, pp. 135-164.

AII-16. B.U. Felderhof, G.W. Ford, and E.G.D. Cohen, 'Two-particle cluster integral in the expansion of the dielectric constant,' Journal of Statistical Physics, Vol. 28, Apr. 1982, pp. 649-672.

AII-17. D.C. Dube, R.S. Yadava, and R. Parshad, 'A formula for correlating dielectric constant of powder and bulk,' Indian Journal of Pure and Applied Physics, Vol. 9, Sept. 1971, pp. 719-721.

AII-18. A.S. Yadav and R. Parshad, 'A formula for dielectric correlation between powder and bulk over wide ranges of permittivities and packing fractions,' Journal of Physics D, Vol. 5, 1972, pp. 1469-1473.

AII-19. V. Twersky, 'Coherent scalar field in pair-correlated random distributions of aligned scatterers,' Journal of Mathematical Physics, Vol. 18, Dec. 1977, pp. 2468-2486.

AII-20. V. Twersky, 'Propagation in pair-correlated distributions of small-spaced lossy scatterers,' Journal of the Optical Society of America, Vol. 69, Nov. 1979, pp. 1567-1572.

AII-21. L. Tsang and J.A. Kong, 'Multiple scattering of electromagnetic waves by random distributions of discrete scatterers with coherent potential and quantum mechanical formalism,' Journal of Applied Physics, Vol. 51, July 1980, pp. 3465-3485.

AII-22. L. Tsang and J.A. Kong, 'Effective propagation constant for coherent electromagnetic wave propagation in media embedded with dielectric scatterers,' Journal of Applied Physics, Vol. 53, Nov. 1982, pp. 7162-7173.

AII-23. V.N. Bringi, V.V. Varadan, and V.K. Varadan, 'The effects of pair correlation function on coherent wave attenuation in discrete random media,' IEEE Transactions on Antennas and Propagation, Vol. AP-30, July 1982, pp. 805-808.

AII-24. V.K. Varadan, V.N. Bringi, V.V. Varadan, and A. Ishimaru, 'Multiple scattering theory for waves in discrete random media and comparison with experiments,' Radio Science, Vol. 18, May-June 1983, pp. 321-327.

AII-25. V.K. Varadan, Y. Ma, and V.V. Varadan, 'Coherent electromagnetic wave propagation through randomly distributed and oriented pair-correlated dielectric scatterers,' Radio Science, Vol. 19 Nov.-Dec. 1984, pp. 1445-1449.

AII-26. M. Lax, 'Multiple scattering of waves. II. The effective field in dense systems,' Physical Review, Vol. 85, Feb. 1952, pp. 621-629.

AII-27. J.K. Percus and G.J. Yevick, 'Analysis of classical statistical mechanics by means of collective coordinates,' Physical Review, Vol. 110, Apr. 1958, pp. 1-13.

AII-28. G.D. Boyd, T.J. Bridges, M.A. Pollack, and E.H. Turner, 'Microwave nonlinear susceptibilities due to electronic and ionic unharmonicities in acentric crystals,' Physical Review Letters, Vol. 26, No. 7, Feb. 1971, pp. 387-390.

## APPENDIX III. MEASUREMENT OF RESONATOR Q USING THE TRANSMISSION METHOD

In Chapter III, we described the experimental set-up used to measure Q values of ring resonators by operating them as transmission filters. This standard technique for measuring Q's, called the transmission method, has been used for microwave resonators for many years and is described by Ginzton (Ref. AIII-1), Beringer (Ref. AIII-2), and others. Here we describe our measurements in terms of a simple model given by Beringer.

To measure the Q of a resonator by the transmission method, a signal source which is isolated from the load is connected by an input coupling network to the resonator. An output coupling network connects the resonator to a detector. By varying the frequency of the source, a resonance curve of transmitted power versus frequency is observed. The resonator Q is determined from the width of this curve.

For our experiments on ring resonators, the input and output coupling networks are taken to be the portions of the straight powder-core dielectric waveguides which pass in close proximity to the ring (c.f. Fig. 2 of Chapter III). The remaining lengths of straight dielectric waveguide, the metal-to-dielectric couplers, and the metal WR-10 waveguides are grouped conceptually with either the source or

the detector, as appropriate.

The relationship between the width of the transmission curve and the Q of the resonator is found using the circuit model shown in Figure AIII-1. In this model, coupling to the resonator is represented by ideal transformers. $R_G$ and $R_L$ are the generator and load impedances. These are assumed to be matched to their respective transmission lines, which have characteristic impedances $Z_1$ and $Z_2$. Finally, the resonator is modeled with an R-L-C series combination.

The first step in the analysis of the model is to transform the generator and load into the central loop, yielding the circuit shown in Figure AIII-2. $Q_0$, the unloaded Q, is then found by putting $R_G$ and $R_L$ equal to zero, yielding

$$Q_0 = \omega_0 L/R, \text{ where } \omega_0 = 1/(LC)^{1/2}.$$

$Q_L$, the loaded Q, is given by

$$Q_L = \omega_0 L/(R + n_1^2 R_G + n_2^2 R_L).$$

By introducing coupling parameters defined as

$$\beta_1 = n_1^2 Z_1/R \qquad \text{and} \qquad \beta_2 = n_2^2 Z_2/R,$$

the relation between $Q_0$ and $Q_L$ becomes

$$Q_0 = Q_L (1 + \beta_1 + \beta_2), \qquad \text{(AIII-1)}$$

which shows that the loaded Q approaches the unloaded Q in the limit of zero coupling.

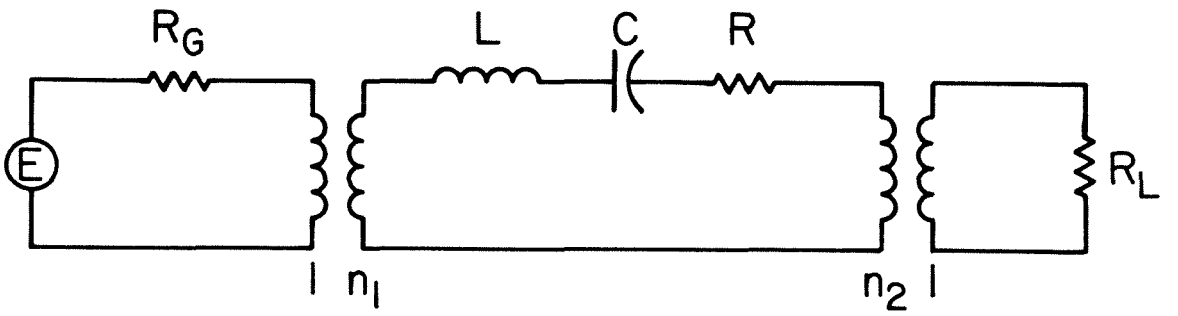


Figure AIII-1: Circuit model for a resonator used as a transmission filter

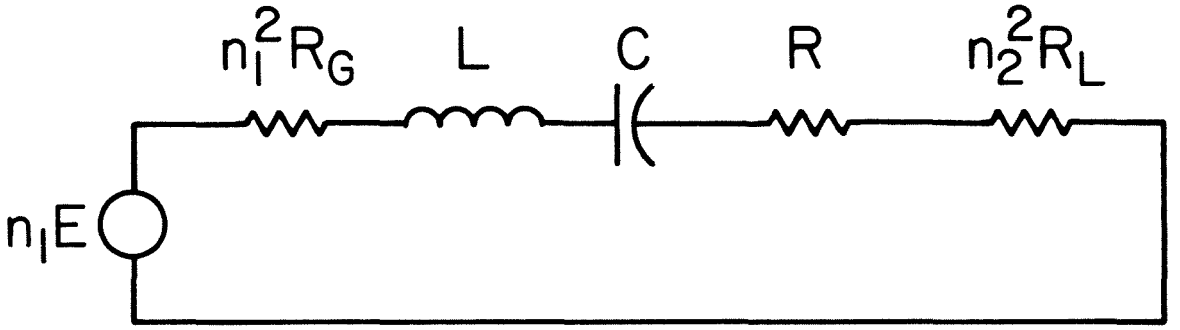


Figure AIII-2: Alternative form for the circuit of Figure AIII-1.

The transmission loss through the system, $T(\omega)$, is defined as the ratio of the power delivered to the load to the power available from the source. It is given by

$$T(\omega) = T(\omega_0)/(1 + Q_L^2(\omega/\omega_0 - \omega_0/\omega)^2), \qquad \text{(AIII-2)}$$

where $T(\omega_0)$ is the transmission loss at resonance and

$$T(\omega_0) = 4\beta_1\beta_2/(1 + \beta_1 + \beta_2)^2. \qquad \text{(AIII-3)}$$

Equation AIII-2 gives a good fit to the transmission loss curves measured for our ring resonators. Setting

$$\omega = \omega_0 + (\Delta\omega/2),$$

gives

$$T(\omega) = T(\omega_0)/(1 + Q_L^2(\Delta\omega/\omega_0)^2),$$

which implies that

$$\omega_0/\Delta\omega = Q_L$$

at the half-power points of transmission. Thus, the loaded Q can be determined by measuring the frequencies of the peak and half-power transmission points. The unloaded Q is found by decreasing the coupling to the resonator until further decreases yield no measurable increase in $Q_L$ (c.f. Eq. AIII-1). $Q_0$ is then equal to $Q_L$ to within the experimental uncertainty.

Given the measured transmission losses and the uncertainties in the Q values for our ring resonator experiments (c.f. Chapter III), Equations AIII-1 and AIII-3 predict that a decrease in $Q_L$ would be observable if the coupling were made sufficiently strong for the transmission loss at resonance to be less than about 20 dB. (Here we

assume that $\beta_1 = \beta_2$.) Unfortunately, with our experimental set-up, the coupling was too weak to allow less than 25 dB transmission loss at resonance, so we could not verify this prediction. For values of transmission loss between 25 dB and 41 dB at resonance, there were no observable changes in $Q_L$.

REFERENCES

AIII-1. E.L. Ginzton, MICROWAVE MEASUREMENTS, McGraw-Hill, New York, 1957, Chapter 9.

AIII-2. R. Beringer, Chapter 7 in 'Principles of microwave circuits,' M.I.T. RADIATION LABORATORY SERIES, Vol. 8, 1948.

## APPENDIX IV. RADIATION LOSS CAUSED BY VARIATION OF THE CORE DIELECTRIC CONSTANT WITH LENGTH

Appendix II treats the effects of material inhomogeneities on electromagnetic wave propagation. Another type of inhomogeneity inherent in all dielectric waveguides consists of the variation of the waveguide parameters with distance along the guide. These imperfections cause power to be lost to reflection and radiation.

For powder core dielectric waveguides, the parameters expected to vary slightly with length are the cross-sectional dimensions and dielectric constant of the core. The effects of variation of the core dielectric constant are of particular interest since it probably would be the most difficult parameter to control in a manufacturing process. In this appendix, an estimate is given of the maximum tolerable size of the deviations of the core dielectric constant from its specified value.

In a real waveguide, the deviation of the core dielectric constant from its ideal value would be a random function of length. However, to avoid the complexities involved in an analysis of the effects of random imperfections (Ref. AIV-1), it is assumed here that the core dielectric constant varies sinusoidally with length. (The loss resulting from the sinusoidal variation can be visualized as

representing that caused by one Fourier component of the actual variation of the dielectric constant with distance.)

In general, imperfections in a dielectric waveguide can cause power to be lost to all other modes (both guided modes and radiation modes). According to Marcuse's analysis (Ref. AIV-2), however, a sinusoidal thickness perturbation can couple only modes whose beat wavelength coincides with the period of the perturbation. (The beat wavelength of two modes is defined as $2\pi$ divided by the difference of their propagation constants. To calculate the beat wavelength, the propagation constant of a radiation mode is to be taken as the z-component of the wave vector of the radiated wave.) Furthermore, since our powder core dielectric waveguides were always designed for single mode operation, there could be no coupling to other guided modes. In this treatment, we also neglect losses due to coupling to the backward travelling dominant mode because such coupling would require a perturbation wavelength equal to half a guide wavelength and it is difficult to imagine a manufacturing process in which such a rapid fluctuation in powder density would be produced inadvertently. (The guide wavelengths of our powder core dielectric waveguides were approximately 2 mm at 94 GHz.) As a result of all these considerations, we calculate here only the losses due to radiation.

To further simplify the calculations, the waveguide is assumed to be a dielectric slab (Fig. AIV-1). The relative dielectric constant of the slab was chosen equal to 4.0 because this value was typical of the core dielectric constants in our channel guides. Similarly, the relative dielectric constant of the material surrounding the slab was chosen as 2.25, corresponding to polypropylene. The mode used to transmit power along the guide was taken to be the lowest-order even TE mode ($TE_0$) because its fields (Fig. AIV-1) are most similar to those of the $E^y_{11}$ mode of channel guide. Finally, assuming a frequency of 94 GHz, the width of the slab was chosen to be 0.32 mm so that the effective refractive index of the $TE_0$ mode would be similar to the values typical of the $E^y_{11}$ mode of our channel guides. (The effective refractive index of a propagating mode of a dielectric waveguide is defined as $\beta/k$, where k is the free space propagation constant and $\beta$ is the propagation constant of the mode.)

Marcuse's analysis (Ref. AIV-2) was used to find the radiation losses suffered by the $TE_0$ mode as a result of sinusoidal variation in the thickness of the slab (Fig. AIV-2). For small amplitudes, the sinusoidal thickness variation produces a sinusoidal variation in the propagation constant of the $TE_0$ mode. By using the characteristic equation of the slab to relate the amplitudes of these two variations, the losses were expressed as a function of the size of the periodic variation in $\beta$.

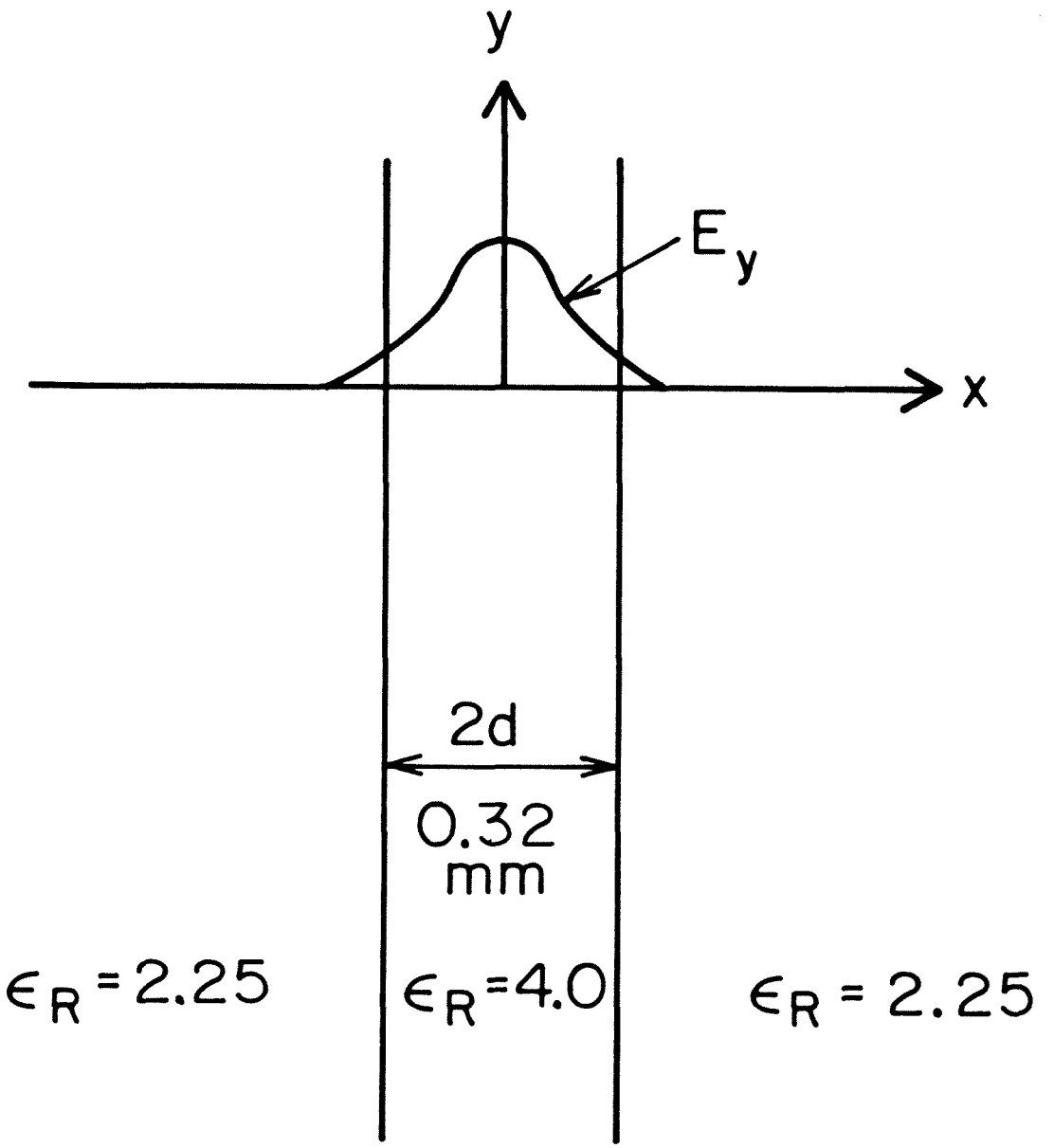


Figure AIV-1: Transverse cross section of the dielectric slab waveguide for which radiation losses were calculated. The electric field distribution is shown for the $TE_0$ mode.

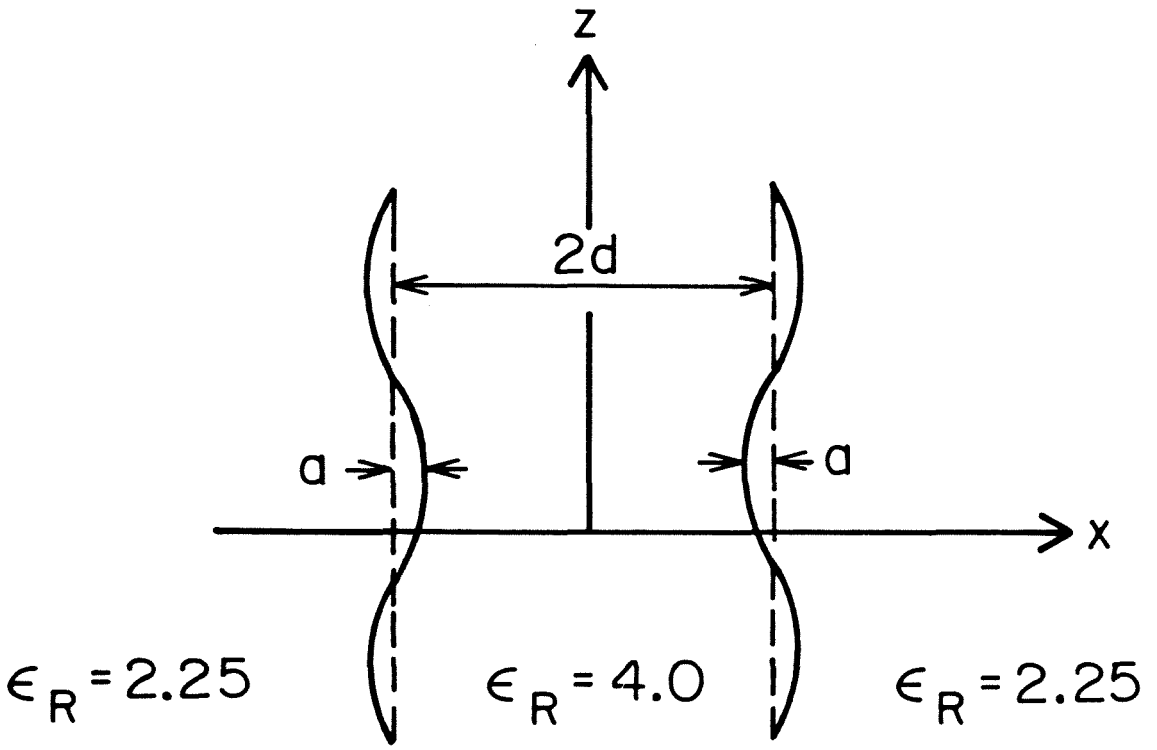


Figure AIV-2: Longitudinal cross section of a dielectric slab with sinusoidal thickness variation

The radiation losses were found to be a strong function of the amplitude of the β variation. For a perturbation period equal to 2.05 cm, a relative variation amplitude of 0.1% for β (i.e., $\Delta\beta/\beta_0 = 0.1\%$, where $\beta = \beta_0 + \Delta\beta\sin(z)$) caused a theoretical radiation loss of 0.3 dB/m. For $\Delta\beta/\beta_0$ equal to 0.4%, the radiation loss was predicted to be 9 dB/m, equal to that of our best channel guides. The value of 2.05 cm was used for the perturbation period because it was the one which produced the strongest (theoretical) radiation. Perturbation wavelengths greater than 4 cm were too long to couple to any radiation modes and hence are not associated with radiation. For shorter periods the radiation losses were not greatly different from the quoted 'worst case' values.

From the results of the above calculation for a slab, we next attempted to estimate the radiation loss for a channel guide with constant channel dimensions but sinusoidally varying core dielectric constant. The channel of this hypothetical guide was surrounded on all sides by a material whose relative dielectric constant equaled 2.25. The channel itself was chosen to have a relative dielectric constant of 4.0 and to have a square cross section with each side being 1.16 mm long. This length was chosen so that the effective refractive index of the $E^y_{11}$ mode at 94 GHz would be the same as for the $TE_0$ mode of the hypothetical slab treated earlier. Using Marcatili's theory (Ref. AIV-3) to relate β to the core dielectric

constant, a value of $\Delta\beta/\beta_0$ equal to 0.1% was found to correspond to a 0.2% relative amplitude variation in the core dielectric constant. A value of $\Delta\beta/\beta_0$ equal to 0.4% corresponded to $\Delta\varepsilon/\varepsilon$ equal to 1%. Thus, we can estimate (crudely) from the slab results that for $\Delta\varepsilon/\varepsilon$ equal to 0.2%, the radiation loss would be about 0.3 dB/m if the perturbation period were 2.05 cm. Similarly, for $\Delta\varepsilon/\varepsilon$ equal to 1%, the radiation loss is estimated to be 9 dB/m.

These results indicate that relatively small periodic perturbations in the types of dielectric waveguides described in this thesis can produce large radiation losses. The fact that we measured negligible radiation from our powder core dielectric guides probably means that any significant periodic imperfections in these guides had periods which were too long to cause coupling to radiation modes.

REFERENCES

AIV-1. D. Marcuse, 'Radiation losses of dielectric waveguides in terms of the power spectrum of the wall distortion function.' Bell System Technical Journal, Vol. 48, Dec, 1969, pp. 3233-3242.

AIV-2. D. Marcuse, 'Mode conversion caused by surface imperfections of a dielectric slab waveguide,' Bell System Technical Journal, Vol.48 Dec. 1969, pp. 3187-3215.

AIV-3. E.A.J. Marcatili, 'Dielectric Rectangular Waveguide and Directional Coupler for Integrated Optics,' Bell System Technical Journal. Vol. 48, Sept. 1969, pp. 2071-2102.